LATERAL CAPACITY OF PILES IN LIQUEFIABLE SOILS

A DISSERTATION

*Submitted in partial fulfillment of the
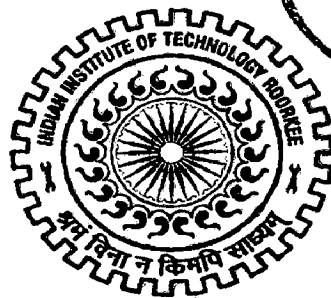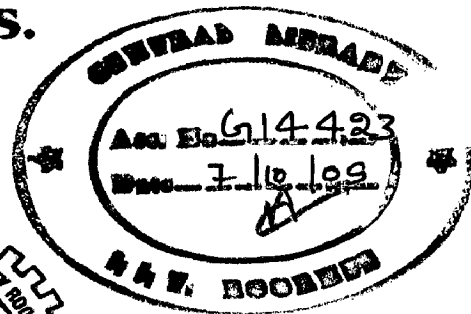requirements for the award of the degree
of*
MASTER OF TECHNOLOGY
in
CIVIL ENGINEERING
(With Specialization in Geotechnical Engineering)

By
KIRAN A.S.

DEPARTMENT OF CIVIL ENGINEERING
INDIAN INSTITUTE OF TECHNOLOGY ROORKEE
ROORKEE -247 667 (INDIA)
JUNE, 2009

CANDIDATE'S DECLARATION

I hereby certify that the work presented in this dissertation entitled "LATERAL CAPACITY OF PILES IN LIQUEFIABLE SOILS" in partial fulfillment of the requirements for the award of the degree of MASTER OF TECHNOLOGY in Civil Engineering, with specialization in Geotechnical Engineering, submitted to the Department of Civil Engineering, Indian Institute of Technology Roorkee, Roorkee is an authentic record of my own work carried out for a period from July, 2008 to June, 2009 under the supervision of Dr. G. Ramasamy, Professor, Department of Civil Engineering and Dr. B. K. Maheshwari, Assistant Professor, Department of Earthquake Engineering, Indian Institute of Technology Roorkee, Roorkee.
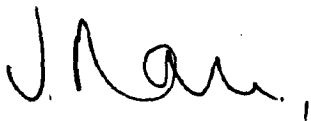
The matter embodied in this dissertation has not been submitted by me for the award of any other degree.

Date: 29th June, 2009   (KIRAN A S)
Place: Roorkee
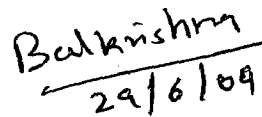
CERTIFICATE

This is to certify that the above statement made by the candidate is correct to the best of our knowledge.

(Dr. G. Ramasamy)   (Dr. B. K. Maheshwari)
Professor,   Assistant Professor,
Department of Civil Engineering,   Department of Earthquake Engineering,
Indian Institute of Technology Roorkee,   Indian Institute of Technology Roorkee,
Roorkee-247 667, India.   Roorkee-247 667, India.

I

ACKNOWLEDGEMENT

(KIRAN A.S.)

ABSTRACT

The performance of piles in liquefying ground under earthquake loading is a complex phenomenon. The process of generation of excess pore water pressure in saturated sand during earthquakes causes loss of shear strength of the ground. Many buildings and transportation facilities supported by deep foundations were damaged due to the loss of bearing capacity and excessive settlement during the 1964 Niigata and 1995 Kobe earthquakes.

Studies of seismic loadings on pile foundations and liquefaction phenomenon have been performed extensively in the last four decades. However, the combined problem of seismic behaviour of piles in liquefiable soil has received relatively less attention, especially the effect of liquefaction on lateral capacity. The present study deals with developing a simplified procedure to evaluate the lateral capacity of piles in liquefiable soils from commonly available field test data (SPT). The excess pore pressure generated due to liquefaction is determined using the method proposed by Seed, Martin and Lysmer. The lateral capacity is then determined using spring model (based on Winkler's hypothesis) incorporating the effect of excess pore pressure on soil stiffness. Layered soil system, ground water level, the earthquake magnitude and duration of earthquake shaking are accounted. Analysis for lateral load on pile foundation is carried out using 'Finite Difference' scheme. A computer code in C++ has been developed for this purpose.

Numerical results have been obtained for typical problems using the package and the effect of normal ground conditions on the pile behaviour is brought out. It has been observed that the lateral capacity of a single pile in liquefiable soil reduces drastically as compared to static case. Using Equivalent Cantilever Approach, design charts are developed to determine the pile head deflection for free and fixed head, fully embedded piles in homogenous soil deposits prone to liquefaction.

LIST OF CONTENTS

LIST OF TABLES

LIST OF FIGURES

LIST OF FLOW CHARTS

LIST OF NOTATIONS

Symbols	Description
σ_{v0}'	Initial effective vertical stress
σ_v'	Net effective vertical stress
a_{max}	Peak horizontal acceleration at the ground surface
g	Acceleration due to gravity
σ_{v0}	Total vertical stress
r_d	Stress reduction coefficient
τ_{av}	Average cyclic shear stress
τ_{max}	Peak cyclic shear stress
z	Depth below the ground
M	Earthquake magnitude.
R	Closest distance to the source
N_m	Measured standard penetration resistance
N_{60}	Value corresponding to 60% energy input
$(N_1)_{60}$	SPT N corrected (except for fines)
C_N	Overburden correction factor
C_E	Correction for hammer energy ratio (ER)
C_B	Correction factor for borehole diameter
C_R	Correction factor for rod length and
C_S	Correction for samplers with or without liners
FC	Fines content in percentage
$(N_1)_{60cs}$	Equivalent clean sand SPT value
θ	Coefficient depending on FC
ω	Coefficient depending on FC
N_{eq}	Equivalent number of uniform stress cycles
T_{eq}	Effective period of each stress cycle
T	Duration of strong earthquake shaking
$\dfrac{\partial U_g}{\partial t}$	Rate of pore pressure build-up
N	Number of applied stress cycles
N_L	Number of cycles to cause liquefaction

Symbols	Description
Δt	small time increment
r_n	Cyclic ratio
r_u	pore pressure ratio
u_0	Excess pore water pressure at time t_0
u_g	Excess pore pressure that would develop at time t
γ	Bulk unit weight
γ_{sat}	Saturated unit weight
γ_{sub}	Submerged unit weight
α	Function of soil properties and cyclic simple shear test conditions
CSR	Cyclic stress ratio
CRR	Cyclic resistance ratio
$CRR_{7.5}$	Cyclic resistance ratio at earthquake Magnitude of 7.5
MSF	Magnitude scaling factor
FS	Factor of safety
E	Youngs modulus of pile material
I	Moment of Inertia of pile
p	Soil reaction
K_h	Modulus of horizontal subgrade reaction
y	Deflection of pile
x	depth below the pile head level
n_h	Coefficient of subgrade reaction
A	Factor depending on relative density
BM	Bending moment
SF	Shear force
L_1	Unsupported length
L_T	Depth of fixity
T	Relative stiffness factor
Q	Lateral load at pile head
M_F	Fixed end moment
M_{act}	Actual maximum moment
D_w	Depth of water table below ground level
d	Diameter of pile

INTRODUCTION

The performance of piles in liquefying ground under earthquake loading is a complex phenomenon due to the effects of progressive build up of pore water pressure in saturated soils. The loss of soil strength and stiffness due to liquefaction may develop large bending moments and shear forces in piles founded in liquefying soil, leading to pile damage. Such failures were prevalent during the 1964 Niigata and the 1995 Kobe earthquakes. When the soil or phreatic surfaces are even slightly sloped, deformations of up to several meters may develop in cases where liquefaction occurs. In such cases, large lateral forces may act on the pile. This phenomenon is commonly referred to as lateral spreading (Klar et al. 2004). Damages related to liquefaction might involve pile foundation failures due to lateral flow of liquefied soils or failure at the boundary between two different soil layers, of which one liquefies and the other does not. Liquefaction also leads to substantial increase in pile cap displacements.

1.1 PILE FOUNDATIONS AND LIQUEFACTION

Dynamic pile-soil interaction analysis has become an important field in Civil Engineering over the past few decades. Several major earthquakes that caused damage to buildings, bridges, port facilities and other infrastructure have brought a lot of attention to how foundations behave under dynamic loading (Fig. 1.1).

Many studies of seismic loadings (vertical as well as lateral) of piles and liquefaction phenomenon have been performed in the past. Yet much has to be revealed especially on the excess pore pressure generated during liquefaction which alters the effective stresses in the soil and thereby change its mechanical behaviour (Maheshwari et al. 2008).

Over the past 25 years a methodology termed the "simplified procedure" has evolved as a standard of practice for evaluating the liquefaction resistance of soils. Following disastrous earthquakes in Alaska and in Niigata, Japan in 1964, Seed and Idriss (1971) developed and published the basic "simplified procedure." That procedure has been modified and improved periodically since that time, primarily through landmark papers

by Seed (1979), Seed and Idriss (1982), and Seed et al. (1985). The simplified procedure was developed from empirical evaluations of field observations and field and laboratory test data (Youd et al. 2001). The strength of this semi-empirical approach is the use of theoretical considerations and experimental findings to establish the framework of the analysis procedure and its components. Sound theory provides the ability to make sense out of the field observations, tying them together, and thereby having more confidence in the validity of the approach as it is used to interpolate or extrapolate to areas with insufficient field data to constrain a purely empirical solution.

Loss of pile capacity   Failure due to shear   Settlement of adjacent ground   Failure due to lateral spreading

Loss of pile capacity & lateral spreading   Failure due to overturning moment   Failure due to transient ground deformation   Failure due to lateral spreading
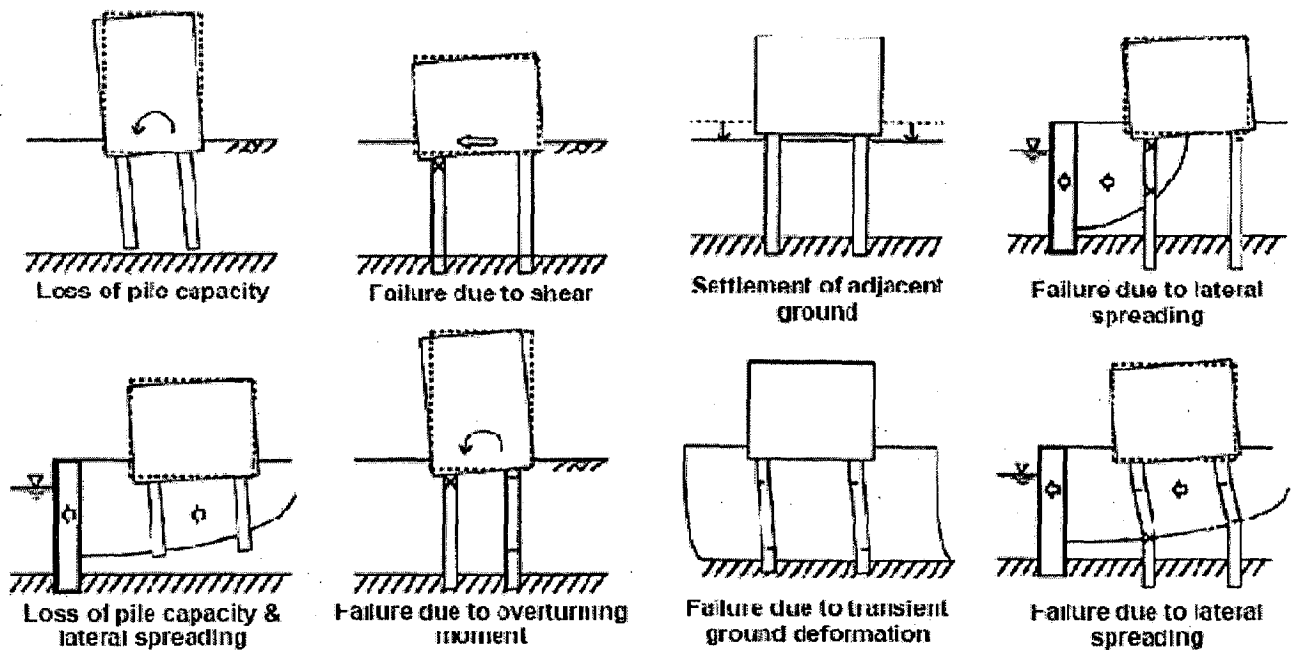
Fig. 1.1 Pile Damage Mechanisms in Liquefied Ground (Tokimatsu et al. 1996)

The available models of liquefaction are based on either (Kagawa and Kraft, 1981)

1) Experimentally observed undrained stress paths during pore pressure build up,

2) A correlation between pore pressure response and volume change tendency of dry soils,

3) Formulation of pore pressure response directly from observed data,

4) Plasticity theory in which the plastic volume change is related to pore pressure build up or

5) Treatment of the soil as a two phase medium.

Different experimental and analytical numerical models have been used to study the behaviour of soil-pile interaction. In general, it is possible to classify the different

2

analytical-numerical models according to three groups - (1) Continuum solution, (2) Finite element Solution and (3) Discrete models such as Winkler models.

Numerical procedures for the analysis of piles founded in liquefying soil have large uncertainties due to lack of understanding of the mechanisms involved in soil–pile interaction in the liquefying soil. Although numerical models based on two-dimensional and three-dimensional finite element analyses (e.g., Hamada et al. 1994; Sakajo et al. 1995; Zheng et al. 1996; Shahrour and Ousta 1998; Finn et al. 2001) provide better insights into this interaction, they are computationally complex and time-consuming. Therefore in recent years, one-dimensional Winkler models based on finite element and finite difference methods for the seismic analysis of pile foundations have become popular amongst designers. In Winkler models, the pile is modelled as a beam and the lateral soil pressure acting on the pile is modelled using a nonlinear spring-dashpot model. These methods are computationally very efficient and give results in a very short time (Liyanapathirana and Poulos, 2005a).

In this dissertation, a simplified procedure to evaluate the lateral capacity of piles in liquefiable soils is described. The excess pore pressure generated due to ground shaking is determined using the model proposed by Seed et al. (1976). The lateral capacity is then determined using spring model incorporating the effect of excess pore pressure on soil stiffness. Analysis for lateral load on pile foundation is carried out using 'Finite Difference' scheme.

1.2 OBJECTIVES

i.   To review the existing numerical models on estimation of pore pressure in liquefiable soils and select a suitable one.

ii. Analysis of laterally loaded piles in liquefiable soils using spring models incorporating the effect of pore pressure.

iii. Development of design charts for analysis of piles in liquefiable soil based on Equivalent Cantilever method.

1.3 SCOPE OF RESEARCH

This Dissertation is an attempt to obtain a simplified procedure for evaluation of lateral capacity of piles in liquefiable soils. The research consists of Study of liquefaction

3

susceptibility of soil, Study of various liquefaction models, Correlating the effective stress reduction due to liquefaction to the soil stiffness (modulus of horizontal subgrade reaction), Using modulus of subgrade reaction approach for the lateral analysis of the pile.

The excess pore pressure generated due to liquefaction is determined using the model proposed by Seed et al. (1976). The lateral capacity is then determined using spring model incorporating the effect of excess pore pressure on soil stiffness. Analysis for lateral load on pile foundation is carried out using 'Finite Difference' scheme. A computer code in C++ is developed for this purpose. Simple design charts are developed for lateral analysis of piles in liquefiable soils subjected to small earthquake accelerations using Equivalent Cantilever method.

The study has been performed for only single pile for one dimensional case. Both fixed and free head piles are considered in the study. The modulus of horizontal subgrade reaction is taken as a function of effective stress only. The pore pressure generation is considered however the dissipation is not considered. The earthquake loading is considered for pore pressure generation only. Lateral analysis is carried out for a particular value of lateral load at pile head. The study accounts to layered cohesionless soil system. Both long and short piles can be analyzed using the proposed method.

1.4 ORGANISATION OF DISSERTATION

This dissertation has been organised into seven chapters. Chapter 2 deals with review of literature. This chapter is primarily focused on past works on liquefaction and lateral load carrying capacity of piles. The combined studies of lateral load carrying capacity of piles considering the effects of liquefaction are reviewed. The pore pressure generation models developed by various researchers are included in the review. Soil liquefaction in some major earthquakes and few cases of liquefaction induced pile damage are also discussed. Chapter 3 deals with Numerical modelling and formulation for liquefaction. The steps and flow chart for the numerical model are described. Chapter 4 deals with the lateral capacity of piles. The procedure of Modulus of Subgrade reaction method and Equivalent Cantilever method for analysis of lateral load carrying capacity of piles under static lateral loading condition is explained. The Modulus of Subgrade reaction method is modified based on the evaluated excess pore pressure due to liquefaction. The procedure

adopted for this is described. Flow chart showing the entire steps is given. Chapter 5 involves the verification of algorithm and solution of a typical problem. The methodology adopted and program developed are verified. The results of lateral analysis of piles in liquefiable soils are explained using a typical problem. In Chapter 6, parametric studies are carried out to evaluate the variation of pile capacity with different locations of liquefiable layer and different homogenous soil deposits subjected to liquefaction. Design charts are prepared for determining pile head deflection in homogenous, cohesionless soil deposits for fully embedded piles. Chapter 7 deals with the summary of the studies conducted and the findings. Based on the results and findings, the conclusions have been drawn and future directions have been stated.

LITERATURE REVIEW

Soil liquefaction is the phenomenon by which soil loses its shear strength for a smaller time period, but that is long enough to cause many failures, loss of human life and major financial losses. It is an aspect of soil behaviour that occurs worldwide during major earthquakes and has much importance on both public safety and financial standpoints (Jefferies and Been, 2006). Occurrence of liquefaction has been reported during a large number of earthquakes in the past (e.g. Shonai (1894), Assam (1897), Kanto (1923), Nepal-Bihar (1934), Fukui (1948), Assam (1950), Jaltipan (1959), chile (1960)). But "Modern" engineering treatment of liquefaction started with the two devastating earthquakes of 1964, i.e. Niigata and Great Alaska Earthquakes, in which seismically-induced liquefaction caused spectacular and devastating effects. Major advances have occurred in both understanding and practice with regard to engineering treatment of seismic soil liquefaction and assessment of seismic site response over the past few decades. Seismic soil liquefaction engineering has evolved by itself into a sub-field, and assessment and treatment of site effects affecting seismic site response is now a mainstream issue addressed in most modern building codes and addressed in both research and practice (Seed et al., 2001).

The past earthquakes such as the 1964 Niigata, 1964 Alaska, 1989 Loma-Prieta, and 1995 Hyogoken-Nambu demonstrated a significant involvement of liquefaction in pile damage (Liyanapathirana and Poulos, 2005a). When liquefaction occurs during earthquakes, pile foundation is subjected to substantial shaking inside the soil which is in liquefied state and having minimum stiffness. Due to severe shaking, the pile may be subjected to severe cracking or even fracture. Significant lateral spreading or down slope displacements occur in a sloping site if the residual strength of soil is less than the static shear stresses. The moving soil exerts stress on the pile foundation resulting in pile damage. Lateral spreading becomes more critical for pile foundations when a non-liquefied layer slides over the top of a liquefied layer (Finn and Fujita, 2002).

The literature has been reviewed under three headings namely 1) Liquefaction and pile damages during past earthquakes, 2) Background studies on liquefaction 3) Lateral response of piles

2.1 LIQUEFACTION AND PILE DAMAGES IN PAST EARTHQUAKES

A few case histories of soil liquefaction during some major earthquakes and liquefaction induced pile damages are summarized here.

2.1.1 Soil Liquefaction in some Major Earthquakes

a) The Alaska Earthquake, March 27, 1964
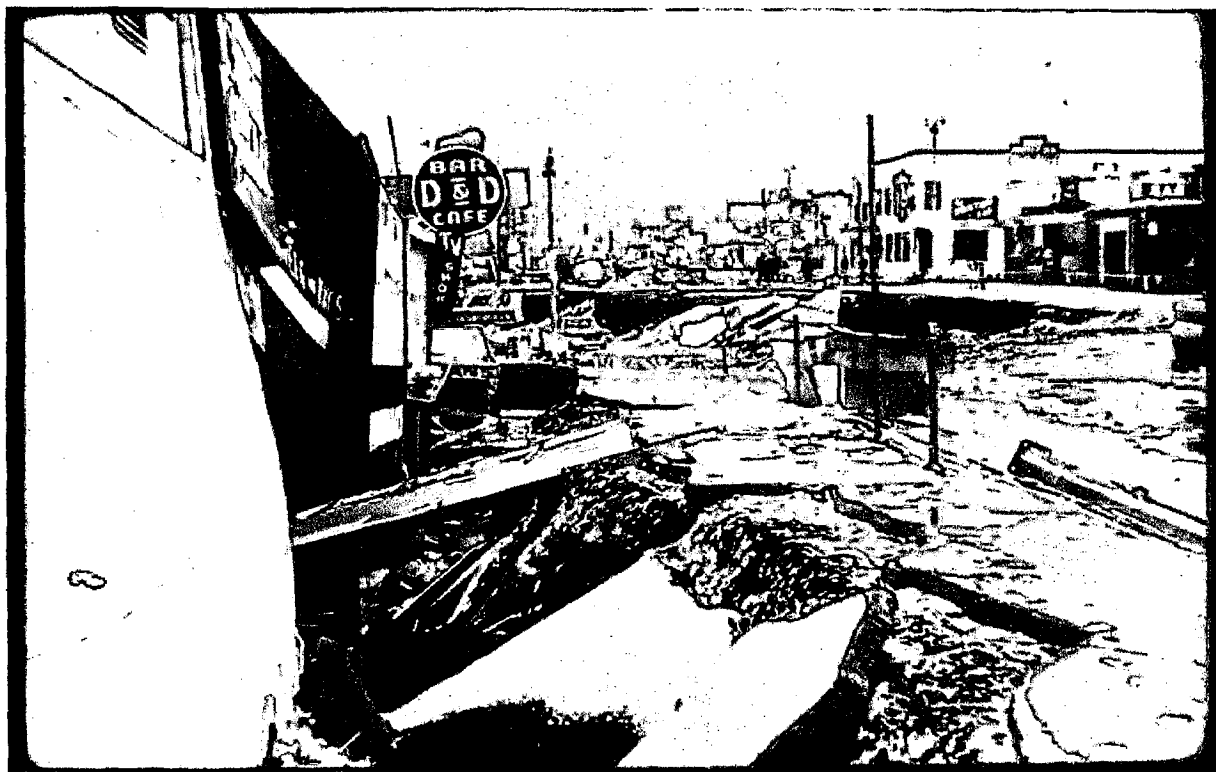
Fig. 2.1 Damage to Fourth Avenue, Anchorage, 1964 Alaska Earthquake
(http://www.smate.wwu.edu/teched/geology/GeoHaz/eq-Alaska64/eq-Alaska64-
09.JPG)

The Earthquake (M = 9.2) was estimated to have produced a peak ground surface acceleration of about 0.15g to 0.20g based on observed patterns of damage to structures. Fig. 2.1 shows the Fourth Avenue buildings in downtown Anchorage after 1964 Alaska Earthquake. It shows the damage resulting from the slide in this area. Before the earthquake, the sidewalk in front of the stores on the left was at the level of the street on the right, which was not involved in the subsidence. The sidewalk subsided 11 feet (3.3

7

m) in response to 14 feet (4.2 m) of horizontal movement of the slide block during the earthquake. Lateral spreading produced a fan- shaped slide 1,800 feet (545.5 m) across that covered about 36 acres (14.6 hectares) and moved a maximum of 17 feet (5.1 m). Movement on the landslide began after about 1 1/2 to 2 minutes of ground shaking and stopped when the shaking stopped. Fig. 2.2 shows the soil profile. The SPT blow count and CPT values are shown in the figure. The open circles are for SPT N values in sandy silt (ML) soils and filled circles are for N values in Naptowne Outwash and silty sand (SM) soils (Boulanger and Idriss, 2004).
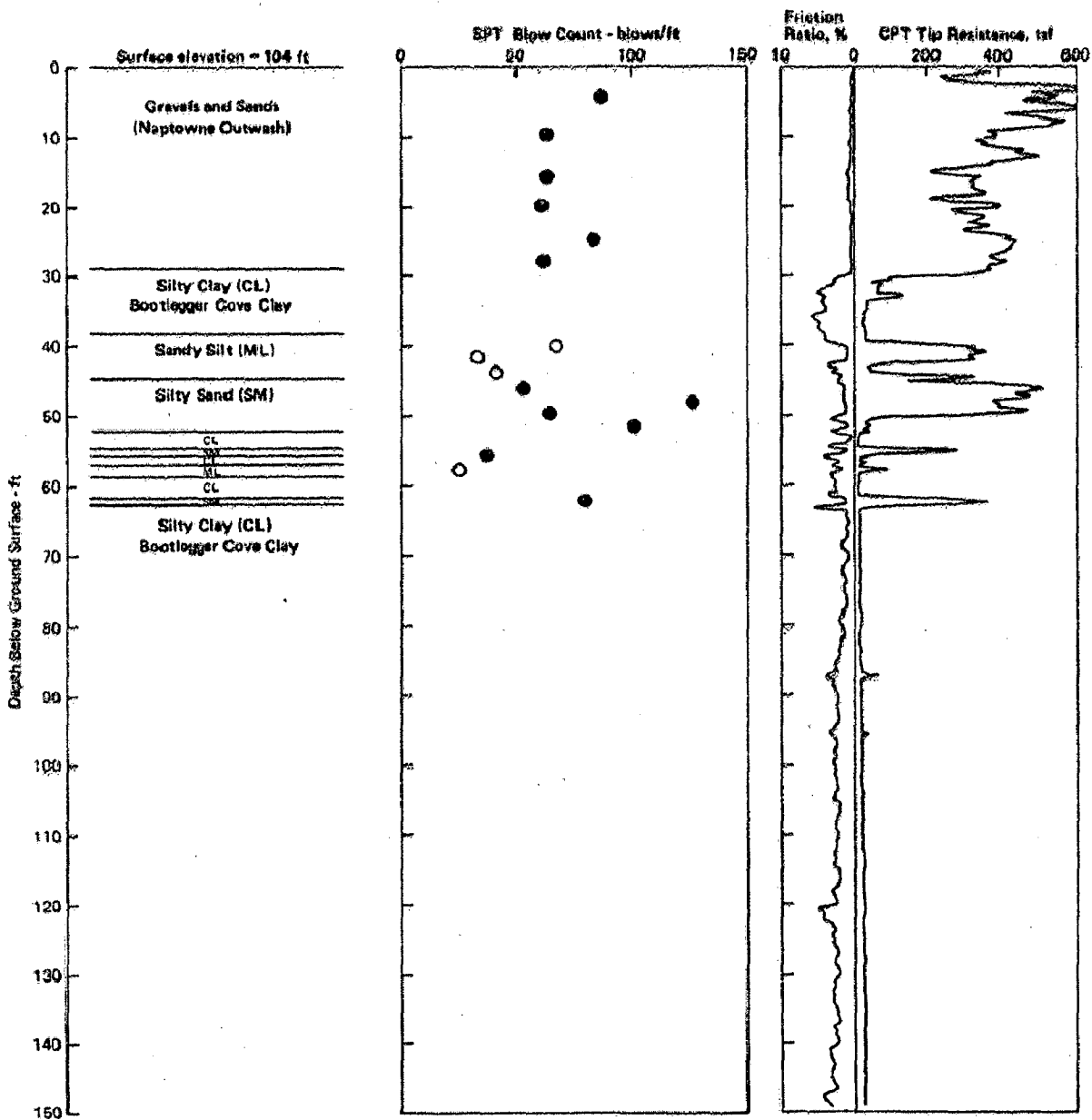
Fig. 2.2 Log of Boring BH3 and CPT Record (Boulanger and Idriss, 2004)

Fig. 2.3 Fissured Highway Embankment, 1964 Alaska Earthquake
(www.smate.wwu.edu/teched/geology/GeoHaz/eq-Alaska64/eq-Alaska64-13.JPG)

Fig. 2.3 shows the eastern approach to Twenty mile River Highway Bridge at Portage. The highway embankment fissured, spread and slumped on underlying alluvium. The road was built on thick deposits of alluvium and tidal estuary mud along the Turnagain Arm of Cook Inlet near Portage, Alaska. These weakened deposits spread laterally away from the road centre toward the edge of the embankment.

b) 1964 Niigata Earthquake, Japan

The 1964 Niigata Earthquake had a magnitude of 7.5. The destruction was observed to be largely limited to buildings that were founded on top of loose, saturated soil deposits. In and around this city, the soils consist of recently reclaimed land and young sedimentary deposits having low density and shallow ground water table. The damaged concrete buildings were built on very shallow foundations or friction piles in loose soil. Similar concrete buildings founded on piles bearing on firm strata at a depth of 20 m did not suffer damage. Fig. 2.4 shows the tilting of buildings at Kawagishi-Cho during 1964 Niigata Earthquake. A remarkable ground failure occurred near the Shinano river bank where the Kawagishi-cho apartment buildings suffered bearing capacity failures and tilted severely. Despite the extreme tilting, the buildings themselves suffered remarkably little

structural damage. Sand boils and ground fissures were observed at various sites in Niigata.

Fig. 2.4 Tilting of buildings at Kawagishi-Cho, Niigata Earthquake, 1964 (www.ce.washington.edu/~liquefaction/selectpiclique/nigata64/tiltedbuilding.jpg)

c) 1988 Armenia Earthquake

The earthquake of December 7, 1988 in Armenia (M~6.8) caused extensive damage to buildings, roadways, and other engineered facilities (Yegian et al., 1994). Fig 2.5 shows a failed highway. It is located near a tributary of Pambak River where the water table was near ground surface. The embankment material is silty sandy compacted fill. The peak ground surface acceleration was about 0.5 g. For this acceleration, free draining gravelly sands are not expected to liquefy. However, the presence of an overlying 30-40 cm relatively impermeable soil layer prevented vertical dissipation of the excess pore-water pressures, as they were being generated by the shaking. As a consequence, high pore-water pressures triggered liquefaction or at least substantially reduced the shearing resistance of this deposit beneath, and particularly near the toes of the embankment. This led to instability of the embankment, resulting in cracking and slip deformations (Fig. 2.6).

10

Fig. 2.5 Photograph of Failed Spitak Highway (Yegian et al., 1994)
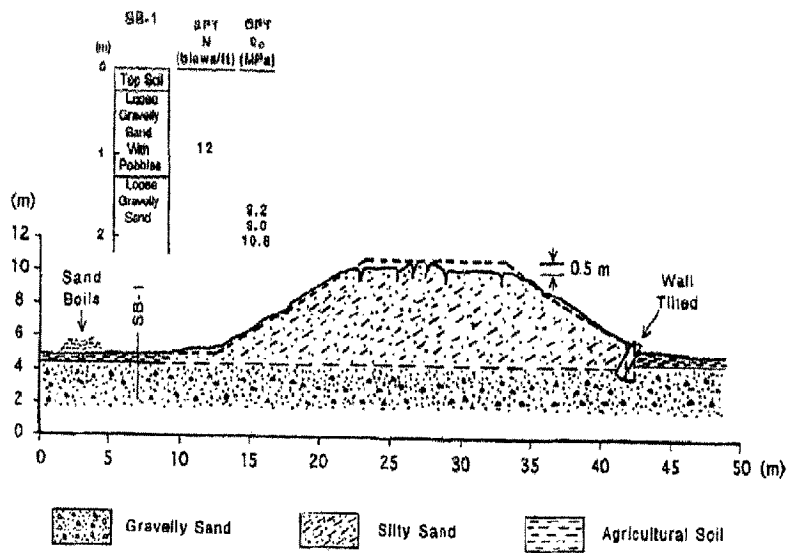
Fig. 2.6 Spitak Highway Embankment Cross Section before and after Failure
(Yegian et al. 1994)

11

d) 1995 Kobe Earthquake

Fig. 2.7 Fallen Bridge Deck, 1995 Kobe Earthquake

(www.ce.Washington.edu/liquefaction/html/main.html)

Fig. 2.7 shows the Nishiyoma Bridge failure during 1995 Kobe earthquake having a magnitude of 6.9. One span of the deck had fallen to the ground. The supports of the bridge were not damaged, but large deformations occurred.

e) 2001 Bhuj earthquake, India

The Bhuj earthquake magnitude, M = 7.7 struck the Kutch area in Gujarat at 8.46 a.m. (IST) on January 26, 2001. It was the most damaging earthquake in India in the last 50 years. This earthquake has caused extensive damage to the life, property and infrastructures (Fig. 2.8). Fig. 2.9 shows failure of a railway embankment at Vaka Nala of about 5 meters height. It suffered extensive damage. The rails were hanging by about 1.0 to 1.5 meters after the earthquake. Ground liquefaction was observed at the base of the embankment. Fig. 2.10 shows a tilted bridge. This pier at the RC bridge near Vondh was found to have a tilt. Considerable liquefaction was observed at the site. Pier supports two spans with different girder/slab depths (EERI Special Earthquake Report, 2001).

Fig. 2.8 Damage to Highway Pavement near Rapar due to Lateral Spreading of Soil (EERI Special Earthquake Report, 2001)

Fig. 2.9 Rail Embankment at Vaka Nala (EERI Special Earthquake Report, 2001)

Fig. 2.10 Damage to the Unequal-height Bed Blocks at RC Bridge near Vondh (EERI Special Earthquake Report, 2001)

2.1.2 Pile Damages due to Liquefaction during Past Earthquakes

Damage to piles during earthquakes has been greatest in areas of liquefaction and particularly lateral spreading. Damage is relatively rare for pile foundations designed according to modern standards and embedded in competent soils that experience negligible permanent deformations during earthquakes. Different mechanisms of pile foundation damage, as excessive deformations or structural damage have been observed in liquefied ground. Liquefaction often causes large transient and permanent ground deformations (laterally or vertically) that impose kinematic loads on the pile foundation. The liquefaction also causes a reduction in pile capacity to resist vertical or lateral loads (i.e., loss of shaft friction, tip bearing capacity, or lateral subgrade reaction) that can lead to excessive deformations under the inertial and static loads from the superstructure (Boulanger et al., 2003). Some of the pile failures reported during past earthquakes are given below.

a) Customs Office Tower, Kandla Port Supported on a Mat–Pile Foundation (Dash et al. 2009)

Kandla is located at the mouth of the Little Rann of Kutch on the south eastern coast of the Kutch district, It is one of the major seaport-city of Gujarat that got affected during 2001 Bhuj earthquake. This area is located about 50 km from the epicenter of the 2001 Bhuj earthquake. The building was founded on 32 cast-in-situ concrete piles and each pile was 18m long. The piles were passing through 10 m of clayey crust and then terminated in a sandy soil. The Port of Kandla is built on natural ground comprising recent unconsolidated deposits of interbedded clays, silts and sands. The profile of the region slopes towards the coast line at about 12.5 m/km. The water table is about 1.2–3.0 m below the ground

The typical borehole profile of the area is given in Fig. 2.11. The soil profile suggests that the upper soil layers consist of 10 m thick deposits of soft silty clay underlain by sand and hard clay minerals. The lower soil layers consist of fine and coarse sand. The Standard Penetration Test (SPT) "N" corrected values for upper sandy layers is less than 15, while the underlying deep sandy layers have SPT values of less than 50. The blow counts N values lies between 15 and 50 of the sandy layers with fines content between 1% and 32% which indicate that the soils are potentially liquefiable under strong and sustained shaking.
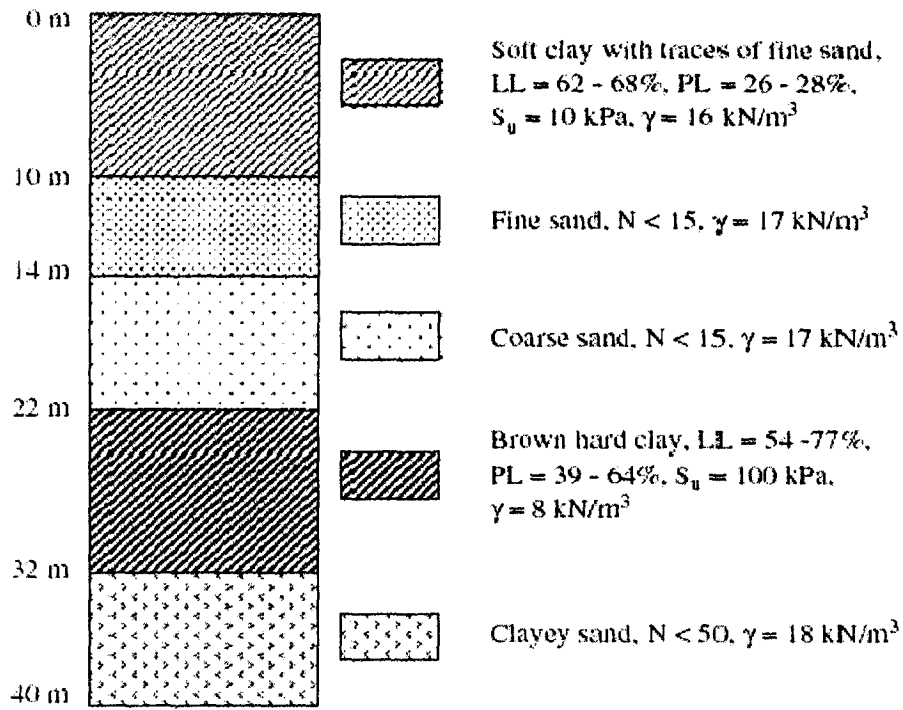
Fig. 2.11 Typical Soil Profile in the Vicinity of Customs Office Tower (Dash et al. 2009)
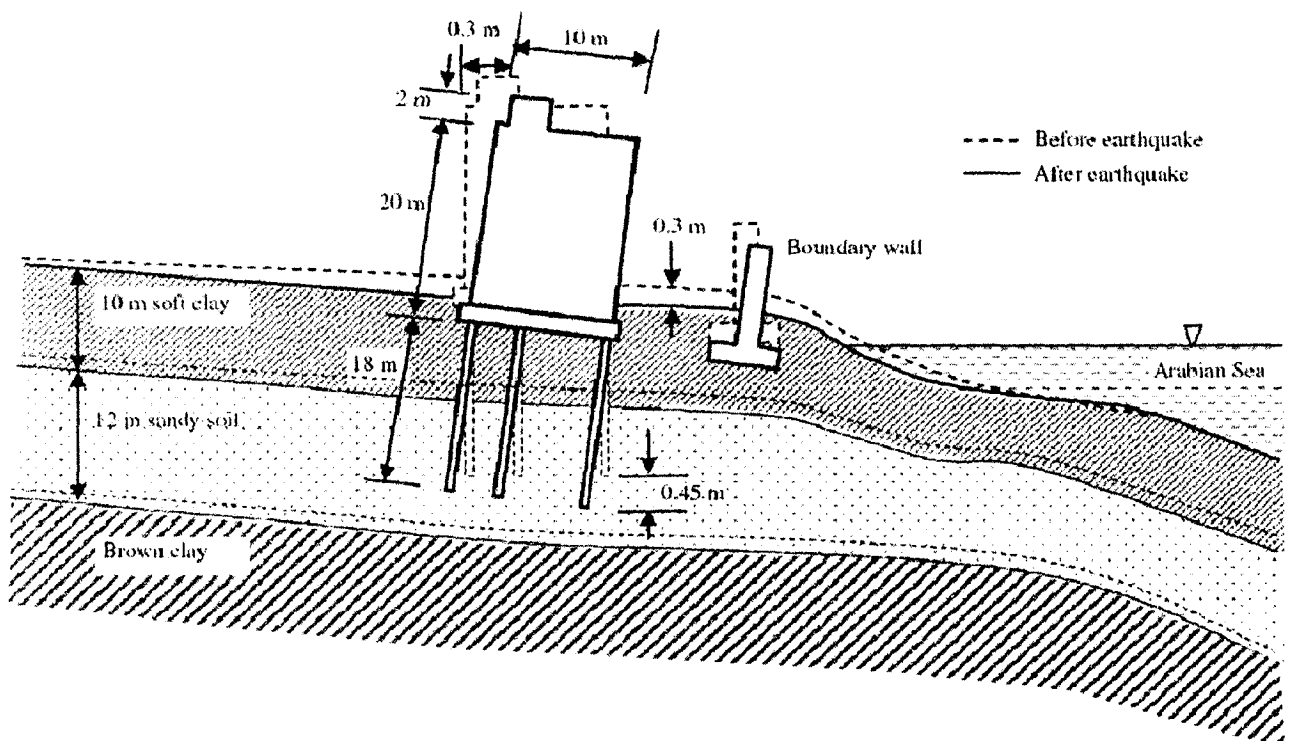
Fig. 2.12 Plausible Settlement Mechanism of Failure Showing the Tilting of the Tower assuming no Structural Failure of Piles (Dash et al. 2009)

The pile-supported building under consideration leaned about 30cm at its top and separated from its adjacent building as shown in Fig. 2.12. The ground in the vicinity of the tower settled about 30cm, resulting in the settlement of mat floors of the building. There were evidences of extensive liquefaction with ejection of sand through ground crack in the vicinity of the building. Lateral spreading was observed at the site.

b) NHK building during the 1964 Niigata earthquake (Hamada, 1992)

It is a four-storey R.C building supported on reinforced concrete piles. The piles were having a diameter of 350 mm and are 11 to 12 m long. 72 piles were investigated and it was found that all were damaged. The piles failed at two portions as shown in Fig. 2.13. Liquefiable layer was found to be about 10m. Only about 2 m of the pile was in non-liquefiable zone.
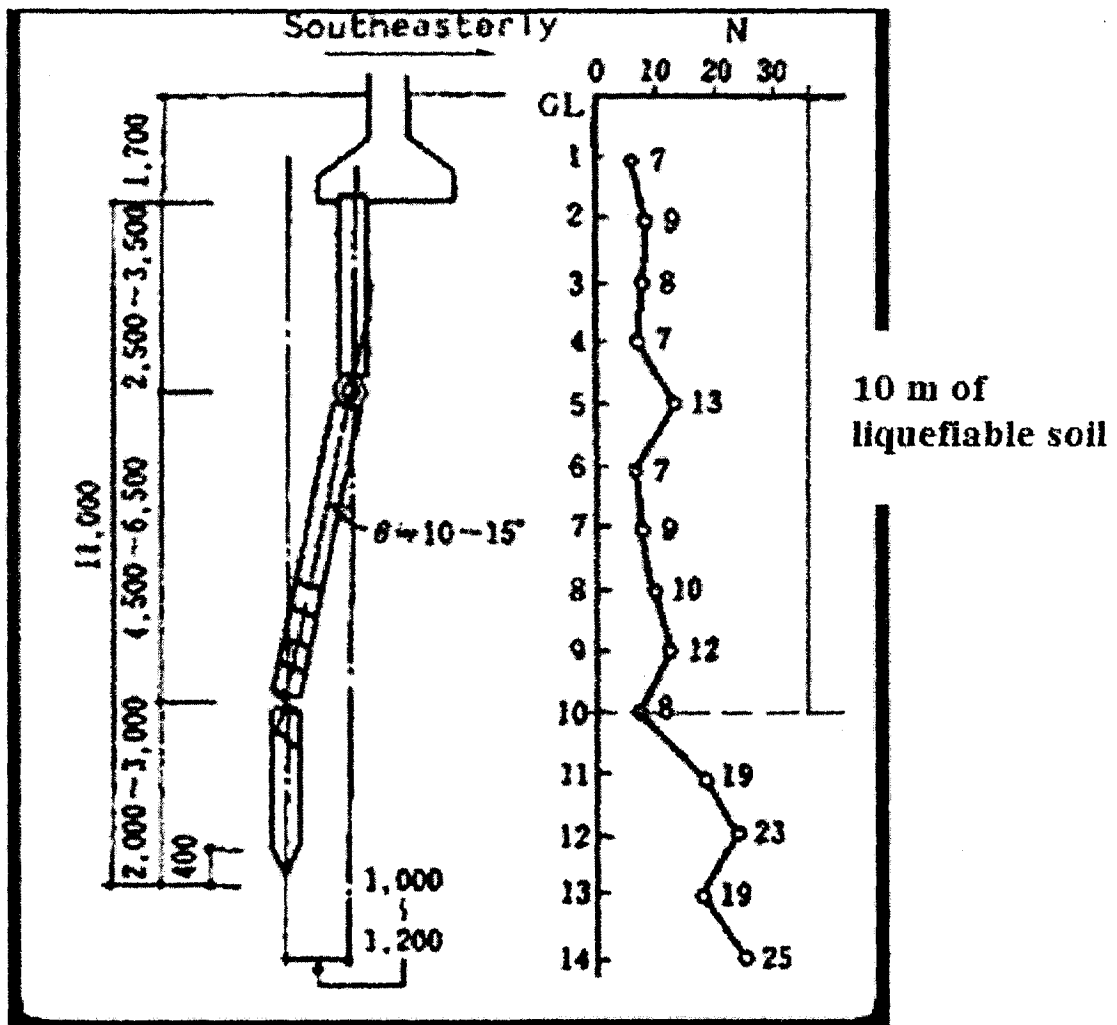
Fig: 2.13 Failed Pile of N H K Building (Hamada, 1992)

c) Failure of Showa Bridge over river Shinano during the 1964 Niigata earthquake (Hamada, 1992)

The pile passes through 10 m of potentially liquefiable soil and is founded on 6 m of competent non-liquefiable soil. The length of the pile in liquefiable zone is 10m and the length of pile in free air/water is 9 m. So during liquefaction, 19 m of the pile was unsupported (Fig. 2.14).
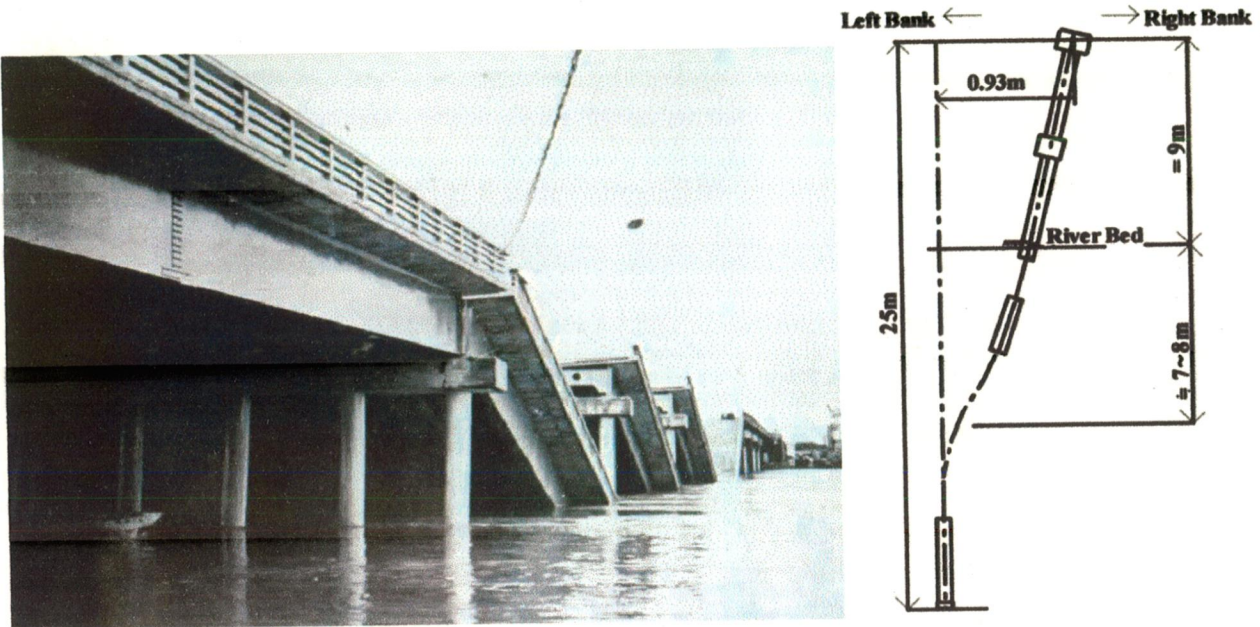
Fig. 2.14: Damage to Steel Piles of Pier 4 of Showa Bridge (Boulanger et al., 2003)

d) Failure of the Yachiyo bridge over river Shinano during the 1964 Niigata earthquake (Hamada, 1992)

This bridge is located adjacent to the Showa Bridge. Extensive lateral spreading occurred in the river and the river width decreased. The foundation of both abutments and piers were Reinforced concrete piles of 0.3m diameter and a length of 10 to 11m. The pile formed a plastic hinge at 8m depth (Fig. 2.15). The depth of liquefiable layer was 8m. The pile head got displaced by about 1.1m.

e) Failure of 4-storey firehouse during the 1995 Kobe earthquake (Tokimatsu et al. 1996)

This building is located at the foot of the Kobe O-Hashi Bridge on Port Island. The building got tilted and moved towards the sea. The building was supported on pre stressed concrete piles of 30 m length and 400 mm diameter. After the earthquake, excavation survey showed that compressional shear failure occurred on the seaside with minor

flexural cracks on the opposite side. From the soil report of the island it is estimated that the top 18 m is most likely to have liquefied during the earthquake.
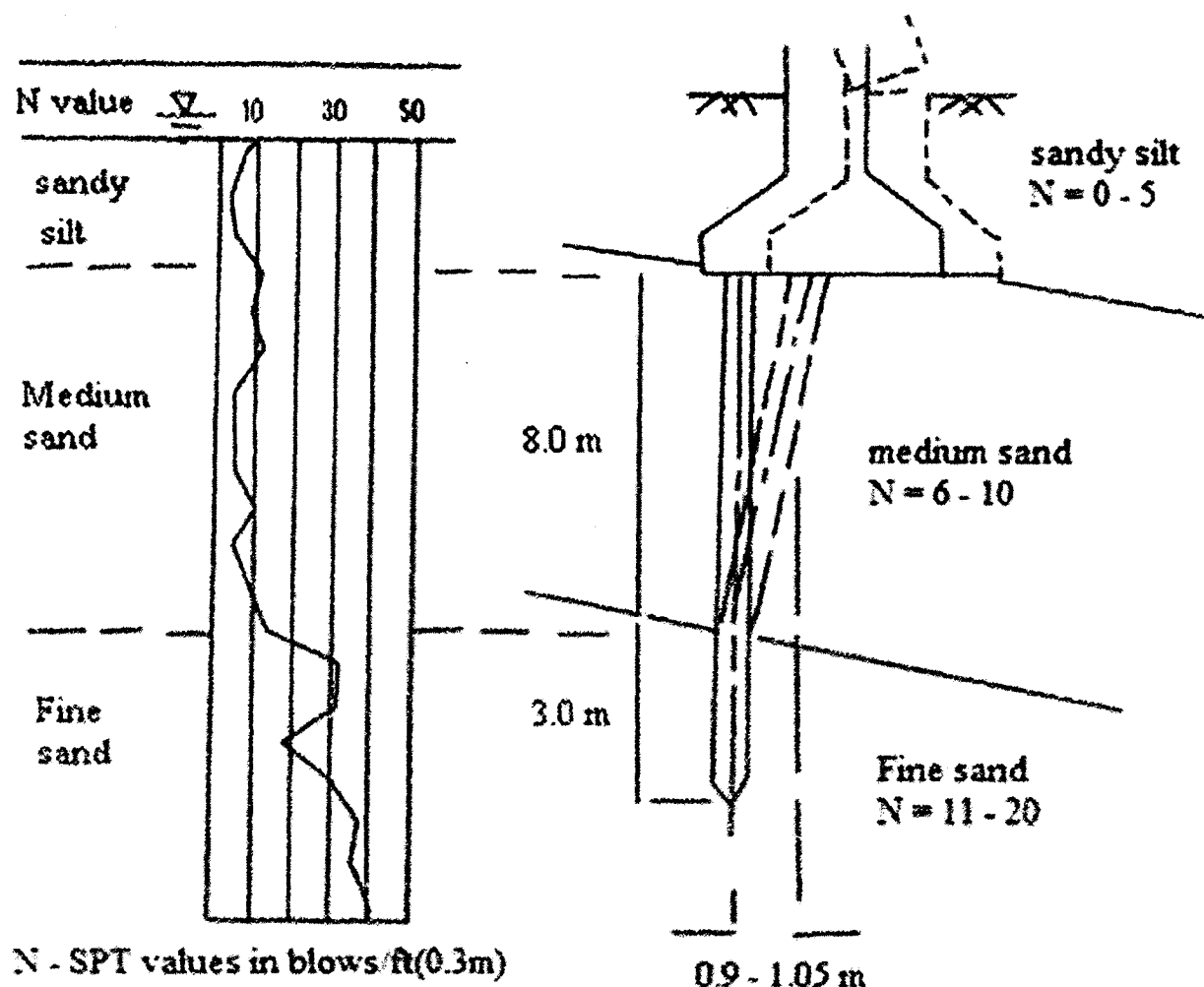
Fig: 2.15 Failure of Yachiyo Bridge (Hamada, 1992)

2.2 BACKGROUND STUDIES ON LIQUEFACTION

Ishihara in his Rankine Lecture (Ishihara, 1993) suggests that the term spontaneous liquefaction was coined by Terzaghi and Peck in 1948. But the subject is much older than that. The Dutch Engineers have been engineering against liquefaction to protect their country from sea. Koppejan et al. in 1948 at the 2nd International Conference in Rotterdam mentioned about flow slides in the approach to a railway bridge near Weesp, Netherlands in 1918, triggered by vibrations from a passing train. During the same time, Hazen's 1918 report on the Calaveras Dam failure was clearly recognized as a phenomenon related to pore pressures and effective stresses (Jefferies and Been, 2006).

The devastating effects of liquefaction sprang up to the attention of geotechnical engineers in 1964 when the Alaska and Niigata earthquake produced spectacular examples of liquefaction induced damage, including slope failure, bridge and building foundation failure, and flotation of buried structures. The excess pore pressure generation under undrained loading conditions forms the hallmark of all liquefaction phenomena. Under both static and cyclic loading conditions, the dry, loose cohesionless soils become dense. When saturated, cohesionless soils in loose state are subjected to these loadings, the soil tries to get denser causing a rise in pore water pressure finally leading to reduced effective stresses (Kramer, 1996). When effective stress reduces, the shear strength reduces greatly and large settlements occurs leading to the phenomenon called "complete liquefaction". (Brennan et al., 2007).

From the mid-1960's intense research has been done for the prediction of liquefaction of soils during earthquakes. Cyclic triaxial tests, cycle simple shear tests and large scale shaking table tests have explained many features of the liquefaction phenomenon. Efforts were made in developing procedures for assessing liquefaction potential of sites underlain by sand deposits using the results of these tests (Peck, 1979). The prominent works done by Martin et al. (1975), Seed et al. (1976), Finn et al. (1977) and Martin and Seed (1979) established the basic understanding of liquefaction in saturated sands.

Martin et al. (1975) developed a quantitative relationship between volume reductions occurring during drained cyclic tests and the progressive increase of pore water pressure during undrained cyclic tests. Using this relationship, the pore pressure build-up during liquefaction can be computed theoretically using basic effective stress parameters of sand.Seed et al. (1976) developed an analytical procedure for evaluating the general characteristics of pore pressure build-up and subsequent dissipation in sand deposits during and after the period of earthquake shaking. Finn et al. (1977) provided a non-linear effective stress analysis method for dynamic response of dry or saturated sands. Martin and Seed (1979) described a simplified procedure which analytically uncouples the analyses of pore-water pressure and dynamic soil response. Liyanapathiana and Poulos (2002a, b) presented an effective stress based numerical model to analyse soil liquefaction when a saturated soil deposit is subjected to earthquake loading. The main advantage of this method is the lesser number of model parameters required as compared to the existing effective stress models.

2.2.1 Numerical Models for Pore Pressure Generation

In liquefying soil the dynamic response is dominated by the progressive build up of pore water pressure. The amount of resistance provided by the soil to deformation at any point in the soil deposit is a function of the effective stress at that point. Therefore, it is important to develop numerical models, which can predict generation and dissipation of excess pore pressure in the soil deposit, which in turn can predict the effective stress.

Some of the numerical models for liquefaction are explained below.

a) **Seed et al. (1976) method:** This paper presents a means for analysing the development and redistribution of pore-water pressures in horizontally stratified deposit of sand, both during and following the period of earthquake shaking. The model can be used to determine the excess pore pressure generated in the soil deposit due to a particular magnitude earthquake and maximum surface acceleration. For the present study, this method is adopted for pore pressure evaluation and hence is discussed in detail in next chapter.

b) **Finn et al. (1977) method:** This method is a non-linear effective stress analysis for the dynamic response of dry or saturated sands.

Generation of pore water pressure (Martin et al. 1975): Consider a cubic element of saturated sand of unit volume and porosity. Let the element be under a vertical effective stress, σ_v', and horizontal stresses $k_0\sigma_v'$. During a drained simple shear test a cycle of shear strain, η, causes an increment in volumetric compaction strain, $\Delta\varepsilon_{vd}$, due to grain slip. During an undrained shear test starting with same effective stress system, the cycle of shear strain, η, causes an increase in pore pressure, Δu given by

$$\Delta u = \frac{\Delta\varepsilon_{vd}}{\frac{1}{E_r'}+\frac{n_e}{k_w}} \tag{2.1}$$

Where E_r' = one-dimensional rebound modulus of sand at an effective stress σ_v'

   k_w = the bulk modulus of water.

   n_e = porosity of sample

For saturated sands $k_w \gg E_r'$ and therefore,

$$\Delta u = E_r' . \Delta\varepsilon_{vd} \tag{2.2}$$

It has been shown experimentally that under simple shear conditions the volumetric strain increment, $\Delta\varepsilon_{vd}$, is a function of the total accumulated volumetric strain, ε_{vd}, and the amplitude of shear strain, η, and is given by

$$\Delta\varepsilon_{vd} = c_1(\gamma - c_2\,\varepsilon_{vd}) + c_3\,\varepsilon_{vd}^2/(\eta + c_4\varepsilon_{vd}) \qquad (2.3)$$

where c_1, c_2, c_3 and c_4 are constants that depend on the sand type and relative density. These constants are evaluated by data plotting of two to three constant strain amplitude tests. For best fit curves, the constants obtained are $c_1=0.80$, $c_2=0.79$, $c_3=0.45$ and $c_4=0.73$.

An analytical expression for the rebound modulus, E_r' at any effective stress level σ_v' is given by the relation

$$E_r' = \frac{\sigma_v'^{\,1-m}}{mk_2\sigma_{v0}'^{\,n-m}} \qquad (2.4)$$

In which σ_{v0}' is the initial value of the effective stress and k_2, m and n are experimental constants for given sand. They can be determined readily from a series of three unloading curves from different σ_{v0}' as shown in Fig. 2.16.

Dissipation of pore water pressure: If the saturated sand layer can drain during shaking there will be simultaneous generation and dissipation of pore water pressure. Thus the rate of increase of pore water pressure will be less than for completely undrained sand. The pore water pressure at time 't' is given by the following equation.

$$\frac{\partial u}{\partial t} = E_r'\,\frac{\partial}{\partial z}\left(\frac{k}{\gamma_w}\frac{\partial u}{\partial z}\right) + E_r'\,\frac{\partial\varepsilon_{vd}}{\partial t} \qquad (2.5)$$

In which u is the pore water pressure, k is the permeability and γ_w the unit weight of water. The first term shows dissipation of pore water pressure. The second term shows the internal generation of pore water pressure. Eq. 2.5 must be solved numerically in conjunction with the equations of motion of the sand layer in order to update continually the values of pore water pressures that are being developed during earthquake shaking.
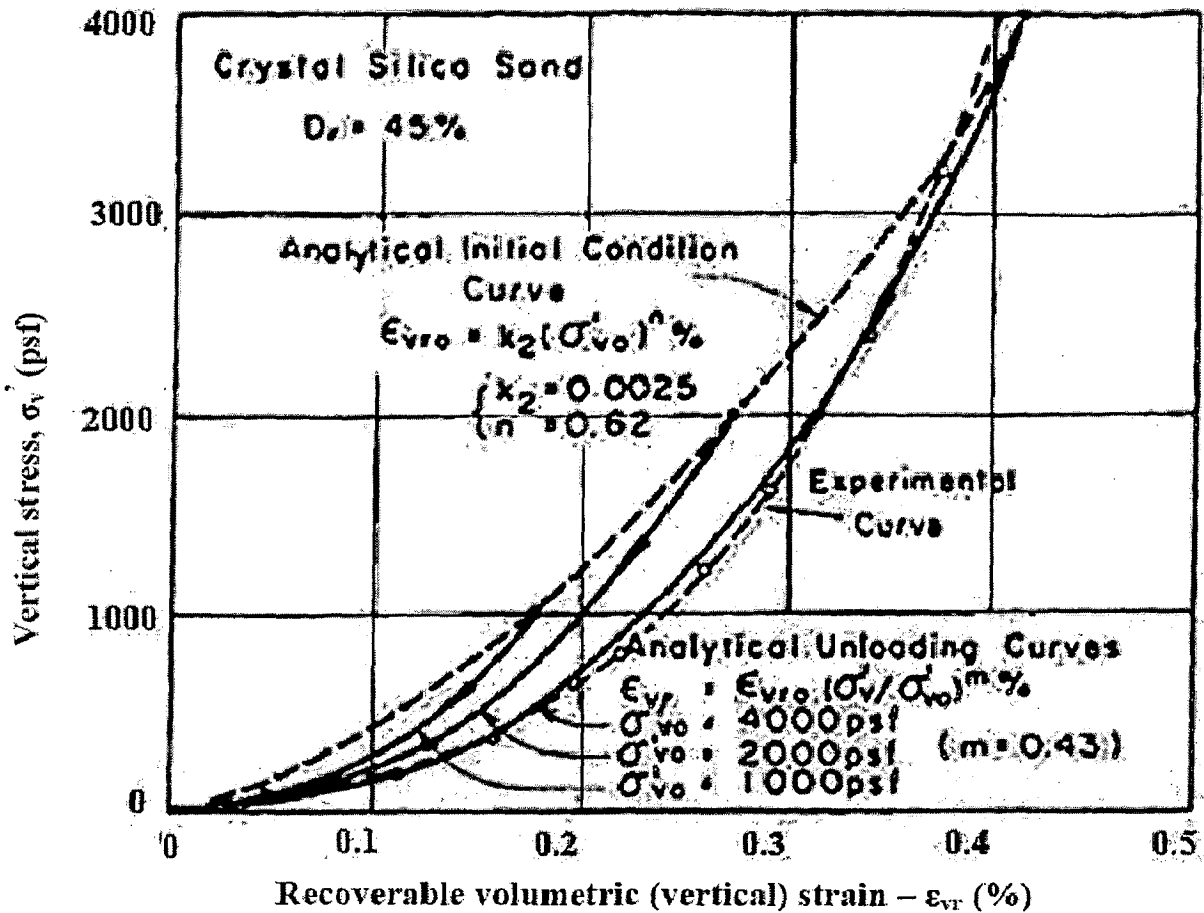
Fig. 2.16 Comparison between Analytical and Experimental One-Dimensional Unloading Curves. (Martin et al. 1975)

c) Kagawa and Kraft (1981) method: A pore pressure generation model solely based on observed pore pressure is presented in the paper. The model is conceptually simple and requires only a limited number of laboratory tests and a few model parameters. All model parameters can be determined from conventional stress controlled, undrained tests employing uniform stress cycles. The model also works well for earthquake type stress variations. An important feature of the model is that it can be used with any non linear dynamic response method that accounts for the time-dependent stiffness degrading effect due to pore pressure build-up in the soil, and it provides a convenient alternative to sophisticated liquefaction models to evaluate the effect of pore pressure generation within soil media.

Assumptions:-

1. Pore pressure generation is due to volume change characteristics.

2. Soil exhibits an identical pore pressure generation in both positive and negative shear stress applications only when the stress histories are the same in both directions and the pore pressure before the stress application are the same.

3. Pore pressure is assumed to develop only in the loading and reloading process.

Pore pressure model: When a potential function for pore pressure build-up, ψ, exists, we can compute the pore pressure increase due to a shear stress change from τ_1 to τ_2 as

$$\frac{\Delta u}{\bar{\sigma}_v} = \int_{|\frac{\tau_1}{\bar{\sigma}_v}|}^{|\frac{\tau_2}{\bar{\sigma}_v}|} \psi(\frac{\tau}{\bar{\sigma}_v}); \quad |\tau_1| \le |\tau_2| \tag{2.6}$$

In which Δu is pore pressure increase, $\bar{\sigma}_v$ is initial effective overburden stress, τ is shear stress. Ψ is considered uniquely determined for a given soil density and a confining pressure following the first assumption and is expressed as

$$\psi = A'[n(N) + f(\frac{u}{\bar{\sigma}_v})] \mid \frac{\tau}{\bar{\sigma}_v} \mid^\beta \tag{2.7}$$

In which A' and β are model parameters. $n(N) =$ memory function that depends on the number of the times a soil element is sheared and $f(\frac{u}{\bar{\sigma}_v}) =$ a function representing the change in the pore pressure generation capability of a soil element caused by an increase in the pore pressure ratio $\frac{u}{\bar{\sigma}_v}$.

Determination of model parameters: Model parameters can be determined by conducting undrained cyclic triaxial tests. When cyclic undrained tests are performed on samples with the same density and confining pressure but for several different stress ratios, the parameter β can be obtained as a function of the number of stress cycles. A method to find β is shown in Fig.2.17. β value typically ranges from 0.0 to 0.3. The model parameter A' is given by

$$A' = \frac{1}{2(\beta+1)(\frac{\tau_d}{\bar{\sigma}_v})^{\beta+1}} \tag{2.8}$$

The pore pressure increase during the N_{th} cycle is given by

$$n(N) = \frac{a}{(a+bN)(a-b+bN)} \tag{2.9}$$

Parameters 'a' and 'b' can be determined using Fig. 2.18. The observed pore pressure increase in the N_{th} cycle in Fig. 2.18 in excess of that in Eq. (2.9) is due to function , $f(\frac{u}{\sigma_v})$.

$$f(\frac{u}{\sigma_v}) = \text{pore pressure increase during } N_{th} \text{ cycle} - n \text{ (N)} \qquad (2.10)$$

d) **Byrne and McIntyre (1994) method:** Byrne and McIntyre (1994) modified Eq. (2.3), and presented the following, simplified, expression for the incremental volumetric strain:

$$\Delta\varepsilon_{vd} = \eta c_1 \exp\left(\frac{-c_2 \varepsilon_{vd}}{\eta}\right) \qquad (2.11)$$

Values of Byrne and McIntyre's constants, C_1 and C_2 are presented in Table 2.1 as a function of relative density and SPT blow count.

The total pore pressure increment, Δu is given by $\Delta u = E'_r . \Delta\varepsilon_{vd}$. E'_r is given by following equation

$$E_r' = \frac{(\frac{\sigma_v'}{P_a})^{1-m}}{m k_2 (\frac{\sigma_{v0}'}{P_a})^{n-m}} \qquad (2.12)$$

where, parameters m, k_2, and n may be obtained from three unloading curves from different initial vertical stresses σ_{v0}'. On the basis of data presented by Martin et al. (1975), and Seed et al.(1978), values of the parameters in Eq. (2.12) were taken as follows: for $D_r = 45\%$; n = 0.62; m = 0.435; and $k_2 = 0.0028$; for $D_r = 60\%$; n = 0.62; m = 0.45 and $k_2 = 0.00167$.

Table 2.1 Byrne and McIntyre's Constants (Byrne and McIntyre, 1994)

$(N_1)_{60}$	D_r (%)	C_1	C_2
5	34	1.00	0.40
10	47	0.50	0.80
20	67	0.20	2.00
30	82	0.12	3.33
40	95	0.06	6.66
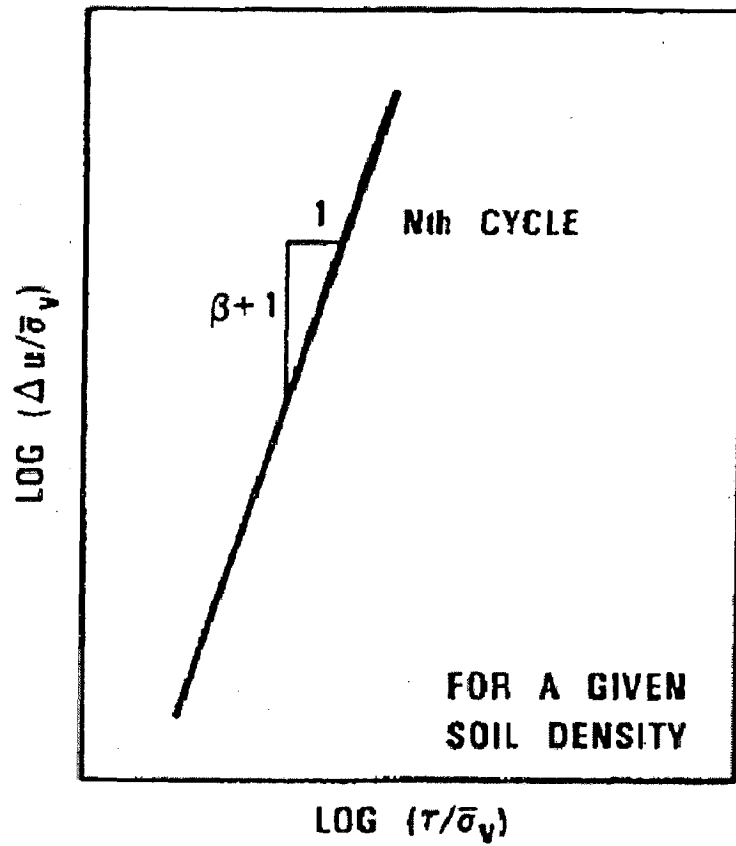
Fig: 2.17 Determination of Parameter β (Kagawa and Kraft, 1981)
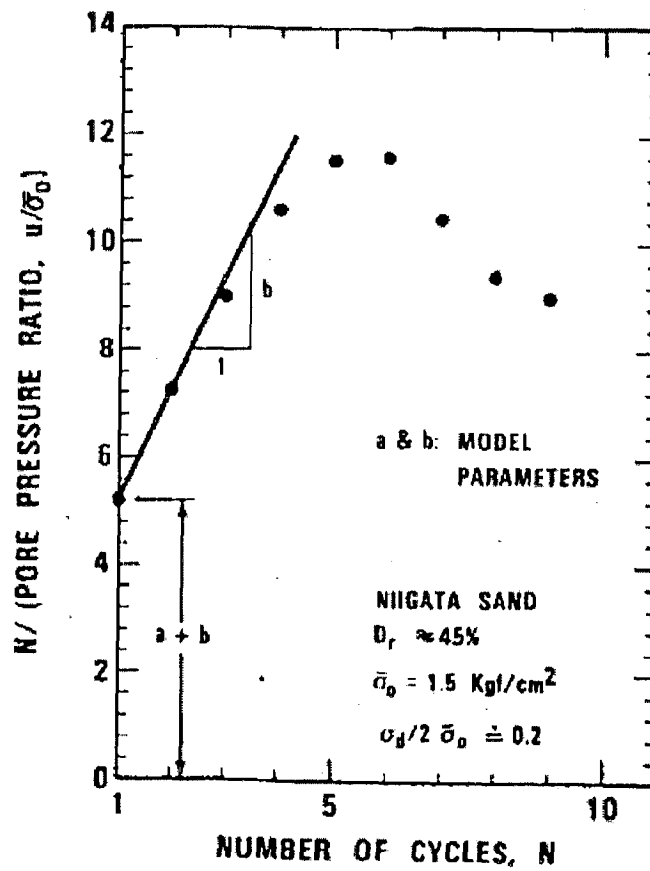
Fig. 2.18 Determination of 'a' and 'b' (Kagawa and Kraft, 1981)

2.2.2 Evaluation of Liquefaction Potential

Evaluation of resistance of the soil to liquefaction is an important aspect of geotechnical engineering practice. A methodology termed the "simplified procedure' has been evolved as a standard of practice for evaluating the liquefaction resistance of soils over the past 38 years. Seed and Idriss (1971) developed and published the basic "simplified procedure" after the disastrous earthquakes in Alaska and Niigata, Japan in 1964. Since then, it has been modified and improved periodically, mainly by papers by Seed (1979), Seed and Idriss (1982), and Seed et al. (1985). In 1985, on behalf of National Research Council, Professor Robert V. Whitman convened a workshop in which 36 experts reviewed the state of art of evaluating liquefaction potential. In 1996, Youd and Idriss convened a workshop of 20 experts to update the "simplified procedure" based on the research done during the past decade. The workshop discussed several field tests which gained common usage for the evaluation of liquefaction resistance such as standard penetration test (SPT), cone penetration test(CPT), shear wave velocity measurements(V_s) and the Becker penetration test (BPT). SPT and BPT are preferred generally because of the more extensive database and past experience (Youd et al., 2001). The procedure based on SPT proposed by the Workshop is adopted for the present study and is explained in section 3.1. Idriss and Boulanger (2006) presented an update for the semi-empirical field-based procedures that are used to evaluate the liquefaction potential. They re-examined the existing procedures and revised relations were proposed.

Gupta and Sharma (1977) reported that Seed and Idriss (1967, 1971) method did not give consideration to the progressive development of liquefaction and spreading of liquefying zone. Also they observed that dense sand liquefy to large extend when analysed using Seed and Idriss (1971) procedure. But from Shake table studies conducted by Gupta and Prakash (1977) observed that sand may not liquefy if relative density is greater than 65% (i.e. dense sand). Gupta and Prakash (1986) proposed that Vibration table studies can be considered to represent the field condition with sufficient degree of confidence.

2.3 LATERAL RESPONSE OF PILES

Pile foundations are frequently subjected to lateral loads in harbour and off shore structures, transmission tower structures, pile supported earth retaining structures and structures in earthquake prone areas. In the design of pile foundations against lateral

loading, two criteria must be satisfied: 1) the pile must have an adequate factor of safety against the maximum lateral loading that might be applied to it, and 2) the deflection that occurs due to a working load must be in an acceptable range that superstructure can withstand (Poulos and Davis, 1980). In liquefiable soils, piles should be designed for lateral loads neglecting lateral resistance of soil layers liable to liquefy. IS 1893 (Part 1, 2002).

Several analytical methods have been proposed to model lateral pile response, none of which can completely account for all factors that influence lateral soil-pile interaction. They include the Elastic Continuum approach, Subgrade Reaction Approach and the concept of p-y curves and the Finite element Method.

2.3.1 Elastic Continuum Approach

The Elastic Continuum using Boundary Element method was widely used to analyze the lateral response of pile between 1960 and 1980. This solution was used by many researchers (e.g., Spillers and Stoll (1964), Poulos (1971), Banerjee and Davies (1978) and Davies and Budhu (1986)) to analyze the response of a pile subjected to lateral loading. All of these analyses are similar in principle; the differences arising largely from details in the assumptions regarding the pile action. The main advantage of this approach is that continuity of soil is taken into account. But it is having number of disadvantages also. The main being, soil is assumed to be homogenous, isotropic and semi infinite, but in reality soil is irregular and Poisson's ratio and Young's modulus changes with depth. To account for this several researchers have proposed solutions for varying soil profiles. Poulos (1973) and Banerjee and Davies (1978) proposed solutions for a layered soil. Banerjee and Davies (1978), and Budhu and Davies (1988) provided solutions for soil with linearly increasing soil modulus with depth. Elastic Continuum using Modified Boundary Element method was proposed to account for soil yielding by incorporating an elasto-plastic soil model. Davies and Budhu (1986) developed a method to predict the behavior of a laterally loaded pile by taking into account soil and pile yielding.

2.3.2 Subgrade Reaction Approach

The subgrade reaction method currently appears to be the most widely used in a design of laterally loaded piles. The method was first introduced by Winkler in 1867 to analyze the response of beams on an elastic subgrade by characterizing the soil as a series of independent linearly-elastic soil springs. The greatest advantage of this method over the

elastic continuum approach is that the idea can be easily programmed using Finite difference or Finite element methods (Juirnarongrit and Ashford. 2005). The soil non-linearity and multiple soil layers can be taken into account. Also for dynamic analysis, this method seems to be easier. The main disadvantage is the lack of continuity, since real soils are to some extent continuous. Barber (1953) developed the solutions to determine the deflections and rotation at the ground surface for cases of constant soil modulus of subgrade reaction, as well as the linearly increasing soil modulus of subgrade reaction with depth. Matlock and Reese (1960) provided the solutions for a soil profile where the modulus of subgrade reaction has some finite value at the ground surface and continues to increase linearly with depth. Davisson and Gill (1963) used the subgrade reaction theory to analyze the behavior of laterally loaded piles in a two-layer soil system for both free and fixed head conditions and provided the results in non-dimensional forms. Ramasamy (1974) used the subgrade reaction theory to study the flexural behavior of axially and laterally loaded piles.

In order to account for soil non-linearity, the linear soil springs are replaced with a series of nonlinear soil springs, which represent the soil resistance-deflection curve so called, "p-y" curve. The p-y curves of the soil have been developed based on the back analysis of the full scale lateral pile load test. Another advantage of p-y curves is that, the error due to soil continuity can be overcome through calibrating p-y curves to full-scale test results. Several researchers have worked on the concept of p-y curves. (e.g., Matlock (1970), Reese et al. (1974), Reese and Welch (1975), Reese et al. (1975), and Ismael (1990)).

Novak (1974) was the first to use a Winkler model for the representation of laterally loaded pile in visco-elastic medium. Winkler type models for seismic analysis of piles in liquefiable soils have been developed by Kagawa (1992), Yao and Nogami (1994), Fujii et al. (1998) and Liyanapathirana and Poulos (2005a). Wilson et al. (2000) presented the first measurements of dynamic p-y behavior for liquefying sand. Boulengar et al. (2003) observed that the subgrade reaction against a pile in liquefying soil is dependent on the excess pore pressures throughout the soil, both near the pile and away from the pile. Liyanapathirana and Poulos (2005a) presented a method to determine the non linear spring constants of Winkler model based on Mindlin's equation. The spring coefficient in the spring dashpot model gets degraded with the amount of pore pressure development. Liyanapathirana and poulos (2005b) presented a pseudostatic approach for pile analysis in

liquefiable soils. Nath (2006) used Winkler model to study the pile soil interaction for axially and laterally loaded piles in liquefiable soils.

2.3.3 Finite Element Method

This method is being extensively used now a day because of the availability of computational power of computers. Also this method can incorporate soil non-linearity as well as soil continuity. This method is the most powerful because, most of the aspects which other methods cannot investigate such as, the stress and strain in the soil mass, the influence of gapping, and the effect of construction sequencing can be studied using this. However the efficiency of this method still depends upon the ability to predict the soil properties and also the accuracy of constitutive soil models. Another disadvantage is the high computation time required especially for $3 - D$ analysis. Several researchers have used Finite element to solve the problem of lateral analysis of piles. A 3-D finite element solution for the laterally loaded pile problem was developed by Desai and Appel (1976). Kooijman (1989) and Brown et al. (1989) used three-dimensional finite elements to develop *p-y* curves. Bransby (1999) implemented a 2-D finite element analysis to find load-transfer relationships for laterally loaded pile and suggested that these curves could be used as *p-y* curves in the analysis of laterally loaded piles.

Finn and Thavaraj (2001) validated their 3-D soil-water coupled analysis method for the results of shaking table tests with group-piles in liquefiable ground under gravitational and centrifugal field. Uzoka et al. (2007) simulated the process of damage to a pile foundation located in reclaimed land with 3 D soil-water-coupled analysis using soil-pile-building model.

29

NUMERICAL MODELING AND FORMULATION FOR LIQUEFACTION

Liquefaction is the phenomenon of transformation of a granular material from a solid to a liquefied state as a consequence of increased pore-water pressure and reduced effective stress. This change occurs most readily in loose to moderately dense granular soils with poor drainage, such as silty sands or sands and gravel containing seams of impermeable sediment. Under earthquake shaking, soil layers may lose its shear strength fully or partially depending up on the amount of excess pore pressure generated. The loss of complete shear strength of soil is termed complete liquefaction. In case of complete liquefaction the effective stress, σ_v' reduces to zero. The soils which lose its strength partially will be referred as partially liquefied soil in this study. For partial liquefaction case, σ_v' will be greater than zero but less than the static effective stress. Complete and partial liquefaction are assessed through the modified 'Simplified Procedure' by Youd et al. (2001). This procedure was first suggested by Seed and Idriss (1971). The excess pore pressure generated in the case of fully liquefiable soil will be greater than or equal to the effective stress under static condition. So the net effective stress will be zero. For partially liquefied soil, excess pore water pressure is generated but is less than the static effective stress. This excess pore pressure generated is estimated adopting the procedure given by Seed et al. (1976).

3.1 EVALUATION OF LIQUEFACTION

The Factor of safety (FS) against liquefaction is evaluated as (Youd et al. 2001)

$$FS = (CRR_{7.5}/CSR)*MSF \qquad (3.1)$$

Where

$CRR_{7.5}$ – Cyclic Resistance ratio at Earthquake Magnitude of 7.5. It is the capacity of soil to resist liquefaction or the cyclic stress required to generate liquefaction for earthquake magnitude 7.5.

CSR – Cyclic Stress Ratio. It is the seismic demand on a soil layer or the cyclic shear stress generated by the earthquake shaking.

MSF – Magnitude Scaling Factor. The methods available to estimate the CRR values are applicable to earthquakes of magnitude 7.5. In order to adjust the values to magnitude smaller or larger than 7.5, Seed and Idriss (1982) introduced this correction factor.

Thus evaluation of liquefaction requires estimation of CRR and CSR.

3.1.1 Estimation of CSR

Seed and Idriss (1971) formulated the following equation for calculation of the cyclic stress ratio.

$$CSR = \left(\frac{\tau_{av}}{\sigma'_{v0}}\right) = 0.65 \left(\frac{a_{max}}{g}\right) \left(\frac{\sigma_{v0}}{\sigma'_{v0}}\right) r_d \qquad (3.2)$$

Where a_{max} = peak horizontal acceleration at the ground surface generated by the earthquake.

g = acceleration due to gravity

σ_{v0} and σ_{v0}' are total and effective vertical overburden stresses at the depth considered respectively and

r_d = stress reduction coefficient which accounts for flexibility of the soil profile (Fig. 3.1).

τ_{av} = average cyclic shear stress

In cyclic stress approach, the basic assumption is that excess pore pressure generation is fundamentally related to cyclic shear stresses, hence the seismic loading is expressed in terms of cyclic shear stresses. The seismic loading can be predicted in two ways: by a detailed ground response analysis or by using a simplified approach (Kramer, 1996). In this study simplified approach is adopted as shown in Eq. 3.2. Here τ_{av} is taken as 0.65 times peak cyclic shear stress, τ_{max}.

Stress reduction coefficient (r_d): For routine practice and non critical projects, the average values of r_d as given by following equations (Liao and Whitman, 1986) may be adopted.

$$r_d = 1.0 - 0.00765z \quad \text{for } z \leq 9.15 \text{ m} \qquad (3.3a)$$

$$r_d = 1.174 - 0.0267z \quad \text{for } 9.15 \text{ m} < z \leq 23 \text{ m} \qquad (3.3b)$$

Where z is the depth below the ground in meters

Values of r_d calculated from Eq. 3.3a and 3.3b are plotted in Fig. 3.1, along with the mean and range of values proposed by Seed and Idriss (1971).

For ease of computation, the mean curve plotted in Fig. 3.1 may also be approximated by the following equation (Youd et al. 2001).

$$r_d = \frac{1.0-0.4113*z^{0.5}+0.04052*z+0.001753*z^{1.5}}{1.0-0.4177*z^{0.5}+0.05729z-.006205*z^{1.5}+0.001210*z^2} \qquad (3.3c)$$

Eq. (3.3c) yields essentially the same values for r_d as (Eq. 3.3a and Eq. 3.3b), but is easier to program and can be used in routine engineering practice.
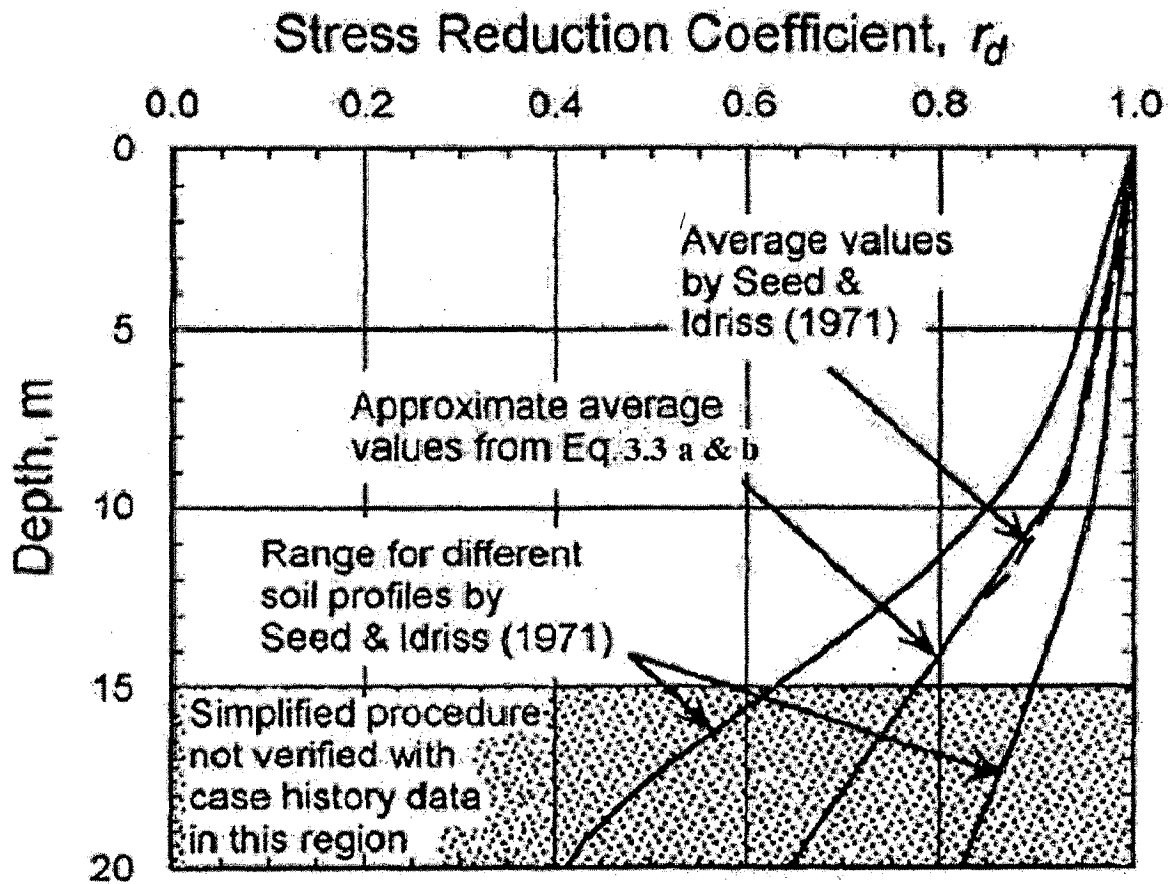
Fig. 3.1. r_d versus Depth Curves Developed by Seed and Idriss (1971) with Added Mean-value Lines. (Youd et al. 2001)

Evaluation of a_{max}: The preferred method for estimating a_{max} is through empirical correlations of a_{max} with earthquake magnitude, distance from the seismic energy source, and local site conditions. For soft sites and other soil profiles where these attenuation relationships are not compatible, a_{max} can be estimated by local site response analyses (Youd et al. 2001). Also value of a_{max} is calculated based on location of site in different seismic zones.

Equation for estimating the median peak acceleration at soft soil sites were given by following equations (Idriss, 1991) and also shown in Fig. 3.2.

For M ≤ 6

$$Ln\,(a_g) = \exp(1.673 - 0.137 * M) - \exp(1.285 - 0.206 * M) * Ln(R + 20) \quad (3.4a)$$

For M > 6

$$Ln\,(a_g) = \exp(2.952 - 0.350 * M) - \exp(2.015 - 0.328 * M) * Ln(R + 20) \quad (3.4b)$$

Where, M = earthquake magnitude.

R = closest distance to the source in km.

Also a number of intensity-acceleration relationships have been proposed as shown in Fig. 3.3 (Kramer, 1996).

3.1.2 Estimation of CRR

A plausible method for evaluating CRR is to retrieve and test undisturbed soil specimens in the laboratory. Unfortunately, in situ stress states generally cannot be re-established in the laboratory, and specimens of granular soils retrieved with typical drilling and sampling techniques are too disturbed to yield meaningful results. To avoid the difficulties associated with sampling and laboratory testing, field tests have become the state-of-practice for routine liquefaction investigations. Several field tests have gained common usage for evaluation of liquefaction resistance, including the standard penetration test (SPT), the cone penetration test (CPT) and shear-wave velocity measurements (Vs). SPT and CPT are generally preferred because of the more extensive database and past experience, but the other tests may be applied at sites underlain by gravelly sediment or where access by large equipment is limited (Youd et al. 2001). Primary advantages and disadvantages of each test are listed in Table 3.1.

CRR based on SPT: Criteria for evaluation of liquefaction resistance based on the SPT have been rather robust over the years. Those criteria are embodied in the CRR versus $(N_1)_{60}$ plot as shown in Fig. 3.4. $(N_1)_{60}$ is the SPT blow count normalized to an overburden pressure of approximately 100 kPa (1 ton/sq ft) and a hammer energy ratio or hammer efficiency of 60%. Fig. 3.4 is a graph of calculated CRR and corresponding $(N_1)_{60}$ data from sites where liquefaction effects were or were not observed following past earthquakes with magnitudes of approximately 7.5.
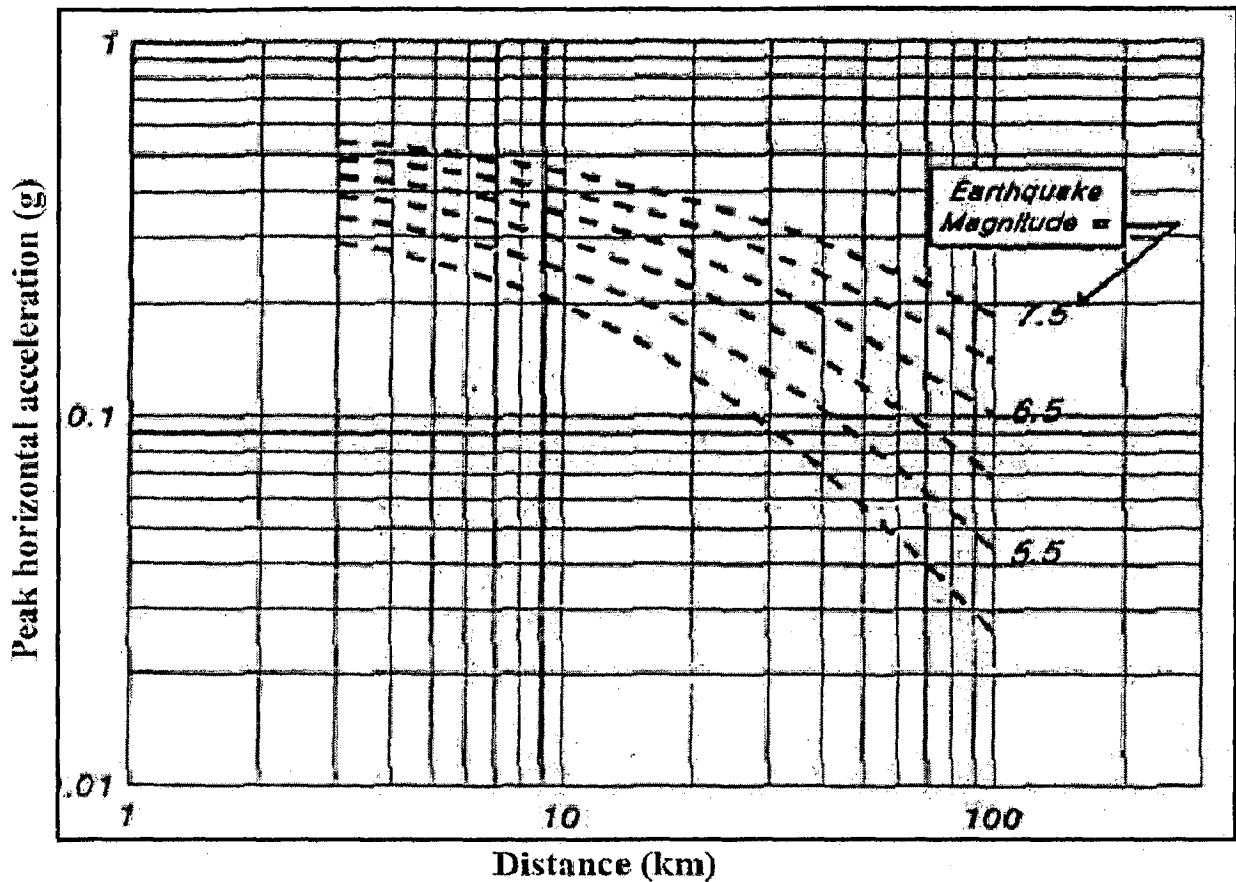
Fig. 3.2 Median Peak Horizontal Acceleration at Soft Soil Sites (Idriss, 1991).
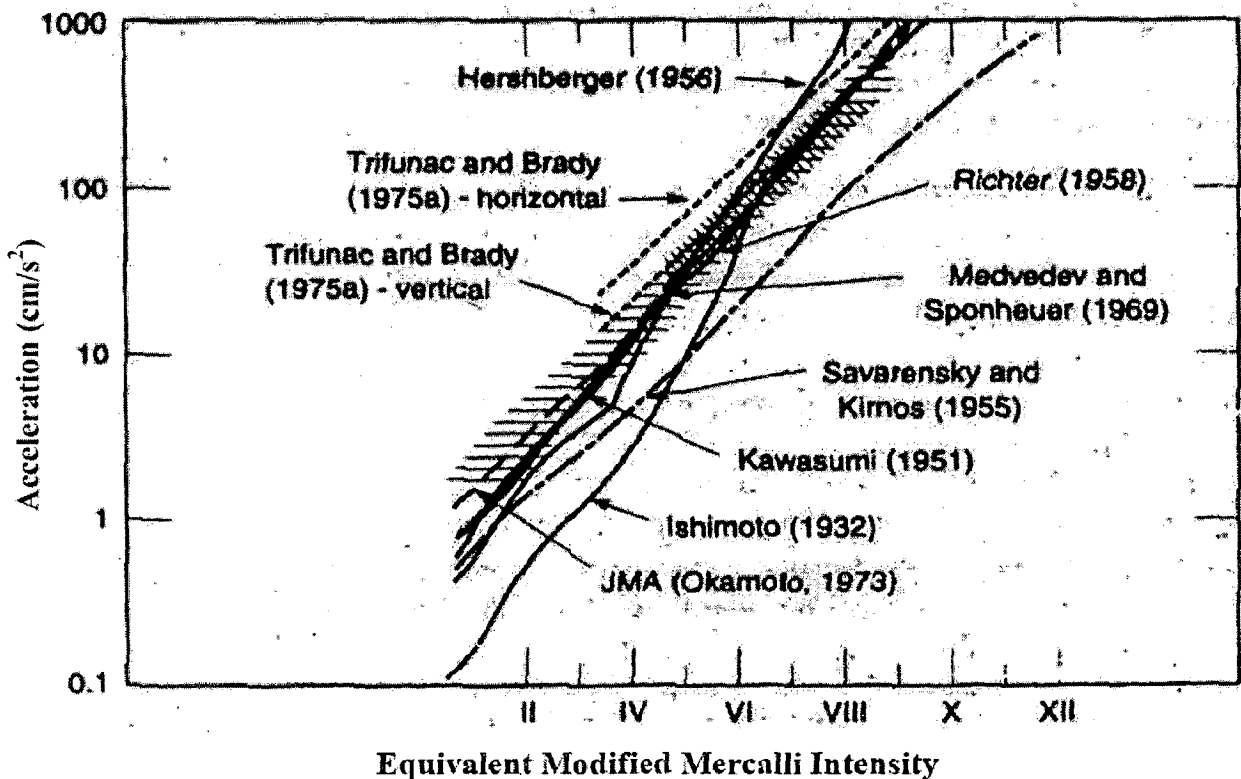
Fig. 3.3 Proposed Relation between Peak Horizontal Acceleration and Modified Mercalli intensity (Kramer, 1996)

34

Table 3.1 Comparison of Advantages and Disadvantages of Various Field Tests for Assessment of Liquefaction Resistance. (Youd et al. 2001)

Feature	Test type		
	SPT	CPT	V_S
Past measurements at liquefaction sites	Abundant	Abundant	Limited
Type of stress-strain behaviour influencing test	large strain	large strain	Small strain
Quality control and repeatability	Poor to good	Very good	Good
Detection of variability soil deposits	Good for closely spaced tests	Very good	Fair
Soil types in which test is recommended	Non-gravel, Sand, Cohesionless	Non-gravel	All
Soil sample retrieved	Yes	No	No
Test measures index or engineering property	Index	Index	Engineering

The SPT values are affected by several factors. Correction should be applied to the values before use. Equation given below incorporates these corrections.

$$(N_1)_{60} = N_m C_N C_E C_B C_R C_S \tag{3.5}$$

Where N_m = measured standard penetration resistance

C_N = factor to normalize Nm to a common reference effective overburden stress

C_E = correction for hammer energy ratio (ER)

C_B = correction factor for borehole diameter

C_R = correction factor for rod length and

C_S = correction for samplers with or without liners.

Corrections to be applied are as shown in the Table 3.2. In addition to these, fines content and grain characteristics also influence SPT results.
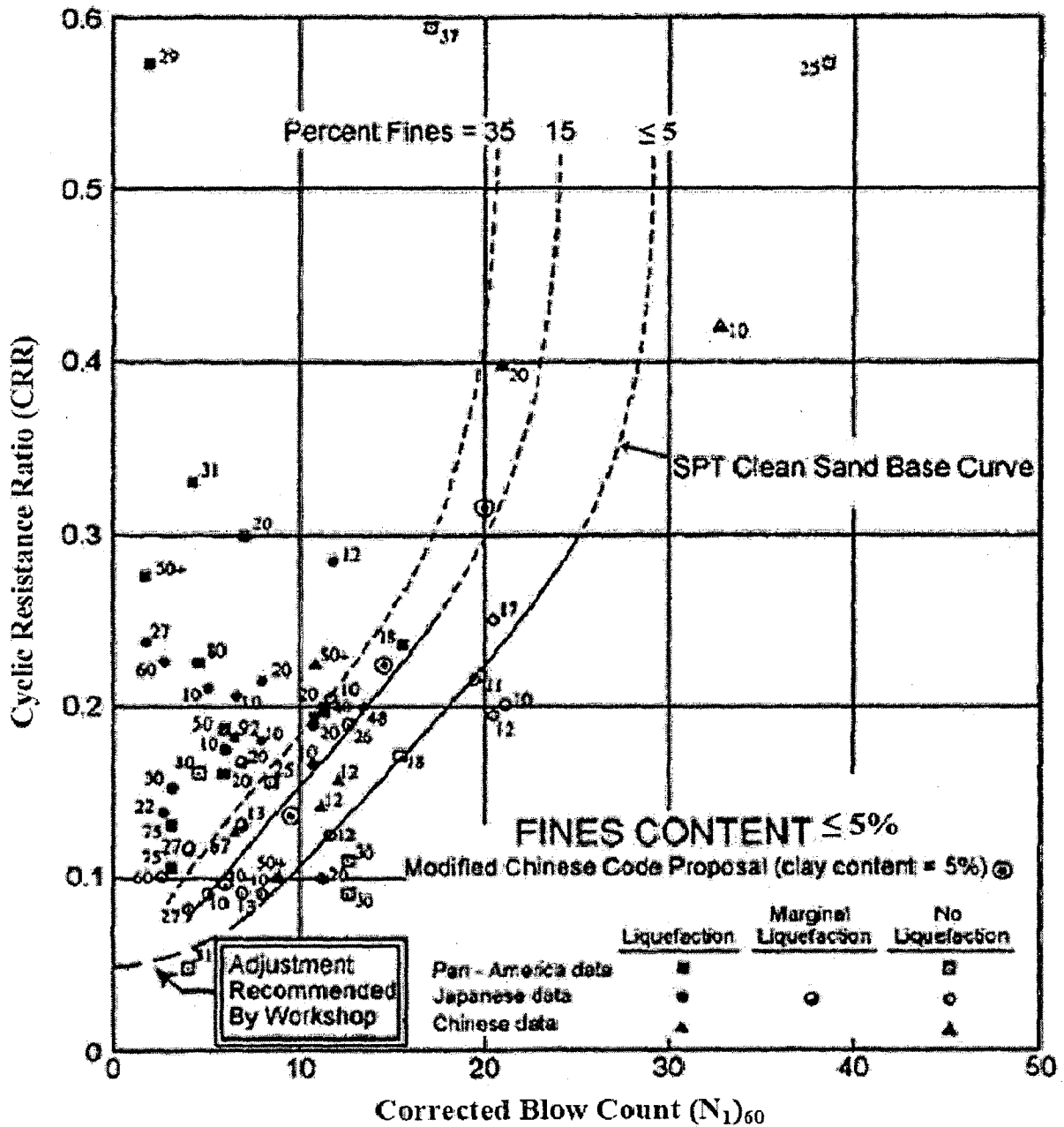
FIG. 3.4 SPT Curve for Magnitude 7.5 Earthquakes with Data from Liquefaction Case Histories (Youd et al. 2001)

The SPT N-values increase with increasing effective overburden stress. Therefore an overburden correction factor is applied, which is calculated from either of following two equations proposed by Liao and Whitman (1986) and Kayen et al. (1992) respectively.

$$C_N = \left(\frac{P_a}{\sigma'_{vo}}\right)^{0.5} \tag{3.6a}$$

$$C_N = \frac{2.2}{1.2 + \frac{\sigma'_{vo}}{P_a}} \tag{3.6b}$$

Where C_N normalizes N_m to an effective overburden pressure σ_{v0}' of approximately 100 kPa. i.e. $P_a = 100$ kPa =1 atmospheric pressure. The maximum value of C_N is limited to 1.7. Eq. 3.6b provides a better fit for pressures up to 300 kPa (Youd et al. 2001).

Table 3.2 Corrections to SPT N Values (Youd et al. 2001)

Factor	Equipment variable	Term	Correction
Overburden pressure	-	C_N	$\left(\dfrac{P_a}{\sigma_{v0}'}\right)^{0.5}$
Overburden pressure	-	C_N	$C_N \leq 1.7$
Energy ratio	Donut hammer	C_E	0.5-1.0
Energy ratio	Safety hammer	C_E	0.7-1.2
Energy ratio	Automatic-trip Donut-type hammer	C_E	0.8-1.3
Borehole diameter	65-115mm	C_B	1.0
Borehole diameter	150mm	C_B	1.05
Borehole diameter	200mm	C_B	1.15
Rod length	< 3m	C_R	0.75
Rod length	3-4m	C_R	0.8
Rod length	4-6m	C_R	0.85
Rod length	6-10m	C_R	0.95
Rod length	10-30m	C_R	1.0
Sampling method	Standard sampler	C_S	1.0
Sampling method	Sampler with liners	C_S	1.1-1.3

For liquefaction resistance calculations and rod lengths < 3 m, a C_R of 0.75 should be applied as was done by Seed et al. (1985) in formulating the simplified procedure. Although application of rod-length correction factors listed in Table 3.2 will give more precise $(N_1)_{60}$ values, these corrections may be neglected for liquefaction resistance calculations for rod lengths between 3 and 10 m because rod-length corrections were not applied to SPT test data from these depths in compiling the original liquefaction case history databases. Thus rod-length corrections are implicitly incorporated into the empirical SPT procedure (Youd et al. 2001).

The $(N_1)_{60}$ values obtained after these corrections can be used to determine the CRR values from the graph given in Fig. 3.4. CRR curves on this graph were conservatively positioned to separate regions with data indicative of liquefaction from regions with data indicative of non-liquefaction. Curves were developed for granular soils with the fines

contents of 5% or less, 15%, and 35% as shown on the plot. The CRR curve for fines contents <5% is the basic penetration criterion for the simplified procedure and is referred as the "SPT clean sand base curve." The CRR curves in Fig. 3.4 are valid only for magnitude 7.5 earthquakes.

Influence of Fines Content: Seed et al. (1985) noted an apparent increase of CRR with increased fines content. Eq. (3.7), Eq. (3.8) and Eq. (3.9) give approximate corrections for the influence of fines content (FC) on CRR. Other grain characteristics, such as soil plasticity, may affect liquefaction resistance as well as fines content, but widely accepted corrections for these factors have not been developed. Hence corrections based solely on fines content should be used with engineering judgment and caution.

The following equations (Youd et al. 2001) were developed by Idriss and Seed for correction of $(N_1)_{60}$ to an equivalent clean sand value, $(N_1)_{60cs}$.

$$(N_1)_{60cs} = \theta + \omega \, (N_1)_{60} \tag{3.7}$$

Where α and β = coefficients determined from the following relationships:

$$\theta = 0 \qquad\qquad \text{for FC} \leq 5\% \tag{3.8a}$$

$$\theta = \exp\left[1.76 - (190/FC^2)\right] \qquad \text{for } 5\% < FC < 35\% \tag{3.8b}$$

$$\theta = 5.0 \qquad\qquad \text{for FC} \geq 35\% \tag{3.8c}$$

$$\omega = 1.0 \qquad\qquad \text{for FC} \leq 5\% \tag{3.9a}$$

$$\omega = [0.99 + (FC^{1.5}/1000)] \qquad \text{for } 5\% < FC < 35\% \tag{3.9b}$$

$$\omega = 1.2 \qquad\qquad \text{for FC} \geq 35\% \tag{3.9c}$$

These equations may be used for routine liquefaction resistance calculations. A back-calculated curve for a fines content of 35% is essentially congruent with the 35% curve plotted in Fig. 3.4. The back-calculated curve for a fines content of 15% plots to the right of the original 15% curve.

Idriss and Boulanger (2006) gave a simpler equation for the correction as follows.

$$(N_1)_{60cs} = (N_1)_{60} + \Delta(N_1)_{60} \tag{3.10a}$$

$$\Delta(N_1)_{60} = \exp\left(1.63 + \frac{9.7}{FC+0.1} - \left(\frac{15.7}{FC+0.1}\right)^2\right) \tag{3.10b}$$

Where FC is fines content in percentage.

The clean-sand base curve plotted in Fig. 3.4 is approximately given by the following equation (Youd et al. 2001).

$$CRR_{7.5} = \frac{1}{34 - (N_1)_{60cs}} + \frac{(N_1)_{60cs}}{135} + \frac{50}{[10(N_1)_{60cs} + 45]^2} - \frac{1}{200} \qquad (3.11)$$

Equation (3.11) is valid for $(N_1)_{60cs} < 30$. For $(N_1)_{60cs} \geq 30$, clean granular soils are too dense to liquefy and are classified as non-liquefiable. Eq. 3.11 may be used in spreadsheets and other analytical techniques to approximate the clean-sand base curve for routine engineering calculations.

Magnitude Scaling Factor (MSF): The clean-sand base or CRR curves in Fig. 3.4 apply only to magnitude 7.5 earthquakes. To adjust the clean-sand curves to magnitudes smaller or larger than 7.5, Seed and Idriss (1982) introduced correction factors termed "magnitude scaling factors (MSFs)." These factors are used to scale the CRR base curves upward or downward on CRR versus $(N_1)_{60}$ plots.

Many investigators have suggested MSF values as shown in Fig. 3.5. For $M < 7.5$, the lower and upper bound values are given, respectively by equations (3.12a) and (3.12b) respectively.

$$MSF = \frac{10^{2.24}}{M^{2.56}} \qquad (3.12a)$$

$$MSF = \left(\frac{M}{7.5}\right)^{-2.56} \qquad (3.12b)$$

where M is the earthquake magnitude.

Eq. 3.12a was proposed by I M Idriss in 1995 during Seed Memorial Lecture. Eq. 3.12b was qiven by Andrus and Stokoe (1997). The MSF values from Eq. 3.12a may be used in engineering practice as this provides a conservative estimate of Factor of Safety against liquefaction (Youd et al. 2001).

3.1.3 Steps to evaluate Factor of Safety

1. Estimate CSR

   a) Calculate r_d using Eq. 3.3c or Fig. 3.1.

   b) Calculate a_{max} from Fig. 3.2 or given based on Earthquake records or seismic zone.

c) Determine the value of total and effective stresses at the point where CSR is to be estimated.

d) Obtain CSR from Eq. 3.2.

2. Estimation of $CRR_{7.5}$

a) Apply corrections to obtain $(N_1)_{60}$ from N_m using the values given in Table. 3.2. For C_N correction, use Eq. 3.6b.

b) Apply the correction of fines to $(N_1)_{60}$ using Eq. 3.10a and Eq. 3.10b to get $(N_1)_{60cs}$.

c) Calculate $CRR_{7.5}$ from Eq. 3.11

3. Compute MSF using Eq. 3.12a.

4. Compute Factor of safety from Eq. 3.1.
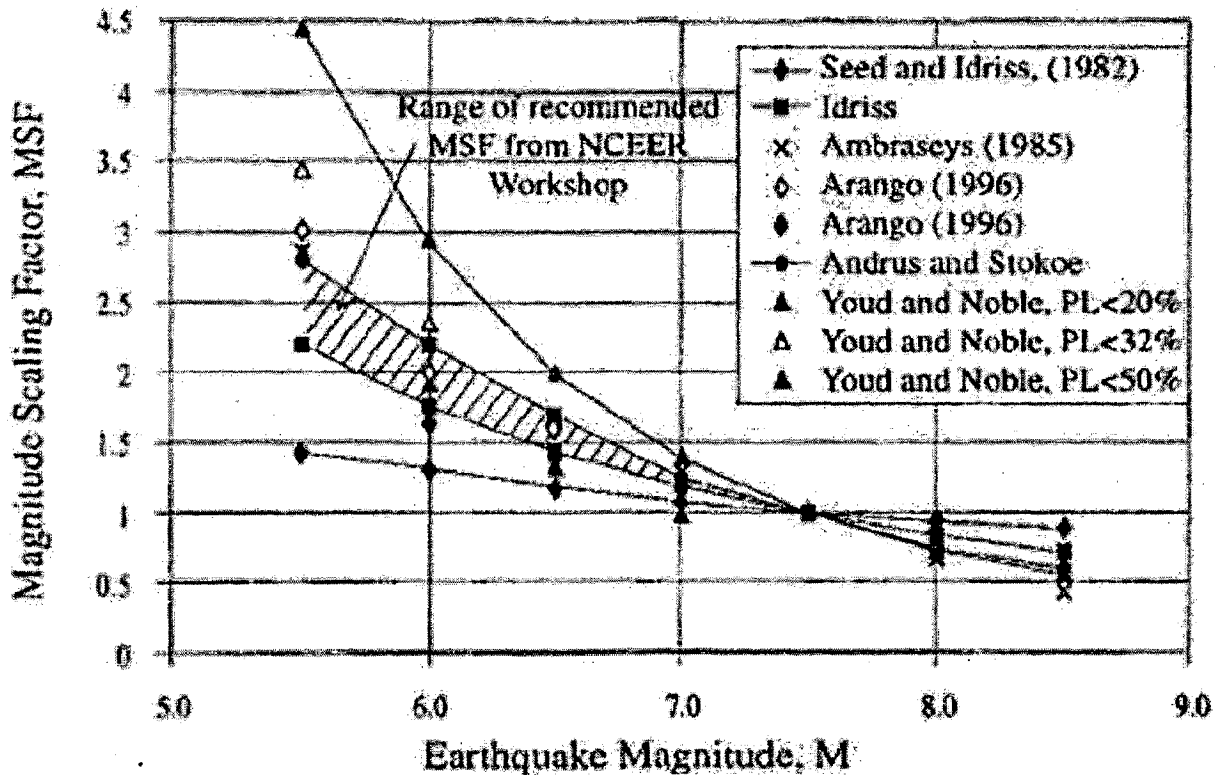
Fig. 3.5. Magnitude Scaling Factors Derived by Various Investigators

(Youd et al. 2001)

3.2 EVALUATION OF GENERATION OF PORE WATER PRESSURE

In recent years much progress has been made in developing procedures for evaluating generation of pore pressure during earthquake shaking. Several pore pressure generation models are available in literature. Some of them are Seed et al. (1976), Finn et al. (1977),

Kagawa and Kraft (1981), Byrne (1991), Byrne and McIntyre (1994) etc. The adopted Seed et al. (1976) method involves both generation and dissipation of pore water pressure. In the present study only pore pressure generation is estimated and dissipation is neglected.

The procedure is as explained below. (Seed et al. 1976)

1. Determine the equivalent number of uniform stress cycles, N_{eq}, and the effective period of each stress cycle, T_{eq}, representing the induced stress history. Corresponding values of N_{eq} and shaking duration for different earthquakes are given in Table 3.3.

Table 3.3 Earthquake magnitude and the corresponding values of N_{eq} and shaking duration (Seed et al. 1976).

Earthquake magnitude	N_{eq}	Duration of strong shaking in seconds
5.5 – 6	5	8
6.5	8	14
7	12	20
7.5	20	40
8	30	60

2. Using ratio $CSR/CRR_{7.5}$ Determine from Fig. 3.6, the number of stress cycles required to produce a condition of initial liquefaction (N_L) for different depths in the deposit.

   Fig: 3.6 give the normalized curve for CSR versus N_L obtained by conducting Cyclic Triaxial tests on 13 sand samples (Jefferies and Bean, 2006). Here the CSR value is normalized by the cyclic resistance ratio at an earthquake magnitude 7.5, which is nothing but $CRR_{7.5}$ given by Eq. 3.11. So find CSR and $CRR_{7.5}$ by 'Simplified Procedure' explained in section 3.1. Then read from Fig. 3.6, the value of N_L.

3. From the known values of N_{eq}/N_L at various depths, the rate of pore pressure build-up, $\dfrac{\partial U_g}{\partial t}$ is determined as follows. For each elemental layer of the deposit, assuming it undrained, find pore water pressure r_u using curve from data as shown in Fig. 3.7 or represented by equation (3.14a) or (3.14b).

$$r_N = [\tfrac{1}{2}(1 - cos\pi r_u)]^{\propto}$$ (3.13a)

$$r_u = \tfrac{1}{2} + \tfrac{1}{\pi} arc\ sin(2r_N^{1/\alpha} - 1)$$ (3.13b)

Where α = a function of soil properties and test conditions. A value of α = 0.7 provides a best fit as shown by dotted lines in Fig. 3.7. r_n and r_u are given by the equations below.

$$r_N = N/N_L$$ (3.14a)

$$r_u = u_g/\sigma_{v0}{}'$$ (3.14b)

where N = number of applied stress cycles.

The rate of pore pressure generation $q = \dfrac{\partial U_g}{\partial t}$, may be approximated by expression

$$q = \frac{u_g - u_0}{\Delta t}$$ (3.15)

where u_0 = the excess pore water pressure at time t_0

u_g = the excess pore pressure that would develop at time $t_1 = t_0 + \Delta t$, if system is undrained.

Δt = Time increment

a) At time $t_0 = 0$, $u_0 = 0$, the pore pressure ratio, r_u is equal to zero. From Fig. 3.7 the value of equivalent undrained cyclic ratio, $r_{N0} = 0$, then at time $(t_0 + \Delta t)$, the value of cyclic ratio if system were undrained would be

$$\overline{r}_{N1} = r_{N0} + \Delta r_N$$ (3.16a)

Where Δr_N= the increase in cyclic ratio for undrained conditions over the time increment, Δt.

b) Δr_N is defined by

$$\Delta r_N = \frac{\Delta N}{N_L}$$ (3.16b)

ΔN = the fraction of equivalent cycle occurring in the time increment, Δt,

N_L = number of cycles required to cause liquefaction under undrained conditions at stress level, τ_{eq}.

Accordingly, $\quad \Delta N = \dfrac{\Delta t}{T} N_{eq}$ (3.16c)

Where T= duration of strong earthquake shaking as given in Table 3.3 for different earthquake magnitudes.

Substituting Eq. 3.16c in Eq. 3.16b, it becomes

$$\Delta r_N = \frac{\Delta t}{T} \frac{N_{eq}}{N_L}$$ (3.16d)

c) Having obtained Δr_N in this way, $\bar{r}_{N1}$ may be determined from Eq. (3.16a) and u_g from Eq. (3.13b) with $r_N = \bar{r}_{N1}$ and $r_u = u_g/\sigma_{v0}$.

d) By repeating step 'c' for the next time increments (t = 2Δt, 3Δt, 4Δt etc.) with newly obtained values of r_{N0} ($r_{N0} = \bar{r}_{N1}$ of previous step), we can obtain u_g at different time increments. Continue the cyclic process and find the pore pressure generated at the end of t = T seconds. It will be the pore pressure generated at the end of earthquake shaking.

4. Repeating step 3 for different depths, the pore pressure generated due to earthquake shaking is determined at all the required soil depths.
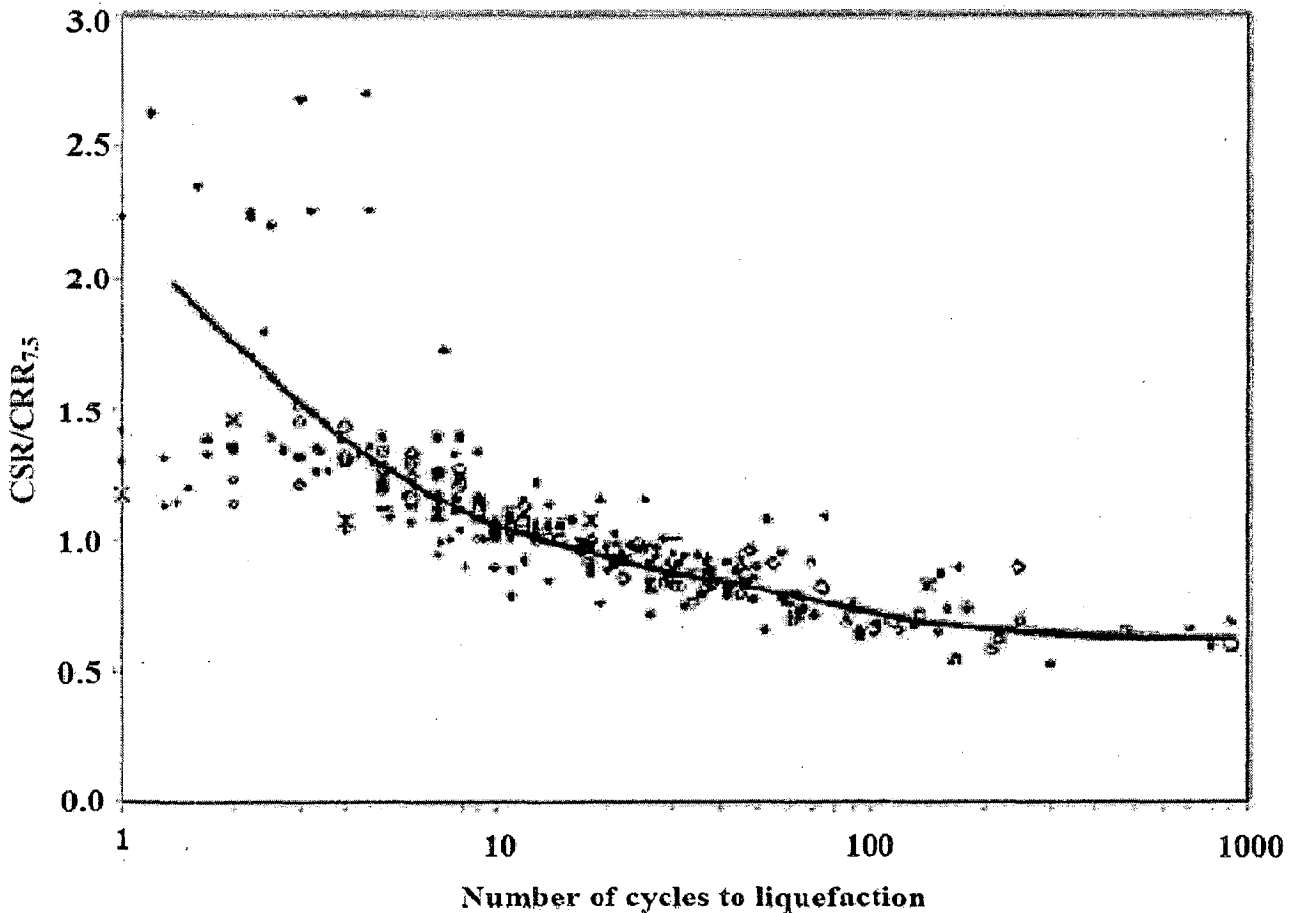
Fig. 3.6 Cyclic Triaxial Test Data Normalized to cyclic Resistance Ratio for M = 7.5, CRR$_{7.5}$ (Jefferies and Bean, 2006)
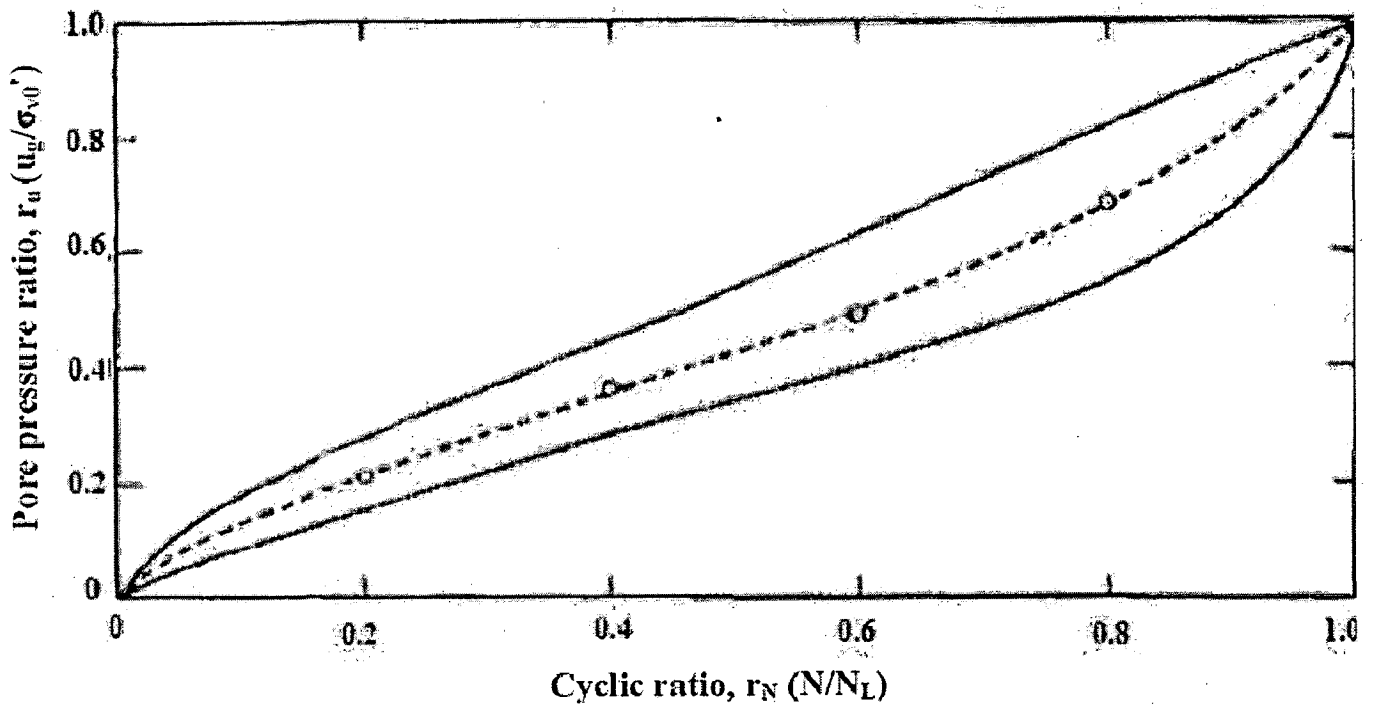
Fig. 3.7 Rate of Pore Pressure Build-up in Cyclic Simple Shear Tests (Seed et al. 1976)

3.3 FLOW CHART

The algorithm of the pore pressure generation model is given below in the form of flow chart (FC. 3.1).

```
                          ╭─────────╮
                          │  START  │
                          ╰─────────╯
                               │
                               ▼
┌──────────────────────────────────────────────────────────────┐
│ Enter the value of γ, γ_sat, water table position, M, and SPT N values, N_eq, T │
└──────────────────────────────────────────────────────────────┘
                               │
                               ▼
              ┌────────────────────────────────────┐
              │    Apply corrections to SPT N values │
              └────────────────────────────────────┘
                               │
                               ▼
┌──────────────────────────────────────────────────────────────┐
│ Calculate CSR and CRR_7.5 using 'simplified procedure' and hence find N_L │
└──────────────────────────────────────────────────────────────┘
                               │
                               ▼
              ┌────────────────────────────────────┐
              │      Enter the time increment, Δt    │
              └────────────────────────────────────┘
                               │
                               ▼
              ┌────────────────────────────────────┐
              │   At t=0, take u_0 = 0, r_{N0} = 0   │
              └────────────────────────────────────┘
                               │
                               ▼
              ┌────────────────────────────────────┐
              │                                      │
              │   Δr_N = (Δt/T)(N_eq/N_L)            │
              │                                      │
              └────────────────────────────────────┘
                               │
         ┌─────────────────────┤
         │                     ▼
         │    ┌────────────────────────────────────┐
         │    │ Calculate r_N = r_{N previous} + Δr_N │
         │    └────────────────────────────────────┘
         │                     │
         │                     ▼
         │    ┌────────────────────────────────────┐
         │    │ Calculate r_u from equation 3.13 b and hence U_g │
         │    └────────────────────────────────────┘
         │                     │
         │                     ▼
         │         ┌──────────────────────────┐
         │         │  t = t_previous + Δt      │
         │         └──────────────────────────┘
         │                     │
         │                     ▼
         │    NO          ╱──────────╲          YES
         └───────────────◄  If t >= T  ►───────────────┐
                          ╲──────────╱                 │
                                                        ▼
                          ┌──────────────────────────────────────┐
                          │ Take final step U_g as the excess pore │
                          │  pressure due to ground shaking         │
                          └──────────────────────────────────────┘
                                                        │
                                                        ▼
                                                  ╭─────────╮
                                                  │  STOP   │
                                                  ╰─────────╯
```

$$\Delta r_N = \frac{\Delta t}{T}\frac{N_{eq}}{N_L}$$

$$\text{Calculate } r_N = r_{N\,previous} + \Delta r_N$$

FC. 3.1 Generation of Pore water pressure

LATERAL CAPACITY OF PILES

In majority of the cases, the safe lateral load is based on limiting the deflection at the pile head and not the ultimate lateral load. In the past, empirical formulations from full-scale lateral load tests were used for pile design practice. Nowadays, theoretical approaches for predicting lateral movement have been developed extensively. Two approaches have generally been employed:-

i. The subgrade reaction approach in which the continuous nature of the soil medium is ignored and the pile reaction at a point is simply related to the deflection at that point.

ii. The elastic approach, which assumes the soil to be an ideal elastic continuum.

The methods based on subgrade reaction approach are briefly explained here along with the methodology adopted in the present study to determine the lateral response of pile in liquefiable soils.

4.1 MODULUS OF SUBGRADE REACTION APPROACH

The subgrade reaction model of soil behaviour, which was originally proposed by Winkler in 1867, characterizes the soil as a series of unconnected linearly elastic springs. The subgrade reaction approach has been widely employed in foundation practice because it provides a relatively simpler means of analysis and enables factors such as non-linearity, variation of soil stiffness with depth, and layering of soil profile to be taken into account. The disadvantage of this soil model is the lack of continuity; real soil is continuous at least to some extend since the displacements at a point are influenced by stresses and forces at other points within the soil.

The differential equation governing the deflection of laterally loaded pile is given by equations given below. (Prakash, 1981)

$$EI\frac{d^4y}{dx^4} = -p \qquad (4.1a)$$

$$p = k_h y \tag{4.1b}$$

$$EI \frac{d^4 y}{dx^4} + k_h y = 0 \tag{4.1c}$$

Where, E = Youngs modulus of pile material

I = Moment of Inertia of pile

p = soil reaction

K_h = Modulus of Horizontal subgrade reaction

y = Deflection of pile

x = depth below the pile head level

Modulus of Horizontal subgrade reaction, K_h for cohesionless soil at a given depth is given by the following relation. (Prakash, 1981)

$$K_h = n_h * x \tag{4.2}$$

Where n_h = coefficient of subgrade reaction (units of force/length^3)

For piles in sand, assuming that the modulus of elasticity depends only on the overburden pressure and the density of the sand, Terzaghi gave the relation as follows. (Poulos and Davis, 1980)

$$n_h = \frac{A\gamma}{1.35} \text{ kN/m}^3 \tag{4.3}$$

Where γ is taken as submerged or dry unit weight of soil as applicable in kN/m^3

Typical values of the factor A applicable to cohesionless soils are shown in Table 4.1. Table 4.1 also shows the correlation between SPT N values and factor A.

Substituting Eq. 4.3 in Eq. 4.2

$$K_h = \frac{A\gamma}{1.35} * x \tag{4.4}$$

$$K_h = \frac{A}{1.35} * \sigma_{eff} \tag{4.5}$$

Where σ_{eff} is the Effective overburden stress given by

$$\sigma_{eff} = \gamma * x \tag{4.6}$$

47

Table 4.1 Values of Factor A (Vide Poulos and Davis, 1980)

Relative density	Loose	Medium	Dense
SPT N Values	4-10	10-30	30-50
Range of values of A	100-300	300-1000	1000-2000
Adopted values	200	600	1500

$$p = K_h \cdot y$$

y = pile deflection at depth x

K_h = Modulus of horizontal subgrade reaction

EI = Flexural rigidity of pile
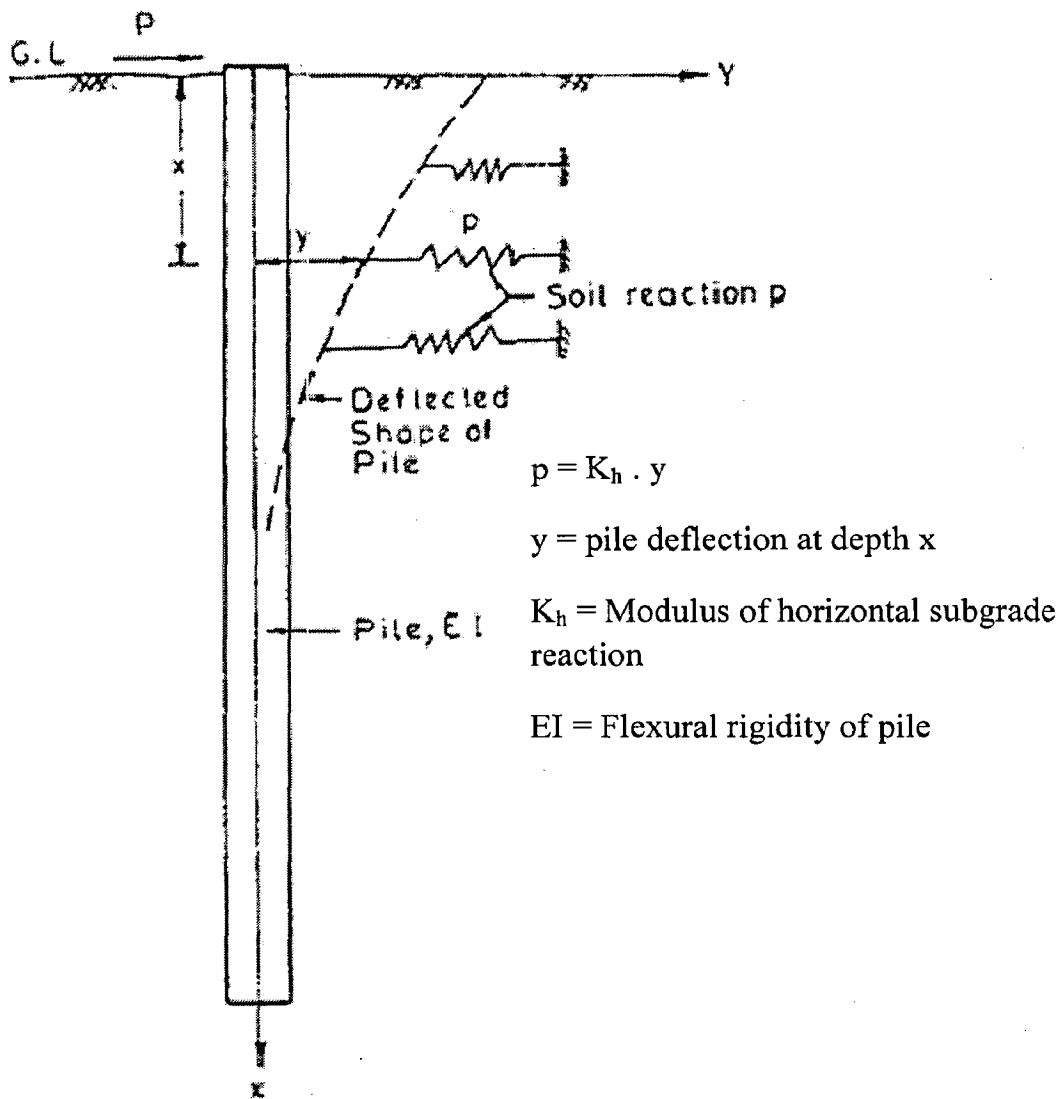
Fig. 4.1 Deflection of Laterally Loaded Pile

The pile can be represented by a number of nodal points as shown in fig: 4.2.
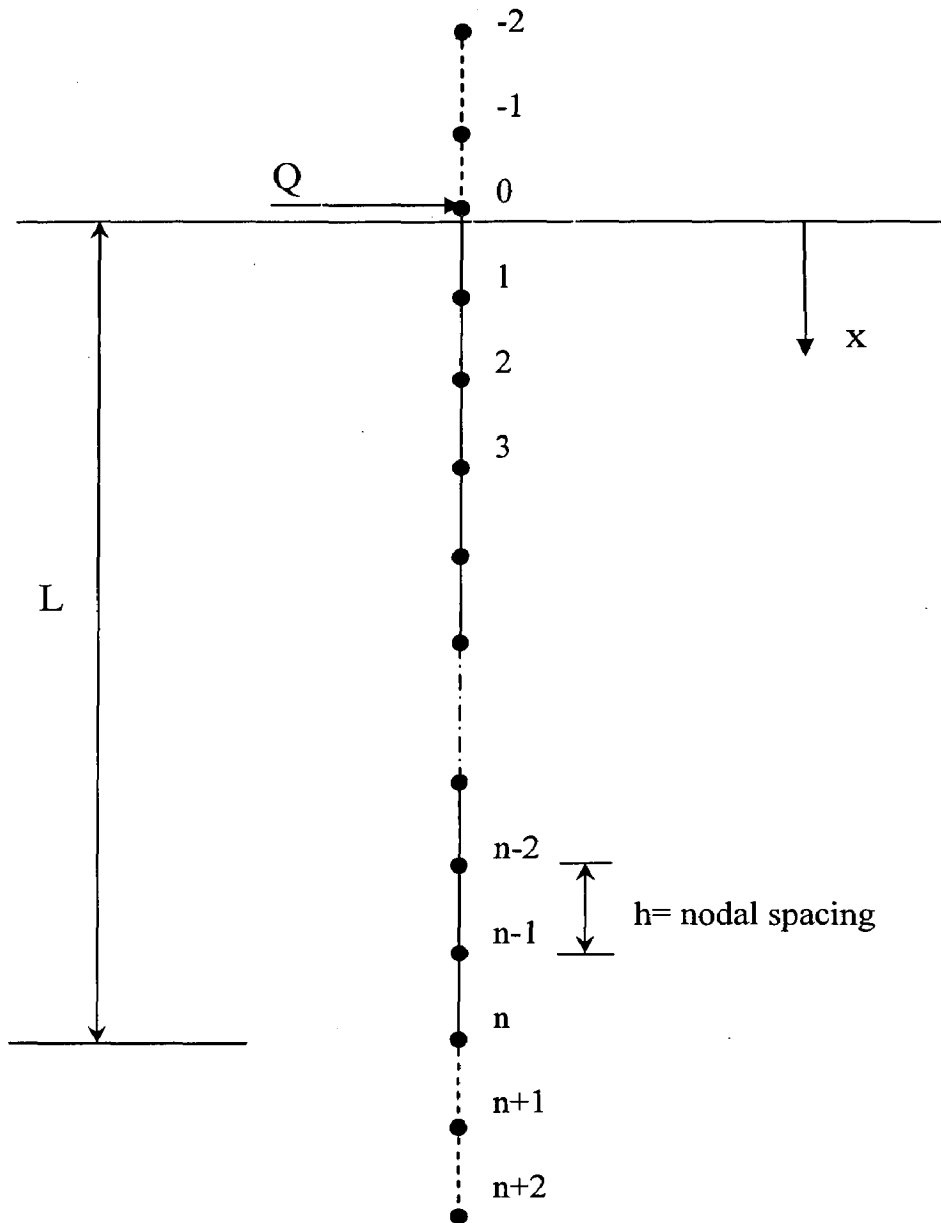
Fig. 4.2 Finite Difference Analysis of Laterally Loaded Pile

Discretizing Eq. (4.1c) using finite differences, at any node i, the differential equation is given by

$$\frac{EI}{h^4}(y_{i-2} - 4y_{i-1} + 6y_i - 4y_{i+1} + y_{i+2}) + K_{hi}y_i = 0 \qquad (4.7)$$

At each nodal point, an equation in the form Eq. 4.7 can be written. The equations involve four additional imaginary nodal points, two near the pile head and two near the pile tip. Thus, for n nodal points on the pile, 'n' equations can be written having (n+4) unknowns. The four unknowns at the imaginary nodal points can be obtained and substituted by

using appropriate boundary conditions. Remaining 'n' unknowns can be obtained by solving the 'n' equations. Thus the solution of equations will give the deflections and hence the moments at the nodal points.

The boundary conditions are as given below. (Poulos and Davis, 1980)

a) Fixed head pile

    i.   At the pile head (x=0), slope=0

$$\text{i.e. } \frac{dy}{dx} = 0 \tag{4.8}$$

    ii. At the pile head (x=0), Shear force (SF) = Applied lateral load (Q)

$$\text{i.e. } EI\frac{d^3y}{dx^3} = Q \tag{4.9}$$

b) Hinged pile head

    i.   At the pile head (x=0), moment =0

$$\text{i.e. } EI\frac{d^2y}{dx^2} = 0 \tag{4.10}$$

    ii. At the pile head (x=0), Shear force = lateral load

$$\text{i.e. } EI\frac{d^3y}{dx^3} = Q \tag{4.11}$$

c) Fixed pile tip

    i.   At the pile tip (x=L), slope=0

$$\text{i.e. } \frac{dy}{dx} = 0 \tag{4.12}$$

    ii. At x= L, deflection=0

$$\text{i.e. } y_n = 0 \tag{4.13}$$

d) Free pile tip

    i.   At x=L, moment=0

$$\text{i.e. } EI\frac{d^2y}{dx^2} = 0 \tag{4.14}$$

    ii. At x=L, shear force=0

$$\text{i.e. } EI\frac{d^3y}{dx^3} = 0 \tag{4.15}$$

After getting deflections, moments (BM) and shear force (SF) may be obtained at any node by following equations.

$$BM_i = EI\frac{d^2y}{dx^2} = \frac{EI}{h^2}\left(y_{i-1} - 2y_i + y_{i+1}\right) \tag{4.16}$$

$$SF_i = \frac{EI}{2h^3}\left(y_{i+2} - 2y_{i+1} + 2y_{i-1} - y_{i-2}\right) \tag{4.17}$$

4.2 EQUIVALENT CANTILEVER METHOD

The Equivalent Cantilever Method proposed by Davisson and Robinson (1965) enables the pile to be treated conveniently as a cantilever. This method is based on Modulus of Subgrade Reaction Approach. The lateral capacity of piles is invariably governed by limiting lateral displacement. The lateral displacement and therefore the lateral capacity of piles can be estimated using 'Equivalent Cantilever method' as explained below (Ramasamy et al. (1987), IS: 2911 (Part 1/Sec 4) – 2002).

The method described below is applicable to both fully and partially embedded piles. In the case of bridge pier foundations, the lateral soil support up to the scour depth is not considered. i.e. the length of pile up to scour depth will have to be treated as unsupported length (L_1).
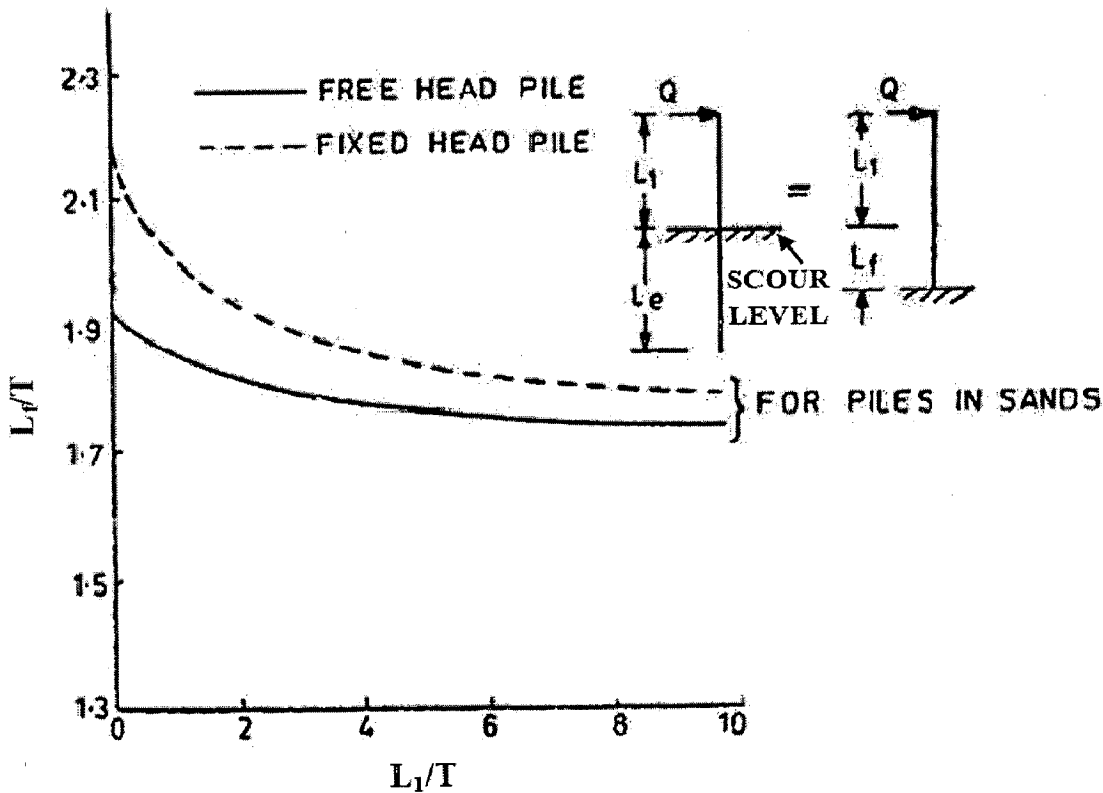
Fig. 4.3 Determination of Depth of Fixity (L_f) (IS: 2911 (Part 1/Sec 4) – 2002).

The pile head deflection of a laterally loaded pile may be computed by analyzing an 'Equivalent Cantilever' (Fig. 4.3). The results presented in Fig. 4.3 are obtained from an analysis based on modulus of subgrade reaction approach. The long flexible pile, fully or partially embedded, is treated as a cantilever fixed at some depth below the ground level. The length of 'Equivalent Cantilever' ($L_f + L_1$) can be obtained using the chart given in Fig. 4.3 where L_f is the depth of fixity.

In Fig. 4.3, T is the relative stiffness factor given by the equation given below. (IS: 2911 (Part 1/Sec 4) – 2002)

$$T = \sqrt[5]{\frac{EI}{n_h}} \qquad (4.18)$$

n_h is given by Eq. 4.3.

Knowing the length of the equivalent cantilever ($L_f + L_1$), the pile head deflection (y) shall be computed using the following equations. (IS: 2911 (Part 1/Sec 4) – 2002)

$$y = \frac{Q*(L_1+L_f)^3}{3*EI} \qquad \text{for free head pile} \qquad (4.19a)$$

$$y = \frac{Q*(L_1+L_f)^3}{12*EI} \qquad \text{for fixed head pile} \qquad (4.19b)$$

Where Q is the lateral load and L_f is depth of fixity.

The fixed end moment (M_F) of the equivalent cantilever is higher than the actual maximum moment (M_{act}) of the pile. The actual maximum moment is obtained by multiplying the fixed end moment of the equivalent cantilever by a reduction factor 'm' given in Fig. 4.4. The fixed end moment of the equivalent cantilever are given by the following equations. (IS: 2911 (Part 1/Sec 4) – 2002)

$$M_F = Q*(L_1+L_F) \qquad \text{for free head pile} \qquad (4.20a)$$

$$M_F = Q*(L_1+L_F)/2 \qquad \text{for fixed head pile} \qquad (4.20b)$$

The actual moment $M_{act} = m*M_F$

4.3 IN LIQUEFIABLE SOILS

The loss of soil strength and stiffness due to liquefaction may develop large bending moments and shear forces in piles founded in liquefying soil, leading to pile damage. Using 'simplified procedure' (Youd et al. 2001), the soil layers which are prone to liquefaction are identified based on the SPT N values. The excess pore pressure generated due to earthquake shaking is determined using Seed et al. (1976) model. From the net effective stress, the modified value of modulus of horizontal subgrade reaction is determined. Using this modified value, the deflection of pile, maximum bending moment and shear force developed can be determined using modulus of subgrade reaction approach. Based on these values the pile can be designed.

4.3.1 Methodology

The procedure adopted in the present study is explained in this section. The different data required as input are listed out. SPT N corrections which seem relevant are only considered. Also the computational procedure carried out is explained.

Input Data: The SPT N values, bulk or saturated densities of soil, earthquake magnitude, position of water table, modulus of elasticity (E) and diameter of pile are the basic data required as input. Corresponding to the earthquake magnitude, the value of equivalent number of uniform stress cycles, N_{eq} (Table 3.3), duration of earthquake shaking (Table 3.3) and peak horizontal acceleration at the ground surface (Fig. 3.2) are obtained from literature.

SPT N value corrections: The observed SPT N values are corrected for overburden stress using Eq. (3.6 b). This equation is reported to provide better correction for overburden pressures up to 300 kPa (Youd et al. 2001). The overburden correction factor commonly adopted earlier is given by the following equation (Peck et al. 1974).

$$C_N = 0.77 * Log_{10}\left(\frac{2000}{\sigma'_{vo}}\right)$$

(4.21)

Where σ'_{vo} is the effective overburden pressure.

A comparison between the corrections given by the two formulae is given in Table 4.2 to show the variation in values

Table 4.2 Comparison between Values of C_N Obtained from Old and New Formulae

Overburden stress, σ'_{v0} (kN/m^2)	$C_N = 0.77 * Log_{10}\left(\dfrac{2000}{\sigma'_{v0}}\right)$	$C_N = \dfrac{2.2}{1.2 + \dfrac{\sigma'_{v0}}{100}}$
20	1.54	1.57
40	1.31	1.38
60	1.17	1.22
80	1.08	1.10
100	1.00	1.00
120	0.94	0.92
140	0.89	0.85
160	0.84	0.79
180	0.81	0.73
200	0.77	0.69
220	0.74	0.65
240	0.71	0.61
260	0.68	0.58
280	0.66	0.55
300	0.63	0.52

It is observed from Table 4.2 that at higher overburden pressure values, there is a significant difference in the value of C_N when computed using the two formulae.

The correction for rod length may be neglected for liquefaction resistance calculations for rod lengths between 3 m and 10 m, because rod-length corrections were not applied to SPT test data from these depths in compiling the original liquefaction case history databases. Thus rod-length corrections are implicitly incorporated into the empirical SPT procedure. Hence this correction is not applied in the present study. The correction for bore hole diameter and sampling method are closer to 1 and hence it is ignored in the study. The correction for energy ratio varies over a wider range and the observed 'N' values corrected for overburden pressure (Eq. 3.6 b) are taken as N_{60} values. (N_{60} – Value corresponding to 60% energy input). The SPT N values are also corrected for the amount of fines present using Eq. 3.10.

Computational Procedure: The analysis of pile subjected to lateral load is based on modulus of subgrade reaction approach and analyzed using 'Finite Difference approach'. The pile is divided into required number of nodal points. The values of CSR, CRR and Factor of Safety at each nodal point are determined using the 'simplified procedure' as explained in section 3.1. Using the curve (Fig. 3.6) given by Jefferies and Bean (2006), the number of cycles to cause liquefaction (N_L) at each nodal point is determined. The soil layer located below water table will be fully liquefied under the occurrence of any one or both of the following conditions.

    i.   If $N_{eq} > N_L$

    ii.   If $CSR > CRR$

Once the soil is fully liquefied, the modulus of horizontal subgrade reaction, K_h is taken as zero at that nodal point otherwise excess pore pressure generated due to earthquake shaking at all other nodal points below the water table is determined using Seed et al. (1976) method as explained in section 3.2. Subtracting these values of excess pore pressures from the corresponding effective stresses under static condition, the net effective stress at all those nodal points is obtained. These net effective stresses are substituted in Eq. 4.5 to get the corresponding modified value of modulus of horizontal subgrade reaction, K_h at all the nodal points. Using these modified K_h values, the lateral capacity of pile is estimated by modulus of subgrade reaction approach as explained in section 4.1.

4.3.2 Program Steps

1. Input the saturated or bulk densities (γ_{sat} or γ) for each layer of soil, the depth of water table below ground level (D_w), modulus of elasticity (E) and diameter of pile (d), boundary conditions of the pile, earthquake magnitude (M) and the applied lateral load, Q.

2. Input the observed values of SPT N along the depth of pile and apply the correction for overburden and percentage fines content.

3. Divide the pile into required number of nodal points. Find the value of SPT N at nodal points by linear interpolation.

4. From Eq. 3.2, evaluate the value of Cyclic Stress Ratio (CSR) at each nodal point.

5. Using the 'simplified procedure' (Youd et al. 2001) explained in section 3.1 for evaluation of liquefaction resistance, determine at each nodal point, the value of CRR and hence find the Factor of safety.

6. Determine the number of cycles to cause liquefaction (N_L) at each nodal point for a particular earthquake magnitude and given soil conditions using the curve (Fig. 3.6) given by Jefferies and Bean, 2006 (using values of CSR, $CRR_{7.5}$ determined in steps 4 and 5).

7. If $N_{eq} > N_L$ or if CSR > CRR ,take the value of horizontal subgrade reaction, K_h as zero at that nodal point

8. Else determine the excess pore pressure generated, U_g at all other nodal points due to earthquake shaking using the model proposed by Seed et al. (1976) (section 3.2).

9. Find the new value of effective stress, σ_v' along all the nodal points by subtracting the excess pore pressure generated from the effective stress under static condition.

10. Determine the value of modulus of horizontal subgrade reaction (K_h) from equation 4.5 using the value of σ_v' from step 8.

11. Then using the value of K_h from step 9, follow the method of lateral analysis of pile in static case using Modulus of subgrade reaction approach. For getting the finite difference solution Gauss-Seidel iteration is adopted.

12. The program gives the CSR, CRR, excess pore pressure generated, net effective stress, K_h, deflection, bending moment and shear force at each nodal point along the depth of pile as output in Microsoft excel worksheet which makes it easier for further analysis of the results and graph plotting.

4.3.3 Flow Chart

The flow chart for the developed computer code for lateral response of pile in liquefiable soils is given below.

```
                          ( START )
                              │
                              ▼
┌─────────────────────────────────────────────────────────────────────┐
│ Enter the value of γ, γ_sat, D_w, E, d, M, Pile boundary conditions,  │
│ Q and SPT N                                                           │
└─────────────────────────────────────────────────────────────────────┘
                              │
                              ▼
              ┌──────────────────────────────────┐
              │ Enter the no. of nodal points     │
              │ required                          │
              └──────────────────────────────────┘
                              │
                              ▼
              ┌──────────────────────────────────┐
              │ Apply corrections to SPT N values │
              └──────────────────────────────────┘
                              │
                              ▼
        ┌──────────────────────────────────────────────┐
        │ Calculate CSR, CRR and FOS using             │
        │ "simplified procedure"                        │
        └──────────────────────────────────────────────┘
                              │
                              ▼
              ┌──────────────────────────────────┐
              │ Calculate the value of N_I        │
              └──────────────────────────────────┘
                              │
                              ▼
                          ╱───────────╲
      NO             ╱  Is N_eq > N_L or  ╲          YES
   ◄─────────────────    Is CSR > CRR      ─────────────────►
                    ╲                    ╱
                     ╲──────────────────╱
        │                                              │
        ▼                                              ▼
┌──────────────────────────────┐              ┌──────────────┐
│ Calculate U_g, modified σ_v'  │              │ K_h = 0      │
└──────────────────────────────┘              └──────────────┘
        │                                              │
        ▼                                              │
┌──────────────────────────────┐                      │
│ Calculate K_h                 │                      │
└──────────────────────────────┘                      │
        │                                              │
        └──────────────────┬───────────────────────────┘
                           ▼
┌─────────────────────────────────────────────────────────────────────┐
│ Calculate deflection, Moment and shear force using modulus of         │
│ subgrade reaction approach                                            │
└─────────────────────────────────────────────────────────────────────┘
                           │
                           ▼
                       ( STOP )
```

FC. 4.1 Lateral Response Analysis of Pile in Liquefiable Soils

VERIFICATION OF ALGORITHM AND BEHAVIOUR OF A PILE IN LIQUEFIABLE SOIL

Using the developed computer program, the lateral capacity of single pile in liquefiable layered soil can be determined. If a soil layer is fully liquefied, that portion of the soil will offer zero lateral resistance to the pile movement. Partially liquefied layers will provide a reduced resistance due to the rise in pore water pressure. Hence the pile will be subjected to larger lateral deflection, bending moment and shear force. The output gives all these parameters along the depth of the pile. Verification of the program formulation for both static and earthquake loading case is carried out. Solution of a typical problem showing the variation of above parameters is discussed in the chapter.

5.1 VERIFICATION OF THE ALGORITHM

The validation of the program for static case is done by comparing the results from program with that given by Reese and Matlock method (Matlock and Reese. 1961, 1962). For earthquake case, the program gave reasonable results for a real pile problem in liquefiable soil.

5.1.1 For Static Lateral Loading Condition

The lateral deflection of a pile along its depth in a cohesionless soil deposit subjected to 100 kN lateral load is evaluated. The pile head and pile tip are free. Soil is medium sand under submerged condition. The input data assumed are as follows.

Saturated unit weight of soil = 20 kN/m^3.

Modulus of Elasticity of pile, E = 2.5 *10^7 kN/m^2

Pile diameter = 0.5 m

Pile length = 10 m

The value of n_h for medium submerged sand as per Eq. 4.3 is 4778 kN/m^3. This value is used for calculating deflection using Reese and Matlock method. In the present study K_h is directly calculated from Eq. 4.5.
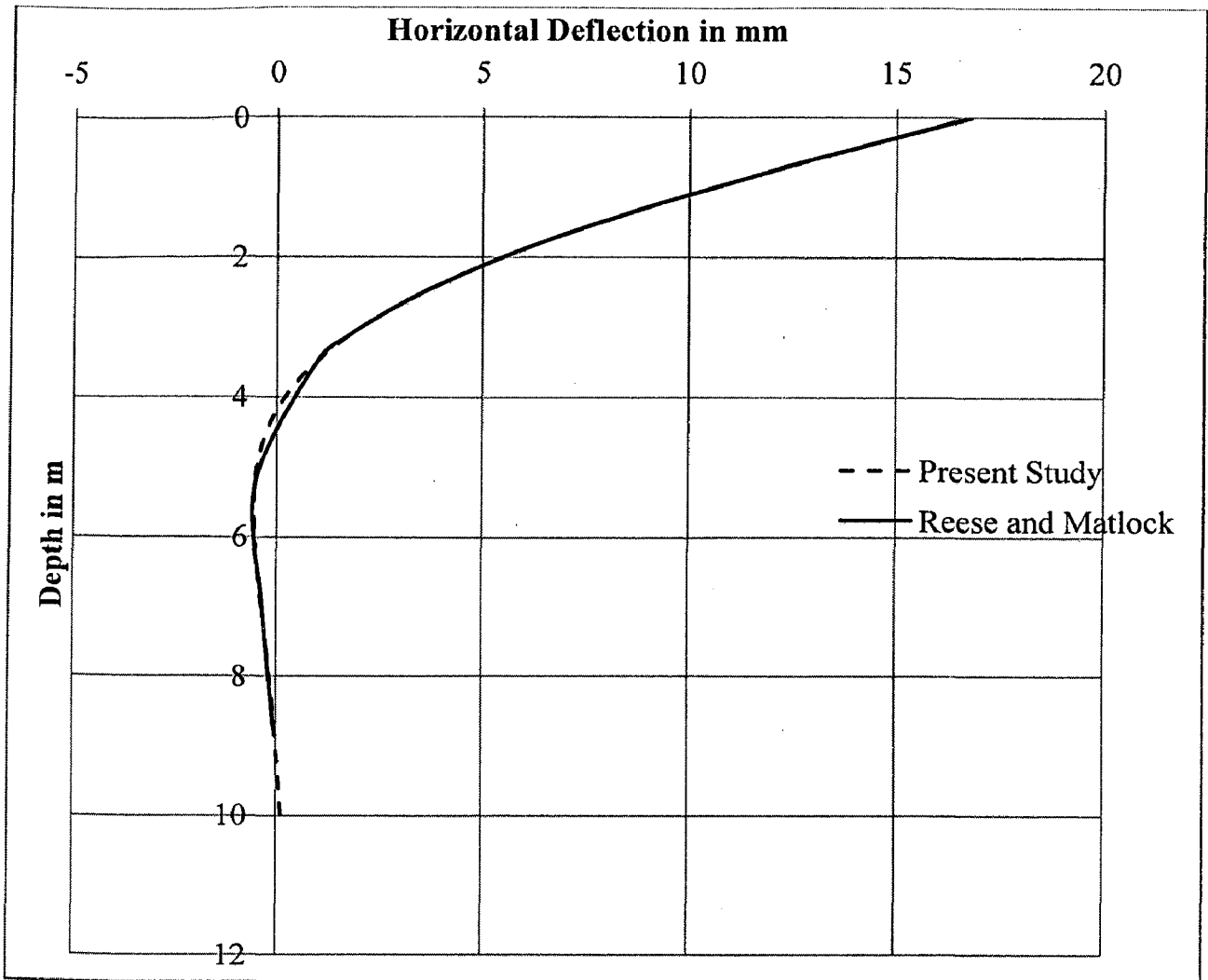
Fig. 5.1 Comparison between Reese and Matlock and Present Study for Lateral Loading

In Fig. 5.1, the variation of horizontal deflection at different depths along the depth of pile has been shown using present study and by Reese and Matlock method (Matlock and Reese. 1961, 1962). It can be observed that the deflections obtained by two approaches are in very good agreement. This validates the computational procedure for static lateral loading.

5.1.2 For Earthquake Loading Condition

The analysis of a single pile during the failure of Yachiyo Bridge over the River Shinano during the 1964 Niigata Earthquake (Hamada, 1992) is carried out. The foundation of both abutments and piers were Reinforced concrete piles of 0.3 m diameter and a length of 10 m to 11 m. The soil profile at the site is as shown in Fig. 5.2. There were three different layers of soil - sandy silt, medium sand and fine sand. For the top 8 m, the pile was surrounded by medium sand and remaining 3 m by fine sand. The actual soil profile

was sloping as shown in the figure. For the present study, it is assumed that the soil profile is horizontal. From the group of piles, a single pile at the corner of pier is selected for the study and is shown in Fig. 5.2.

It was reported by Hamada (1992), that the pile formed a plastic hinge at 8 m depth. The depth of liquefiable layer was 8m. The pile head got displaced by about 1.1 m in an earthquake magnitude of 7.5.
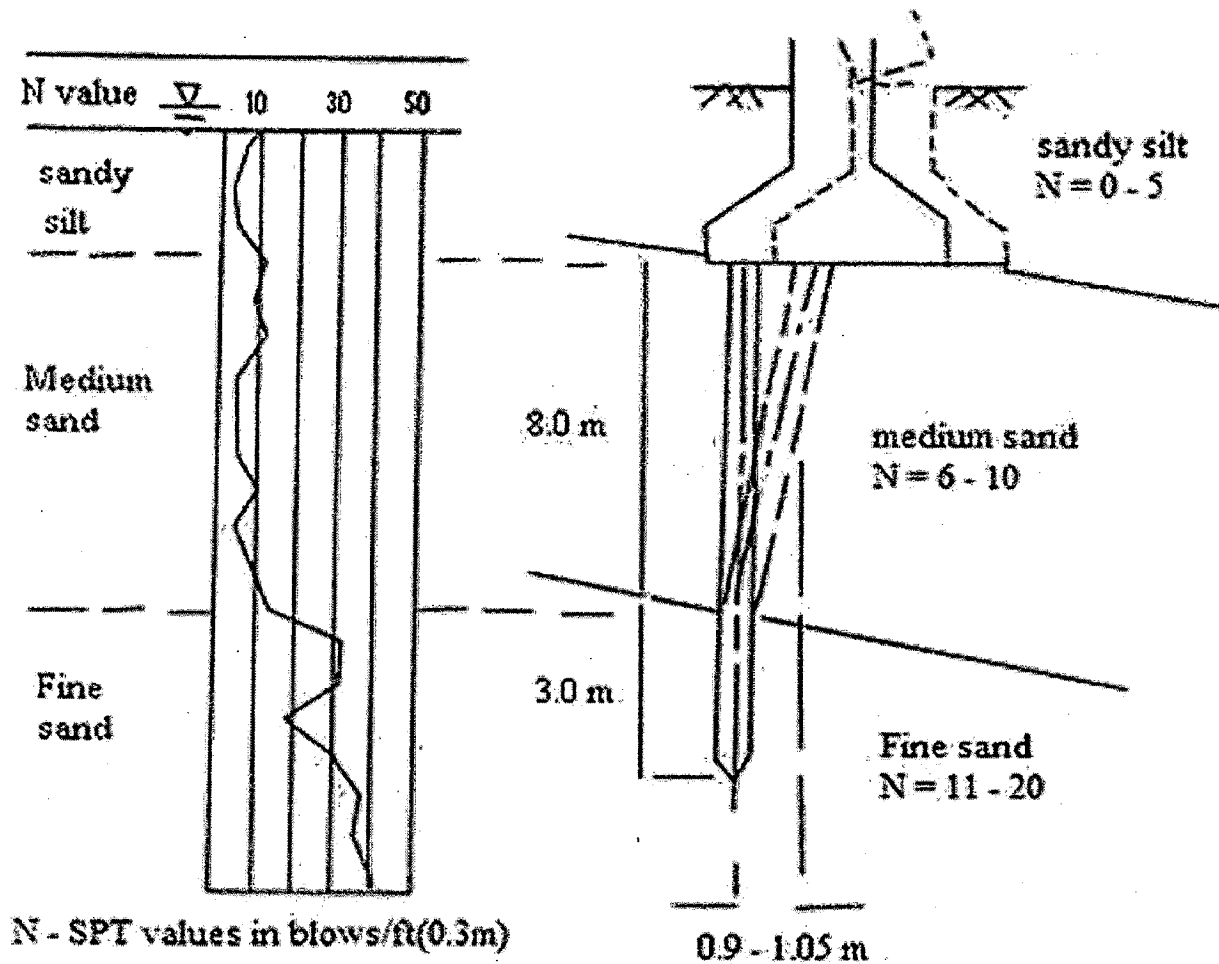

Fig. 5.2 Soil Profile beneath Yachiyo Bridge (Hamada, 1992)

The following data are assumed

> Saturated unit weight = 19 kN/m^3
>
> Modulus of Elasticity of pile, E = 2.5 * 10^7 kN/m^2
>
> Maximum surface acceleration, a_{max} = 0.15g
>
> Load= 100 kN
>
> Pile head = fixed

Table 5.1 Generation of Pore pressure

Depth from pile head (m)	SPT N_m	σ'_0 for SPT N correction	C_N	SPT N Cor $(N_{60})cs$	CSR	CRR	CSR/$CRR_{7.5}$	N_L	r_N (N_{eq}/N_L)	r_u (U_g/σ'_{v0})	$(\sigma_{v0'})$ static kN/m²	U_g kN/m²	(σ_v') EQ kN/m²
1	9	27.19	1.49	13.45	0.200	0.150	1.337	4.34	4.607	1	9.19	9.19	0
2	12	36.38	1.41	16.88	0.199	0.184	1.078	9.47	2.111	1	18.38	18.38	0
3	5	45.57	1.33	6.64	0.197	0.090	2.199	1.00	20	1	27.57	27.57	0
4	6	54.76	1.26	7.55	0.196	0.097	2.017	1.00	20	1	36.76	36.76	0
5	12	63.95	1.20	14.35	0.195	0.159	1.227	5.67	3.527	1	45.95	45.95	0
6	7	73.14	1.14	7.97	0.193	0.101	1.917	1.78	11.209	1	55.14	55.14	0
7	10	82.33	1.09	10.87	0.191	0.126	1.519	3.20	6.246	1	64.33	64.33	0
8	13	91.52	1.04	13.52	0.189	0.150	1.255	5.25	3.810	1	73.52	73.52	0
9	30	100.71	1.00	29.90	0.186	0.466	0.399	10071.53	0.002	0.007	82.71	0.60	82.11
10	19	109.9	0.96	18.18	0.182	0.199	0.917	25.65	0.780	0.632	91.9	58.06	33.84
11	30	119.09	0.92	27.60	0.178	0.361	0.492	5334.67	0.004	0.012	101.09	1.17	99.92

EQ – Earth Quake

U_g – Excess pore pressure generated during Earthquake

σ_v' - Effective stress

r_u – Pore pressure ratio

$(N_{60})cs$ – SPT N corrected

62

Table 5.2 Comparison of Lateral Pile Responses for Static and Earthquake Case

Depth (m)	K_h [static] (kN/m^2)	K_h [Earth quake] (kN/m^2)	Deflection static (m)	Deflection Earth quake (m)	Moment [static] (kNm)	Moment [Earth quake] (kNm)
0	0	0	0.02247	0.78471	-122.9	-487.3
1	2814.93	0	0.01628	0.76019	-22.9	-387.3
2	7178.04	0	0.00780	0.69667	31.3	-287.3
3	3858.90	0	0.00246	0.60423	29.5	-187.3
4	5968.79	0	0.00010	0.49294	18.2	-87.3
5	15084.58	0	-0.00044	0.37286	6.3	12.7
6	9522.16	0	-0.00034	0.25404	1.1	112.7
7	15664.11	0	-0.00013	0.14657	-0.9	212.7
8	22643.52	0	-0.00002	0.06050	-0.8	312.7
9	61032.03	60590.82	0.00001	0.00590	-0.3	412.7
10	38863.39	14310.52	0.00001	-0.00716	0	155.1
11	67897.92	67115.18	0	-0.00462	0	0

The results of the problem, solved using present method are shown in Table 5.1 and Table 5.2. The earthquake magnitude was 7.5. Corresponding values of N_{eq} and T are 20 and 40 seconds respectively. Table 5.1 shows the generation of excess pore water pressure. The observed SPT N values are corrected for overburden pressure by multiplying it with C_N. C_N is determined using Eq. 3.6 b. The values of CSR at different depths are evaluated from Eq. 3.2. From the corrected SPT N values, obtain the values of CRR along the pile depth using 'Simplified Procedure' explained in section 3.1.2. Find the ratio of CSR to $CRR_{7.5}$ at the nodal points. From Fig. 3.6, determine the values of N_L corresponding to CSR/ $CRR_{7.5}$ values. When the value of CSR > CRR or N_{eq} > N_L, the value of net effective stress reduces to zero. For other nodal points, find the value of cyclic ratio (r_N) and pore pressure ratio (r_u) by Seed et al. (1976) explained in section 3.2. Multiply pore pressure ratio by the static effective overburden stress to obtain the value of excess pore pressure generated. Subtract this excess pore pressure generated from the value of static effective stress to obtain the value of net effective stress. It can be observed from Table

5.1 that up to a depth of 8 m, the value of net effective stress is zero because the soil is fully liquefied up to 8 m. This agrees with the reported value of liquefaction depth.

A comparison between the K_h values for static and earthquake case is given in Table 5.2. K_h values for earthquake and static loading cases are determined from Eq. 4.5 using the net effective stress and static effective stress values respectively. Using these K_h values, the lateral deflection of pile is determined using Modulus of Subgrade Reaction Approach as explained in section 4.1. The bending moment along the depth of pile is given by Eq. 4.16.

Table 5.2 also shows the variation of lateral deflection and bending moment with depth for static and earthquake cases. The lateral load acting on the pile is not known. However, for an assumed value of 100 kN, the pile head deflection is about 0.78 m. The pile head will give a deflection of 1.1 m (as reported by Hamada, 1992) when a lateral load of 140 kN is applied. It can be observed that the calculated moment at 8.0 m increases from about zero under static condition to very high value under Earthquake condition which could have caused formation of plastic hinge at that depth as reported in this case. Also soil at 8 m depth forms the interface between fully liquefied and partially liquefied layers, which can also be a possible reason for failure as reported by Uzuoka et al. (2007). These show that the adopted method gives reasonable results and thus verifies the developed algorithm for earthquake loading.

5.2 BEHAVIOUR OF A PILE IN LIQUEFIABLE SOIL

The solution of a typical problem showing the lateral response of a single pile in liquefiable soils under earthquake loading is illustrated. For this the input data are taken from the case study of 10 storey Hokuriku building during the 1964 Niigata earthquake (Bhattacharya, 2003).

5.2.1 Input Data and Problem statement

Fig. 5.3 shows the soil profile at site. The building has a basement floor of 7 m height and is founded on reinforced concrete piles. The diameter of the reinforced concrete pile is 0.4 m and pile length is 12 m. The pile head is free and the pile tip is fixed. The pile head is 7 m below ground level (Bhattacharya, 2003). The pile passed through 5 m of liquefiable soil and remaining through dense soil.

. The remaining data are assumed as follows

Modulus of Elasticity of pile, $E = 2.5 * 10^7$ kN/m^2

Position of water table = at Ground level

Saturated unit weight = 19 kN /m^3.

Lateral load applied at pile head, Q = 25 kN

Maximum ground surface acceleration, a_{max} = 0.125 g

Earthquake Magnitude, M = 7.5

Number of uniform stress cycles, N_{eq}=20
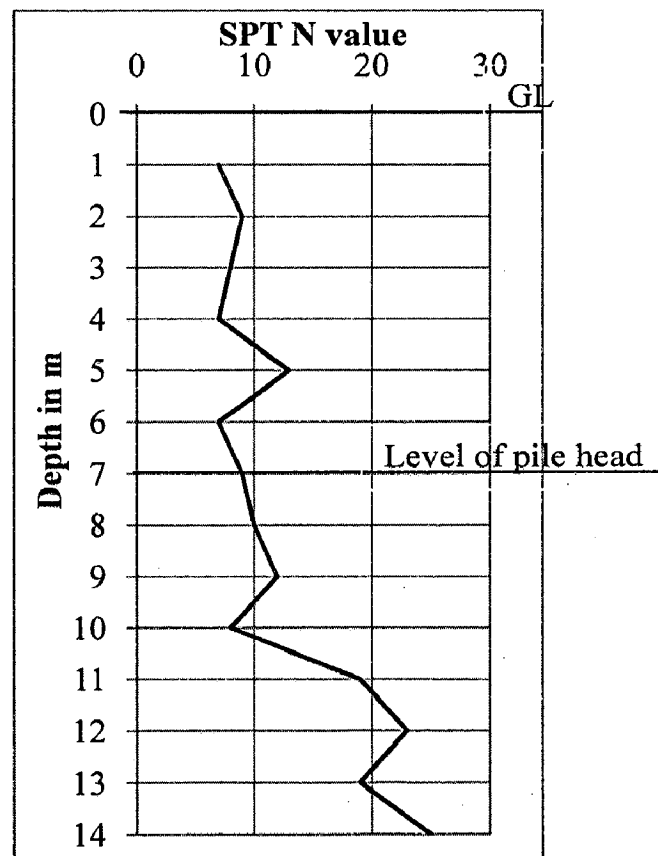
Duration of strong shaking, T = 40 s

Fig. 5.3 Soil Profile for 10- storey Hokuriku Building (Bhattacharya, 2003)

Table 5.3 shows the generation of excess pore pressure. The procedure of pore pressure generation and determination of lateral pile responses are same as explained in the previous problem (section 5.1.2). The shear force is evaluated using Eq. 4.17. The results of the problem under static lateral loading and Earthquake loading cases are given in Table 5.4. Comparisons of these results are shown in Fig. 5.4 to Fig. 5.7.

Table 5.3 Development of Pore Pressure

Depth from pile head (m)	SPT N_m	σ'_{v0} for SPT N correction	C_N	SPT N Cor $(N_{60})cs$	CSR	CRR	CSR/$CRR_{7.5}$	N_L	r_N (N_{eq}/N_L)	r_u (U_g/σ'_{v0})	(σ'_{v0}) static kN/m²	U_g kN/m²	(σ'_v) EQ kN/m²
1	10	72.19	1.145	11.447	0.168	0.131	1.278	4.954	4.037	1	9.19	9.19	0
2	12	81.38	1.092	13.110	0.166	0.147	1.134	7.664	2.610	1	18.38	18.38	0
3	8	90.57	1.045	8.358	0.165	0.104	1.588	2.851	7.016	1	27.57	27.57	0
4	19	99.76	1.001	19.021	0.164	0.208	0.786	57.795	0.346	0.310	36.76	11.41	25.35
5	23	108.95	0.961	22.101	0.163	0.248	0.655	216.734	0.092	0.117	45.95	5.35	40.60
6	19	118.14	0.924	17.553	0.161	0.192	0.841	41.010	0.488	0.409	55.14	22.53	32.61
7	25	127.33	0.890	22.237	0.160	0.250	0.638	348.119	0.057	0.083	64.33	5.32	59.01
8	23	136.52	0.858	19.726	0.158	0.217	0.728	84.585	0.236	0.232	73.52	17.08	56.44
9	23	145.71	0.828	19.043	0.156	0.209	0.745	75.158	0.266	0.254	82.71	21.00	61.71
10	23	154.9	0.800	18.407	0.152	0.201	0.757	69.336	0.288	0.270	91.9	24.80	67.10
11	23	164.09	0.774	17.811	0.149	0.195	0.764	66.306	0.302	0.279	101.09	28.23	72.86
12	23	173.28	0.750	17.253	0.144	0.189	0.765	65.719	0.304	0.281	110.28	31.00	79.28

EQ – Earth Quake
U_g – Excess pore pressure generated during Earthquake
$(N_{60})cs$ – SPT N corrected
σ'_v - Effective stress

r_u – Pore pressure ratio
r_N – N/N_L

Table 5.4 Variation of Lateral Pile Responses with Depth for Static Lateral Loading and Earthquake Case

Depth from pile head(m)	K_h static kN/m^2	K_h EQ kN/m^2	y_{static} (m)	y_{EQ} (m)	BM_{static} kNm	BM_{EQ} kNm	SF_{static} kN	SF_{EQ} kN
0	0	0	0.00982	0.04292	0.00	0.00	25.00	25.00
1	2366.1	0	0.00597	0.03128	25.00	25.00	17.94	25.00
2	5476.3	0	0.00292	0.02044	35.88	50.00	2.89	25.00
3	5021.1	0	0.00101	0.01119	30.78	75.00	-7.63	25.00
4	16319.4	11253.9	0.00008	0.00433	20.61	100.00	-10.83	0.64
5	24020.4	21221.7	-0.00019	0.00065	9.12	76.28	-9.21	-30.64
6	22452.5	13277.8	-0.00017	-0.00060	2.19	38.71	-5.00	-33.62
7	33857.4	31055.6	-0.00008	-0.00061	-0.88	9.05	-1.67	-20.21
8	33948.3	26063.3	-0.00002	-0.00034	-1.14	-1.70	0.12	-6.37
9	36765.6	27432.8	0.00000	-0.00012	-0.64	-3.70	0.47	-0.41
10	39380.7	28753.8	0.00001	-0.00001	-0.21	-2.51	0.33	1.39
11	41814.2	30139.3	0.00000	0.00001	0.02	-0.91	0.18	1.49
12	44083.6	31691.1	0.00000	0.00000	0.15	0.46	0.13	1.38

Where y – Pile Deflection

      BM – Bending moment

      SF – Shear Force

5.2.2 Evaluation of Modulus of Subgrade Reaction (K_h)

The observed SPT N values are corrected for overburden correction and these values are shown in Table 5.3. The values of CSR, CRR and N_L are obtained. When the value of CSR > CRR or $N_{eq} > N_L$, the excess pore pressure generated becomes equal to the effective stress. The net effective stress reduces to zero and hence the value of K_h also becomes zero. From Table 5.3, it can be observed that for the top 3m layer, net effective stress value reduced to zero, which means the soil is completely liquefied and hence K_h = 0. For the remaining points, the rise in pore water pressure is determined. This value is reduced from the value of static effective stress to obtain the net effective stress. Based on this net effective stress, the modified value of K_h is determined. The amount of excess pore water pressure developed, static and net effective stress are shown in Table 5.3. Comparison of K_h for static lateral loading and earthquake loading is given in Table 5.4. Using these reduced K_h values, lateral response analysis is carried out.

5.2.3 Generation of Excess Pore Water Pressure

Fig. 5.4 shows the variation of pore pressure ratio with depth. It can be observed from the figure that the pore pressure ratio is unity up to 3 m. This shows that excess pore pressure generated up to 3 m is very high and is equal to the effective overburden stress. So the soil up to 3 m is fully liquefied. Below 3 m, the pore pressure ratio is less due to the presence of comparatively stronger soil (larger SPT N values). The larger pore pressure ratio in top layers explains the larger value of deflection at pile head under earthquake loading.
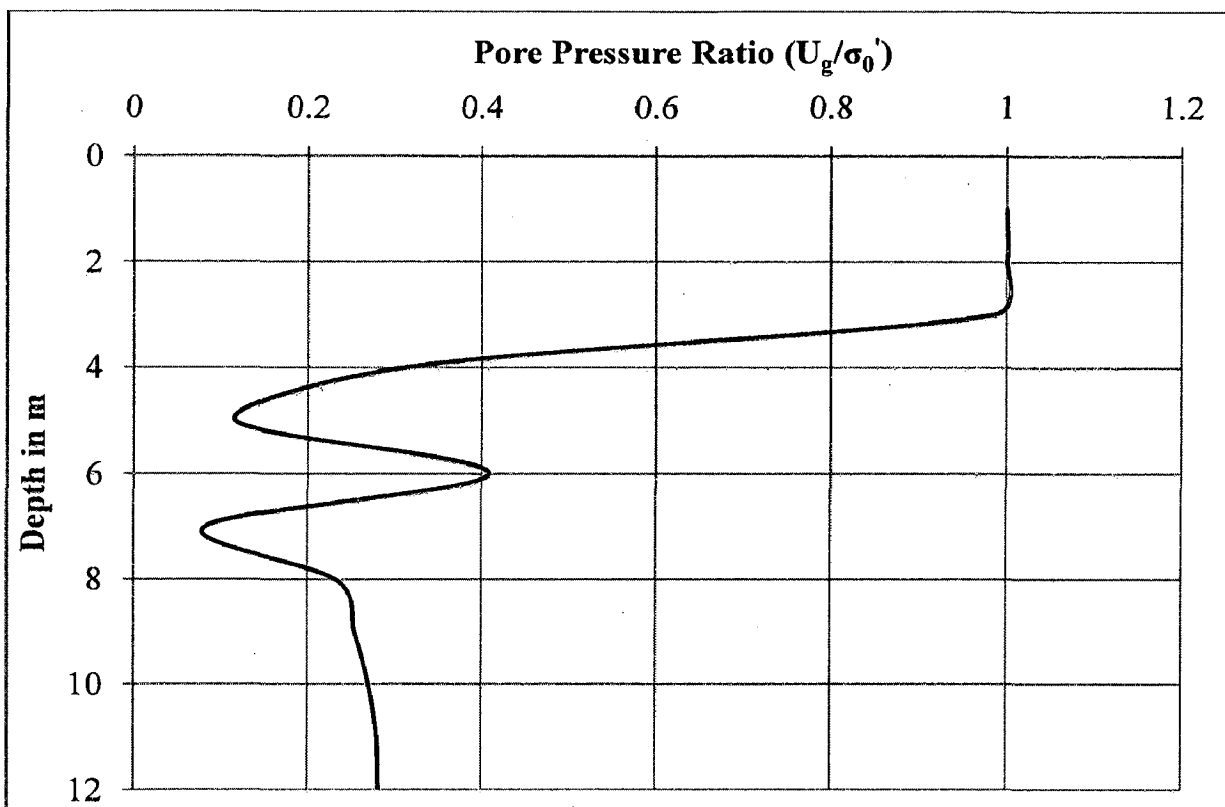
Fig 5.4 Variation of Pore Pressure Ratio with Depth

5.2.4 Effect of Liquefaction on Pile Head Deflection

In Fig. 5.5, the variation of pile deflection along the depth of pile for static and earthquake loading are shown. The pile head deflection is obtained as 9.8 mm and 42.9 mm respectively for static lateral loading and earthquake loading case. It shows that due to liquefaction, deflection increased by about 4.38 times. This explains the dangerous effect of liquefaction on pile deflection.
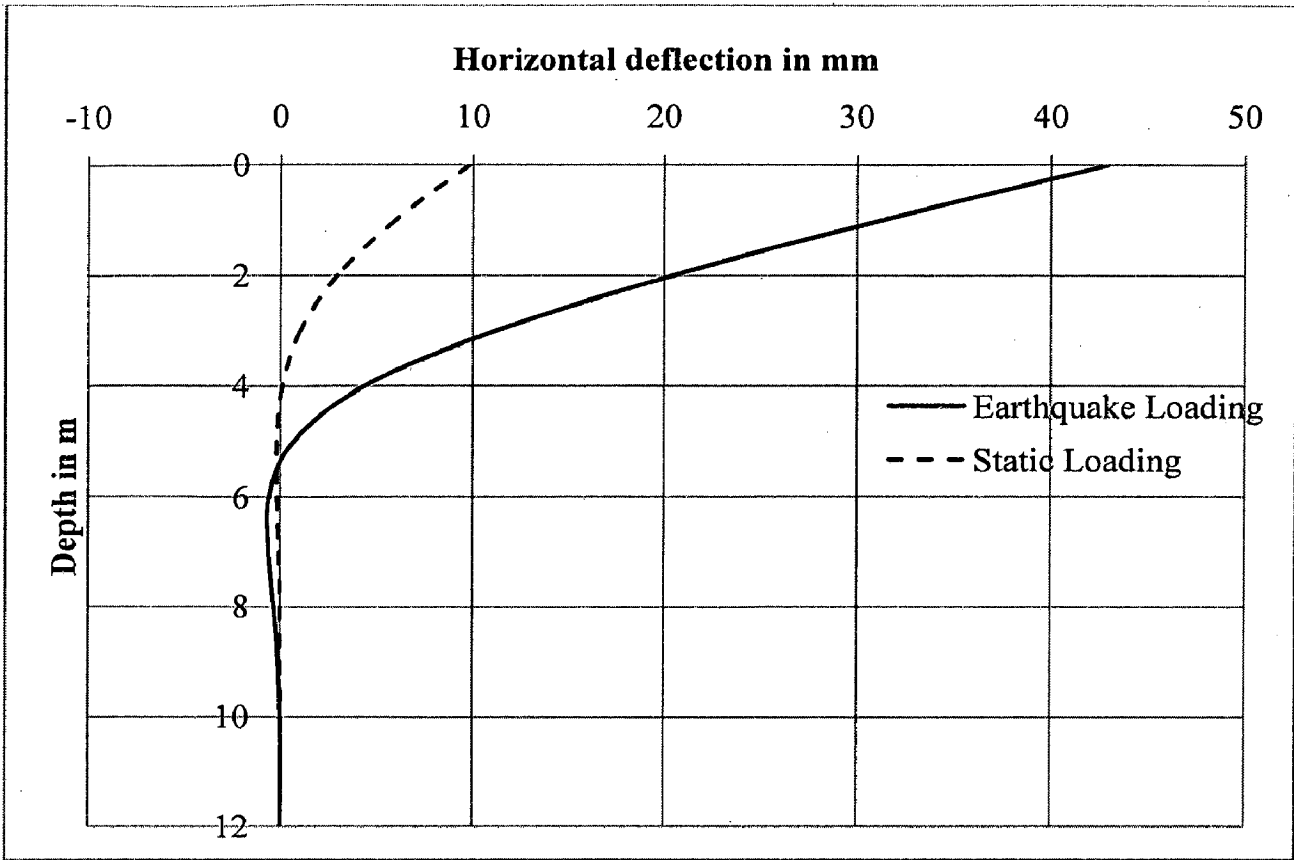
Fig. 5.5 Deflection along the depth of pile

## 5.2.5 Effect of Liquefaction on Bending Moment
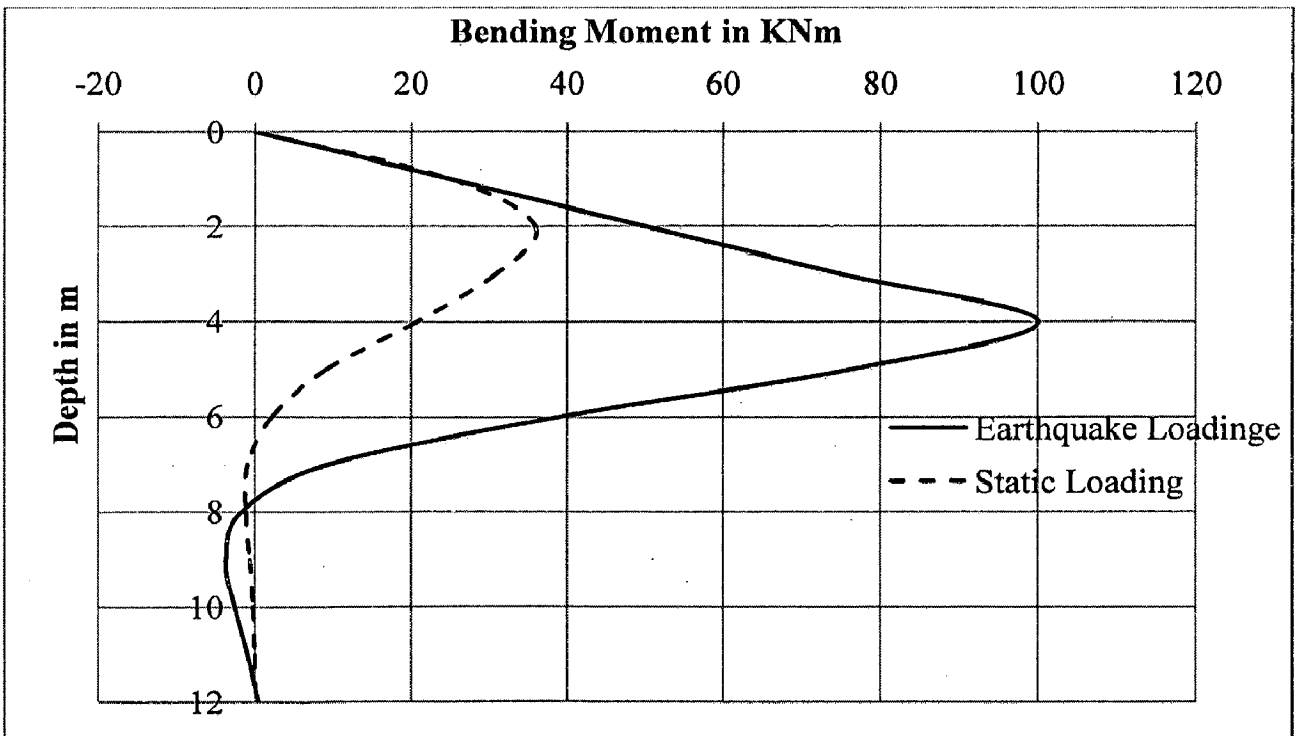
Fig. 5.6 Bending Moment Variation along the Depth of Pile

In Fig. 5.6, the variation of Bending Moment along the depth of pile for static and earthquake loading are shown. The maximum value of bending moment increased from about 36 kNm for static loading to 100 kNm for earthquake loading. It shows a 2.8 times increase from the static case value. These results explain the structural failure of piles in many case of pile foundation failure under Earthquakes reported in the literature (e.g. NHK building, 1964 Niigata earthquake). So during design in liquefiable soils, a higher value of Factor of safety should be applied for bending moment.

5.2.6 Effect of Liquefaction on Shear Force
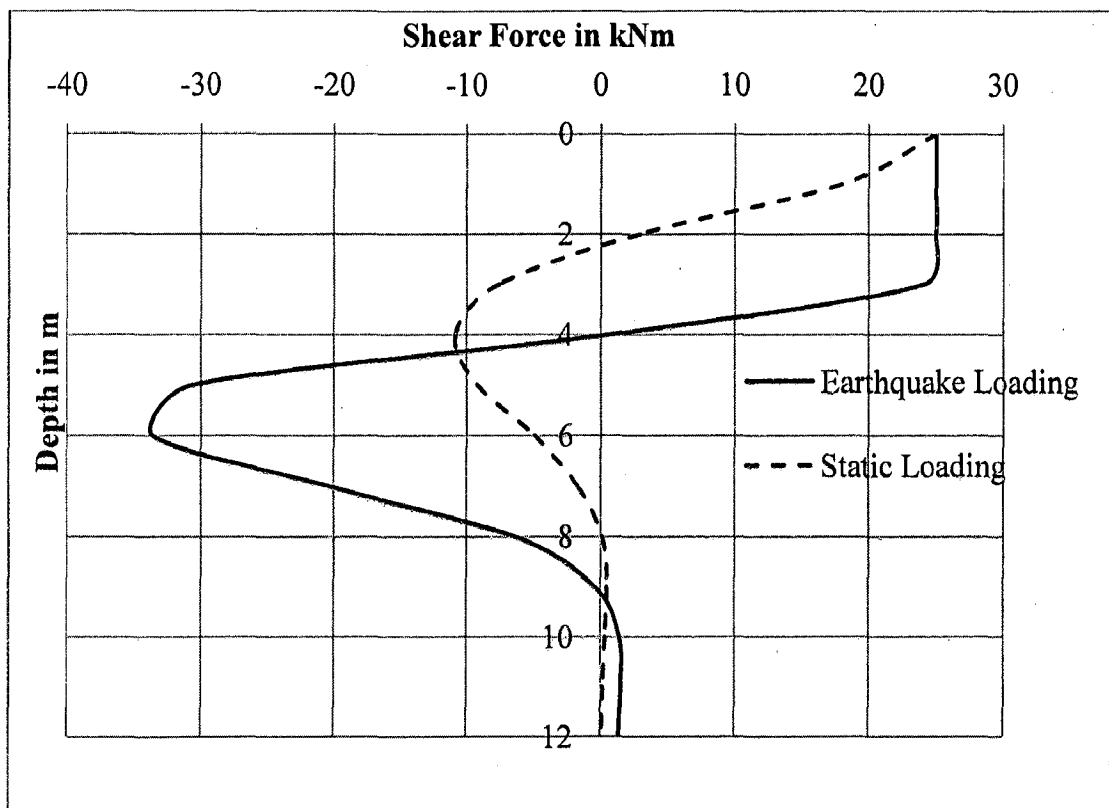
Fig. 5.7 Shear Force Variation along the Depth of Pile

In Fig. 5.7, the variation of Shear Force along the depth of pile for static and earthquake loading are shown. Increase in Shear force can cause damage to structures founded on pile foundations. The maximum shear force increased by about 1.3 times from 25 kN for static loading to 33 kN for Earthquake loading. This shows that sufficient consideration should be given to Shear Force during pile design in liquefiable soils.

PARAMETRIC STUDY

Parametric studies are carried out to illustrate the possible reduction in pile capacity under earthquake loading due to liquefaction. Using the program, studies are carried out to evaluate the effect of location of liquefiable layer and homogenous soil deposits having different SPT N values on pile capacity. Design charts are prepared for determining pile head deflection in homogenous, cohesionless soil deposits for fully embedded piles.

6.1 EFFECT OF LOCATION OF LIQUEFIABLE LAYER ON LATERAL CAPACITY OF PILE

The effect of position of liquefiable layer in a layered soil deposit on the lateral response of a pile is studied. A layered soil deposit of 20 m depth (Fig. 6.1) is assumed with a weak liquefiable layer of 5 m. Three different positions of this 5 m liquefiable layer are considered. In the first case, top 5 m is assumed as liquefiable, in the second case, 6-10 m is assumed liquefiable and in the third case, 11-15 m is liquefiable. The data assumed are given below.

Lateral load at the top = 25 kN

Pile length = 20 m

Pile diameter = 0.5 m

Modulus of Elasticity of pile, $E = 2.5*10^7$ kN/m^2

Water table = at ground level

Saturated unit weight = 19 kN/m^3

Earthquake magnitude = 7.5

Maximum ground surface acceleration is 0.1g

The SPT N value for partially liquefiable layer is taken as 15 and for liquefiable layer as 8. The pile is assumed as fixed head pile.
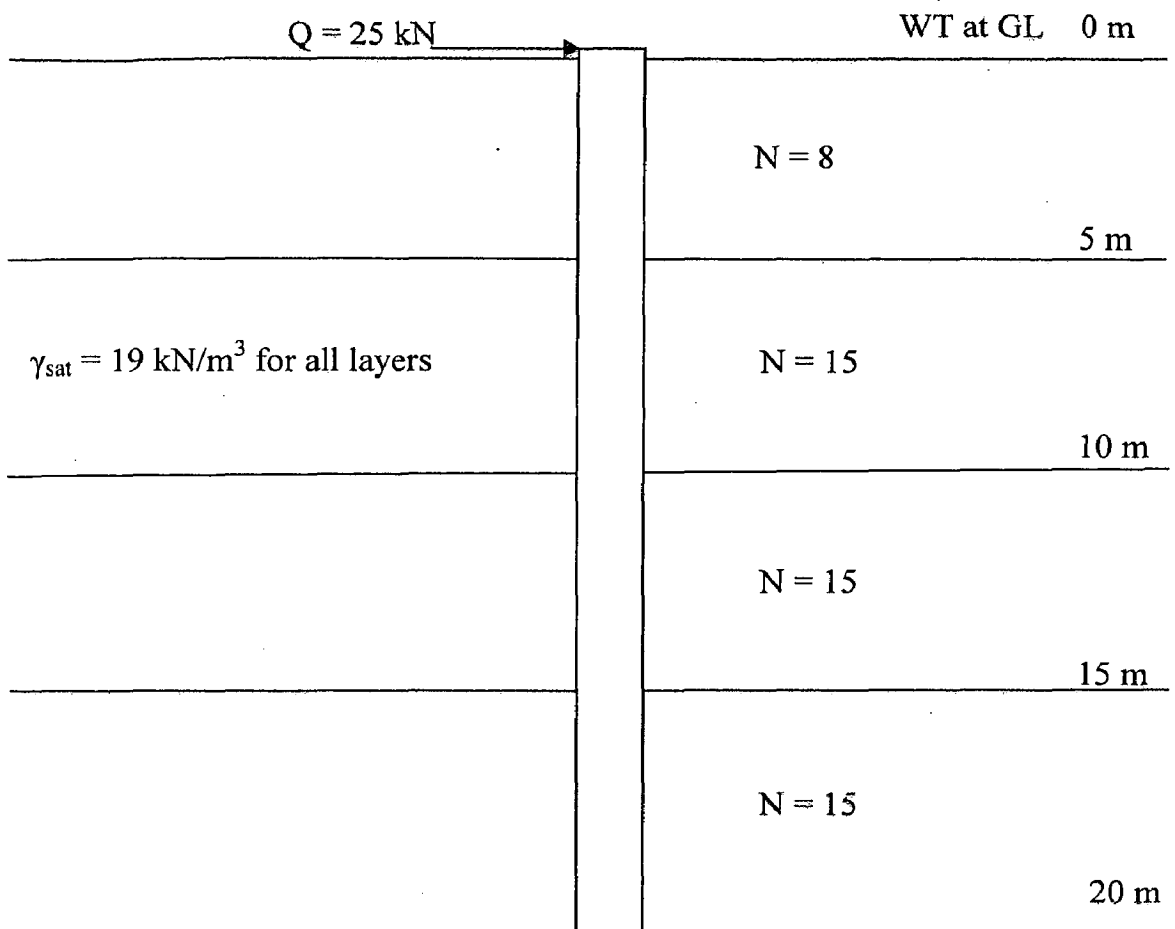
Q = 25 kN →   WT at GL   0 m

N = 8

                                                                    5 m

$\gamma_{sat} = 19$ kN/m³ for all layers   N = 15

                                                                    10 m

N = 15

                                                                    15 m

N = 15

                                                                    20 m

Fig. 6.1 Layered Soil with 5 m Liquefiable Layer at Top

The analysis of the problem is carried out using the developed program and pile deflections for the three cases are determined. In Fig. 6.2, the variation of pile deflection along the depth of pile for three different positions of fully liquefiable layer is shown. It can be observed that when the fully liquefiable layer is at the top, the condition becomes highly critical as far as lateral capacity is considered. The pile head deflection increased by several times. But when the liquefiable layer is in intermediate, the effect seems to be very less whatever is its position in between. However the presence of intermediate fully liquefiable layer in gently sloping grounds can cause lateral spreading which is not considered in this case (Finn and Fujita, 2002). Also the existence of non liquefiable layer at the ground surface has significant influence on the maximum bending moment of pile (Miura et al., 1991).
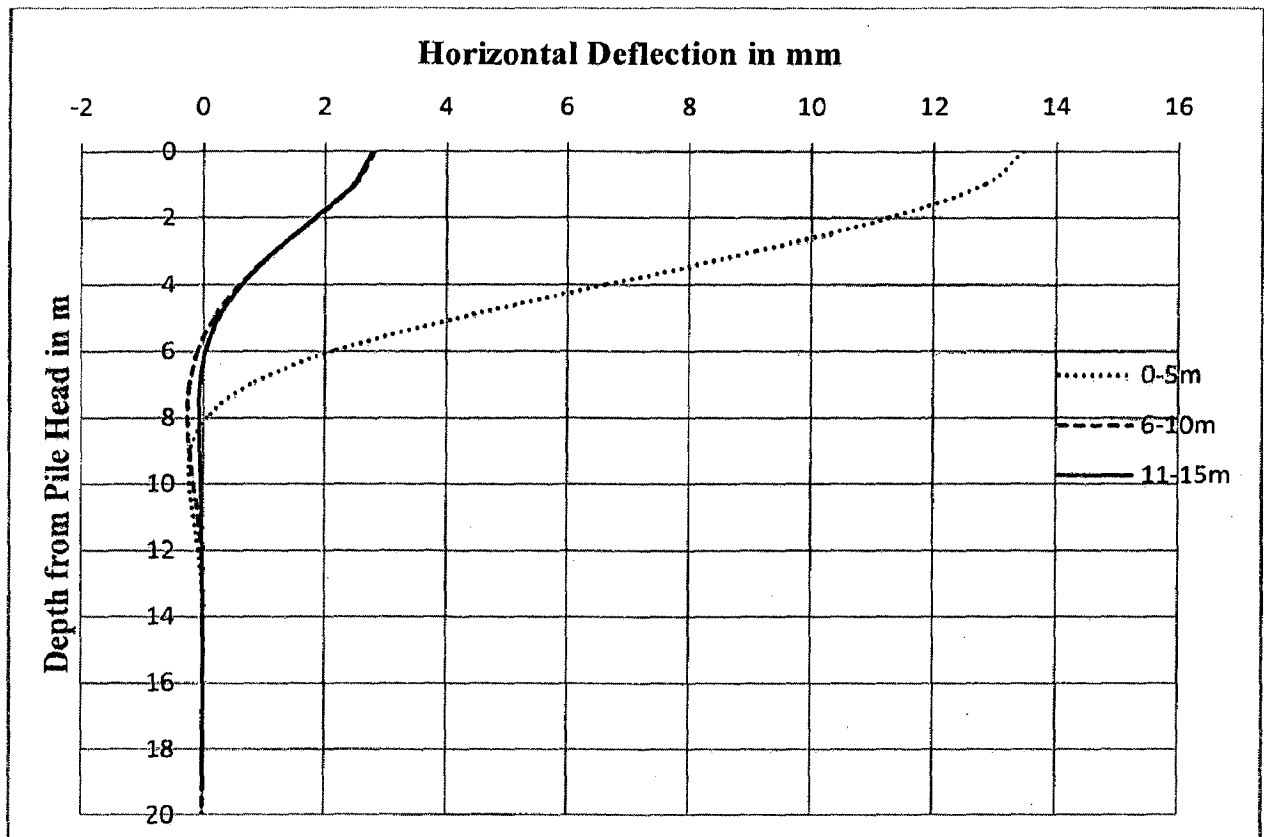
Fig. 6.2 Comparison of Pile Head Deflection for Different Position of Liquefiable Layer

6.2 VARIATION OF PILE RESPONSE IN LIQUEFIABLE SOIL WITH RESPECT TO SPT N

The variation of pile head deflection and maximum bending moment for different SPT N values are studied. For this, lateral response of a pile in homogenous cohesionless soil is analyzed for a fixed head pile. The data is the same as assumed in section 6.3.1 except that the value of earthquake magnitude is taken as 6.5 and pile length as 15 m.

Fig. 6.3 and Fig. 6.4 show the variation of pile head deflection and bending moment with SPT N values. Very large value of deflection (746 mm) and bending moment (459.5 kNm) are observed for SPT N = 5. It is because of complete liquefaction of a larger depth of top soil layer. When SPT value increases more than 12, the pile head deflection and maximum bending moment are reduced to allowable values. For higher values of SPT N there is not much effect of liquefaction in the soil layers. This is because soil becomes comparatively denser as SPT N value increases and dense soils are not prone to liquefaction.
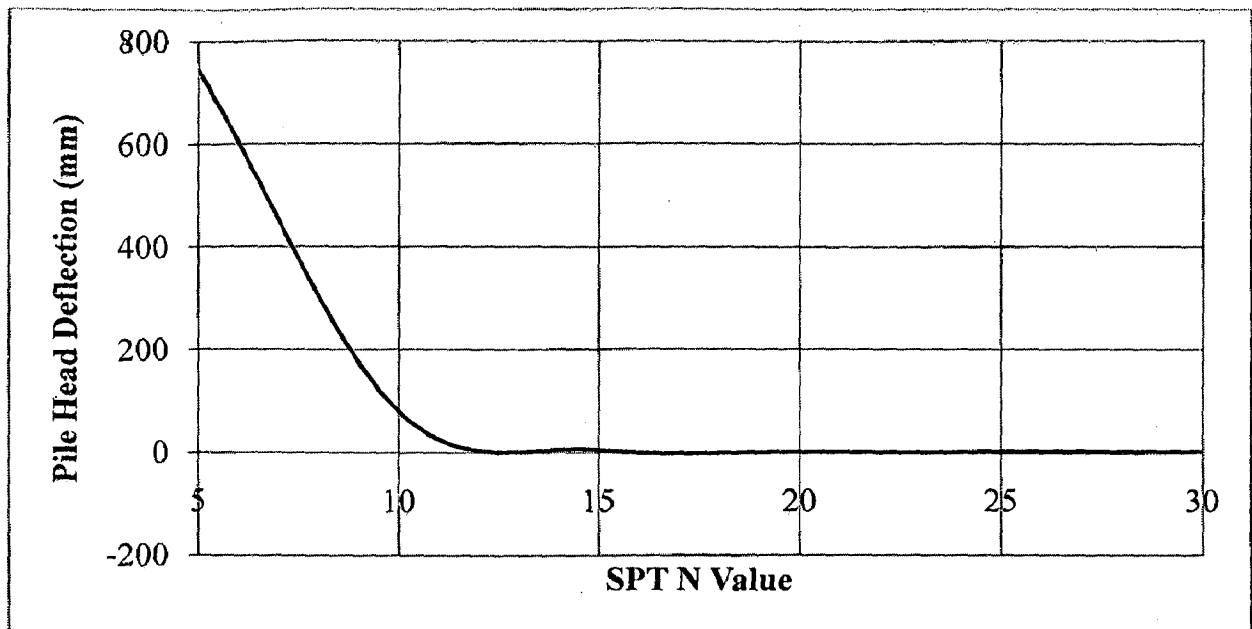
Fig. 6.3 Variation of Pile Head Deflection with SPT N Values
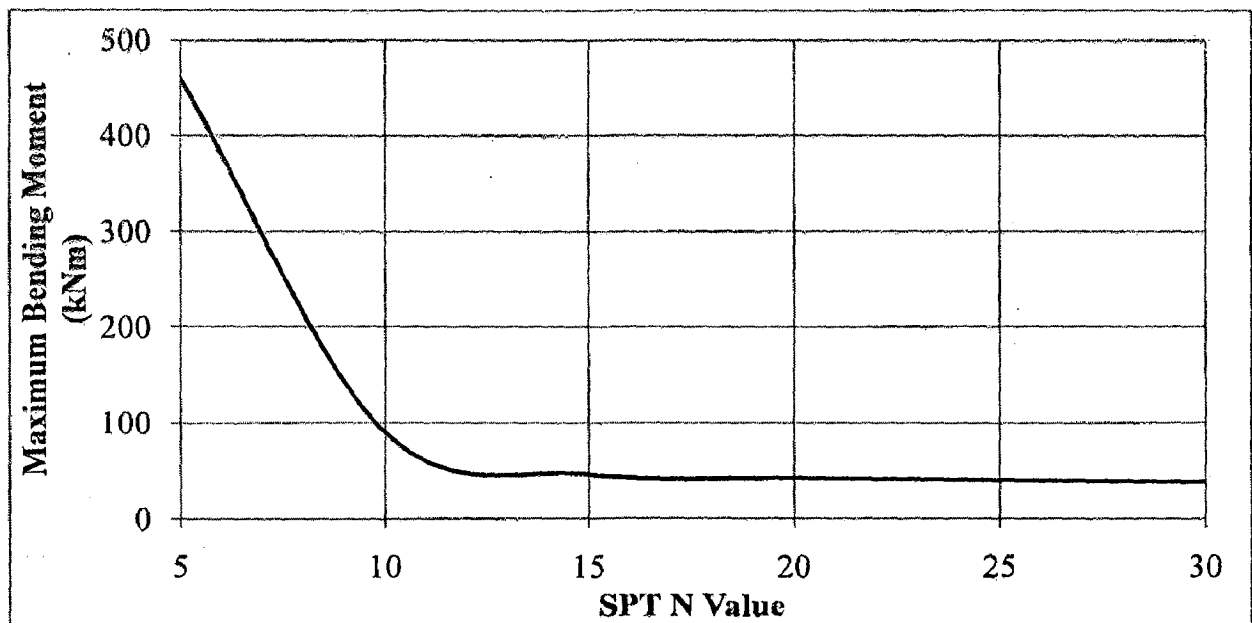
Fig. 6.4 Variation of Maximum Bending Moment with SPT N values

6.3 DESIGN CHARTS

In the case of partially liquefiable soils, the net effective stress will be greater than zero but less than the static effective stress due to the generation of excess pore pressure. Due to the reduced effective stresses, the values of modulus of horizontal subgrade reaction (K_h) also get reduced as it is directly proportional to the net effective stress (Eq. 4.5). This leads to the reduction in the lateral capacity of piles. The analysis of piles in partially

liquefiable, homogenous cohesionless soils is carried out for lateral loads. From these results, simplified design charts are developed using Equivalent cantilever approach for those soils.

Using the procedure discussed in section 4.3, the pile head deflection, y for long piles in homogenous soil deposits (assuming constant value of SPT N throughout the soil depth) are determined for any particular value of lateral load. Homogenous deposits of SPT N from 5 to 30 are considered in the study. Using the determined y values, the value of depth of fixity, L_f is determined using Eq. 4.19. Relative stiffness factor (T) is determined from Eq. 4.18. The values of L_f/T (Fixity factor) as a function of SPT N value and maximum ground surface accelerations are shown in Fig. 6.5 to 6.14. In these charts, only fully embedded piles are considered. Also the charts give values of L_f/T for maximum ground surface acceleration (a_{max}) up to 0.2 g only. For piles having some unsupported length or $a_{max} > 0.2$ g, analysis should be carried out using the basic procedure described in section 4.3.

Design charts for free head piles are shown in Fig. 6.5 to 6.9. Design charts for fixed head piles are shown in Fig. 6.10 to 6.14. A problem to illustrate the procedure for using these design charts is also discussed.

6.3.1 Free Head Piles

Fig. 6.5 to Fig. 6.9 shows the design charts for lateral design of fully embedded free head piles in homogenous cohesionless partially liquefiable soils for different values of earthquake magnitude. In each figure (for a particular value of earthquake magnitude), the relation between fixity factor (L_f/T) and SPT N values for different ground surface accelerations ranging from 0.05 g to 0.2 g are given. Also the design chart for lateral analysis of piles for static loading case is provided. For static case the curve is horizontal to the X- axis with a Fixity factor of around 1.95.

The charts are useful to determine the pile head deflection in partially liquefiable soils only. For example in Fig. 6.5, consider the curve for $a_{max} = 0.1$ g. Here below SPT N = 10, the soil deposit will be subjected to complete liquefaction at the top leading to unsupported length. So for these cases, curve cannot be extended and problem should be solved using the program developed. For earthquake magnitude of 8 (Fig. 6.9), the soil

undergoes complete liquefaction for $a_{max} = 0.2$ g for higher values of SPT N also. So the curve corresponding to it is not provided.
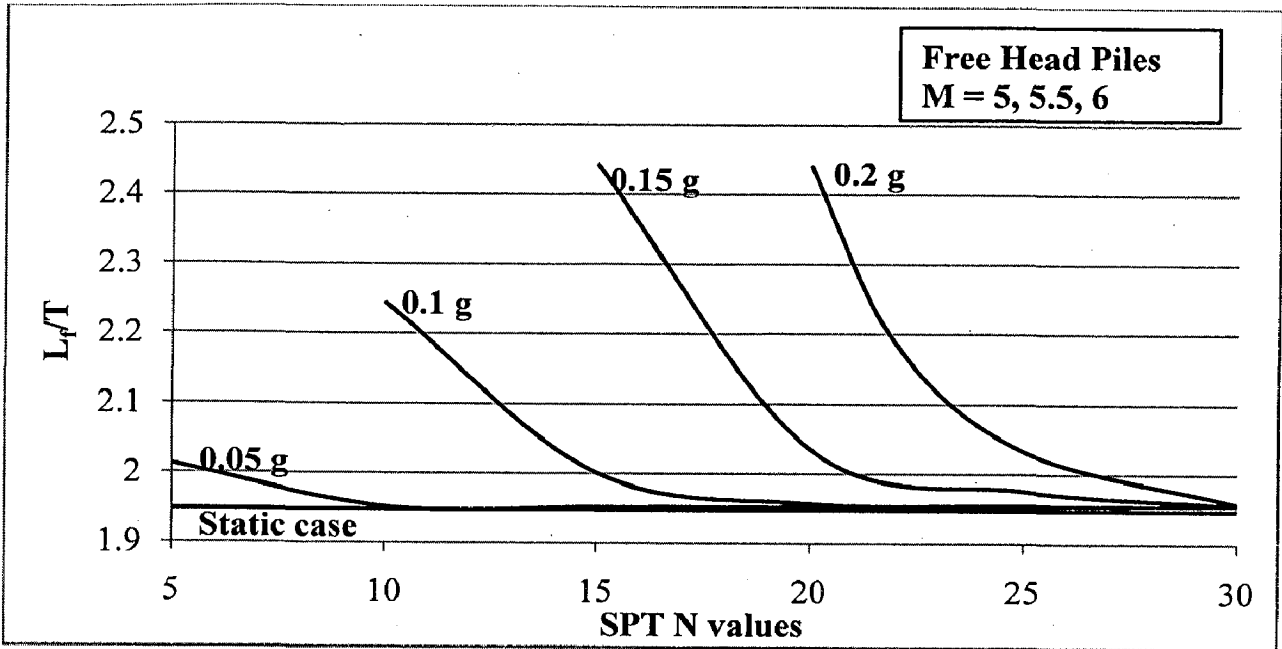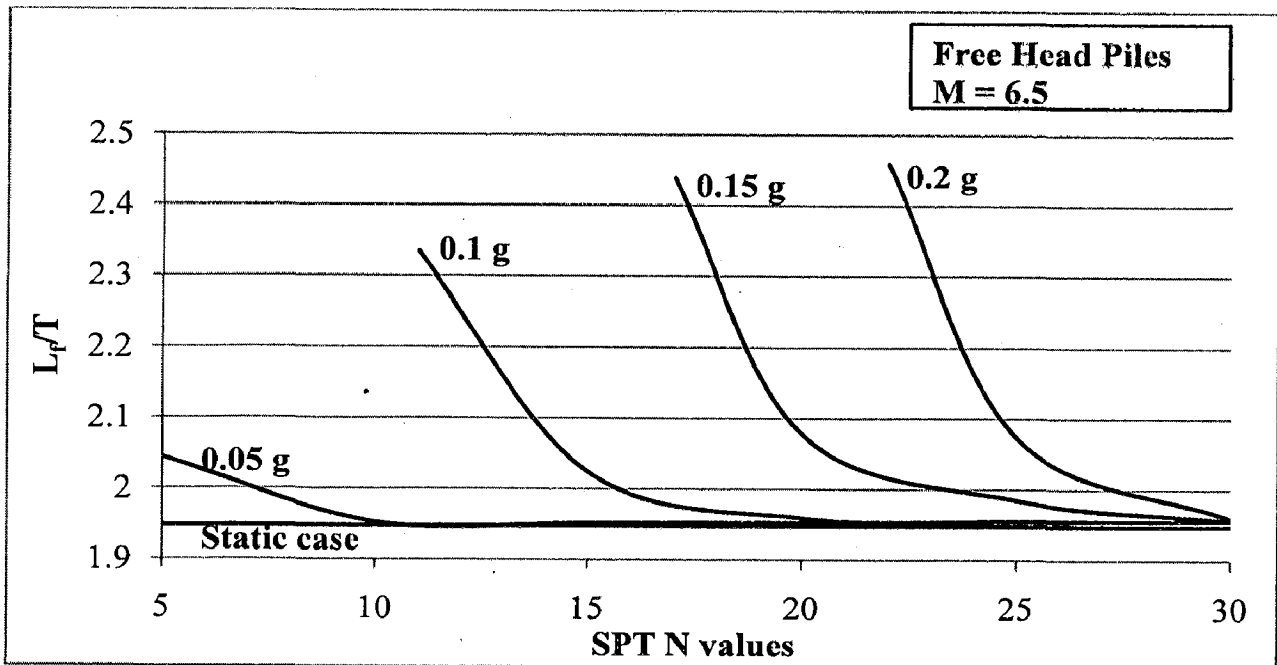

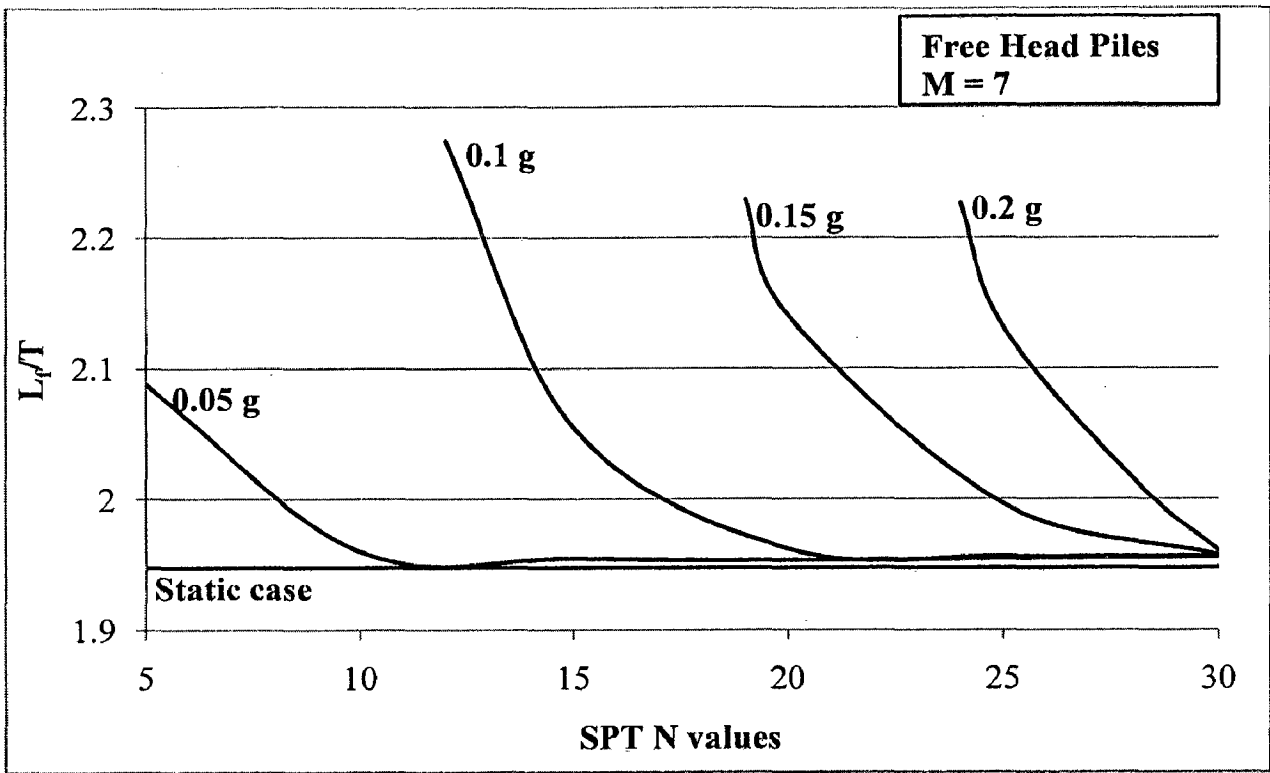Fig. 6.5 L_f/T Vs N for M=5, 5.5 and 6

Fig. 6.6 L_f/T Vs N for M=6.5
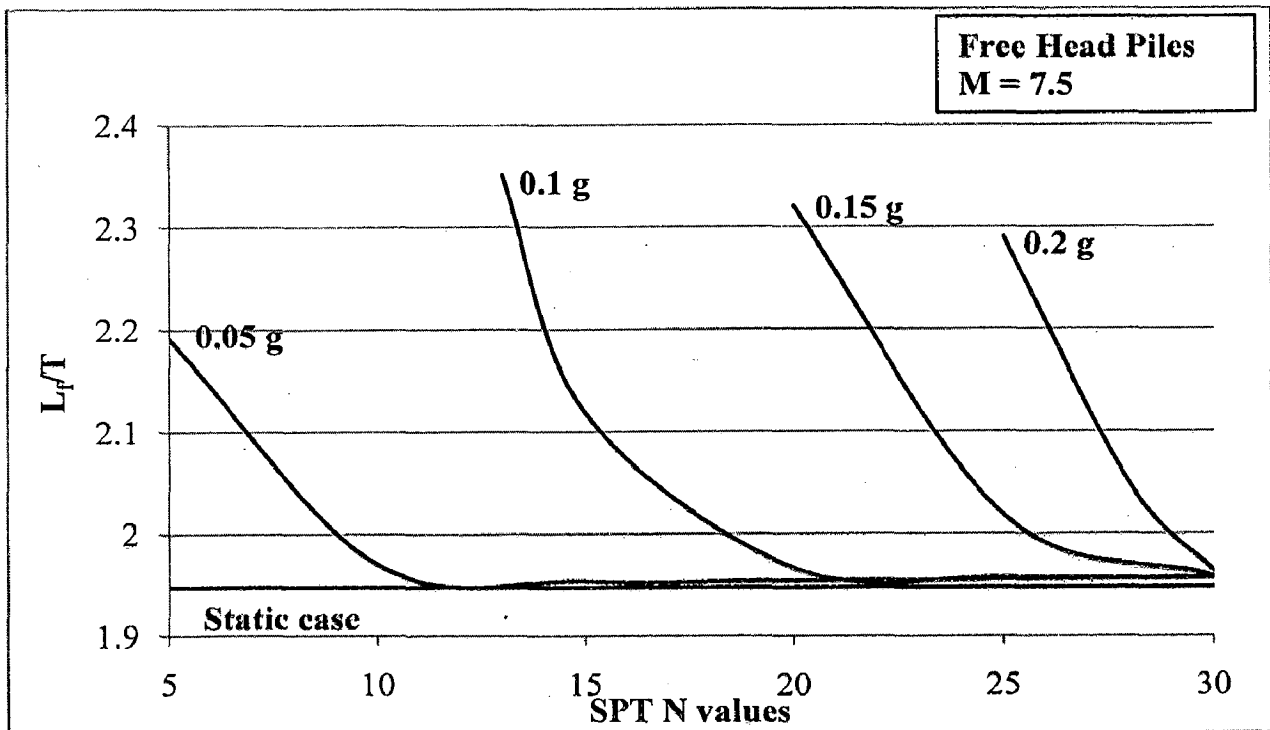
Fig. 6.7 L_f/T Vs N for M=7
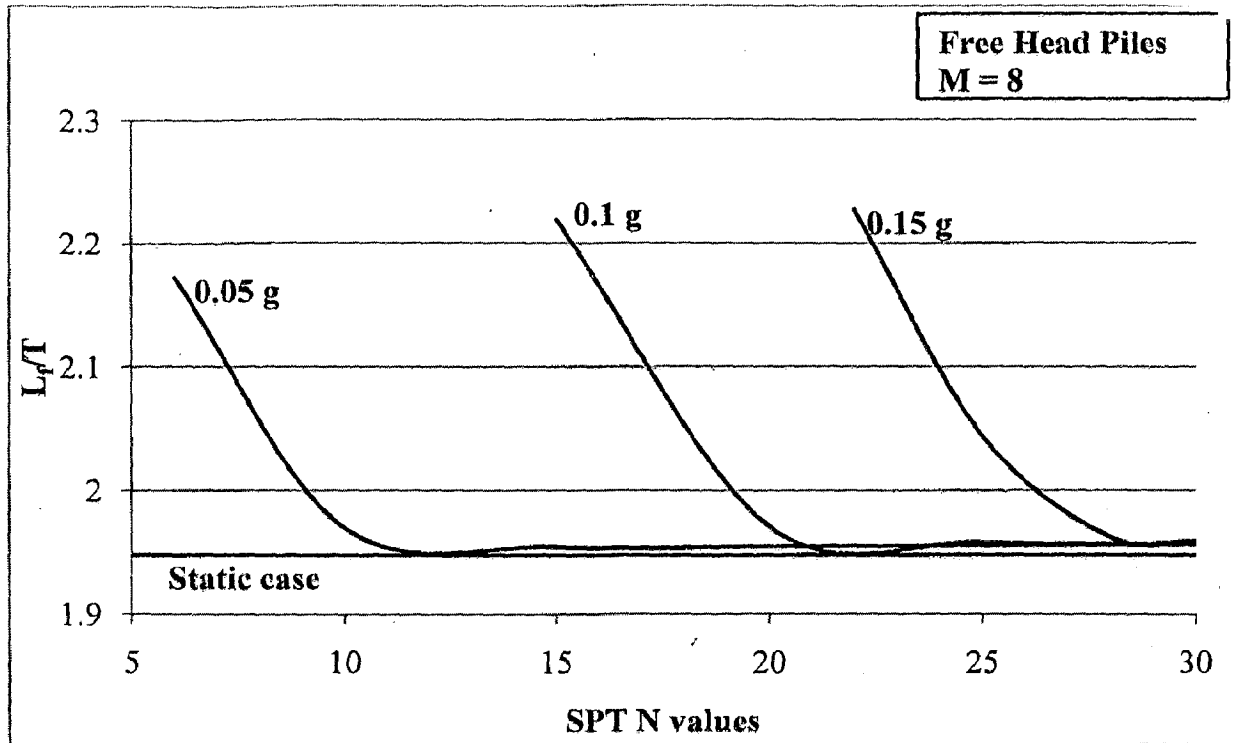

Fig. 6.8 Lf/T Vs N for M=7.5

Fig. 6.9 L_f/T Vs N for M=8

6.3.2 Fixed Head Piles

From Fig. 6.10 to Fig. 6.14, the design charts for lateral design of fully embedded fixed head piles in homogenous cohesionless partially liquefiable soils for different values of earthquake magnitude are shown. In each figure (for a particular value of earthquake magnitude), the relation between fixity factor (L_f/T) and SPT N values for different ground surface accelerations ranging from 0.05 g to 0.2 g are given. Also the design chart for lateral analysis of piles for static loading case is provided. For static case the curve is horizontal to the X- axis with a Fixity factor of around 2.24.

The charts are useful to determine the pile head deflection in partially liquefiable soils only. For example in Fig. 6.11, consider the curve for a_{max} = 0.15 g. Here below SPT N = 17, the soil deposit will be subjected to complete liquefaction at the top leading to unsupported length. So for these cases, curve cannot be extended and problem should be solved using the program developed. For earthquake magnitude of 8 (Fig. 6.14), the soil undergoes complete liquefaction for a_{max} = 0.2 g for higher values of SPT N also. So the curve corresponding to it is not provided.
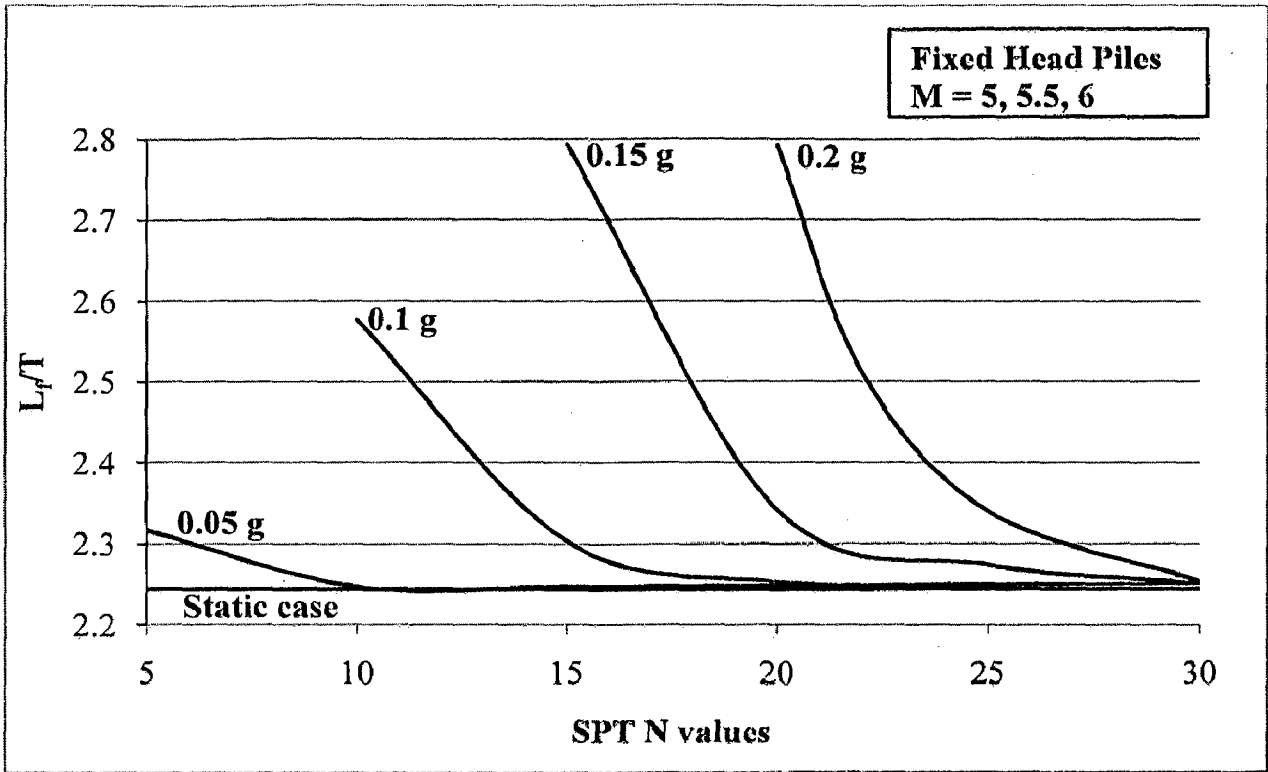
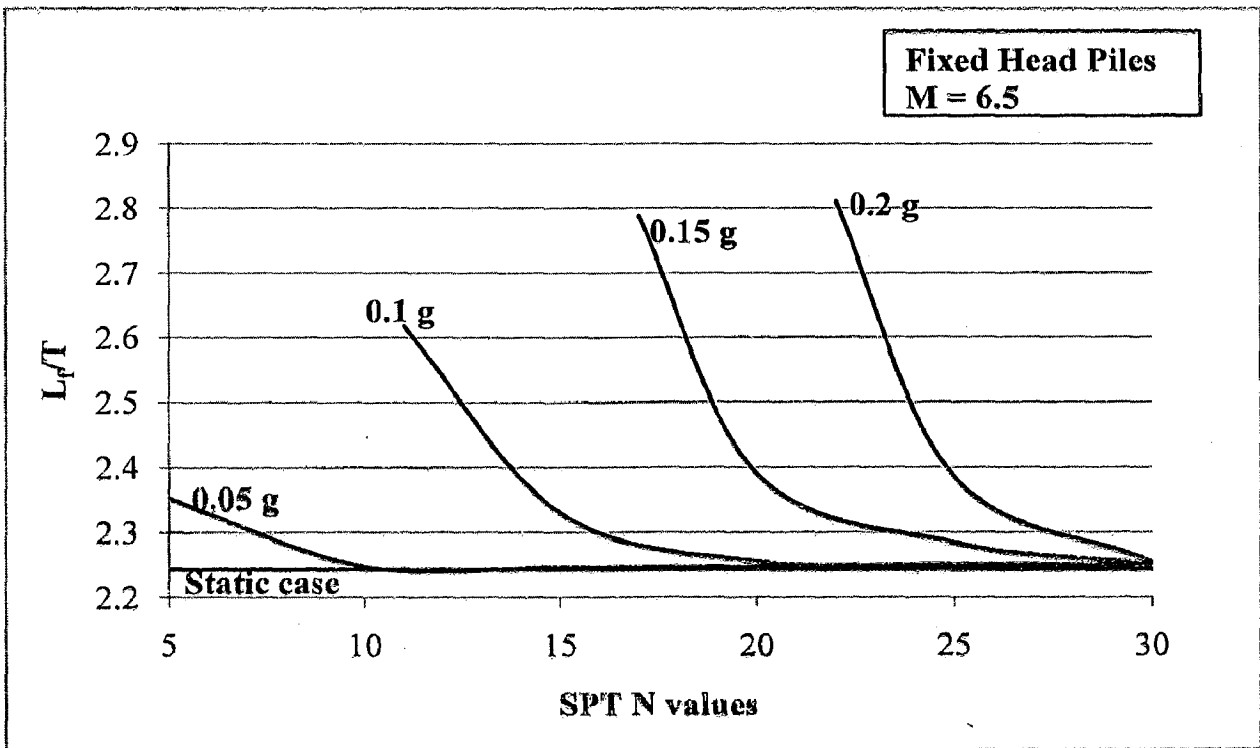Fig. 6.10 L_f/T Vs N for M=5, 5.5 and 6
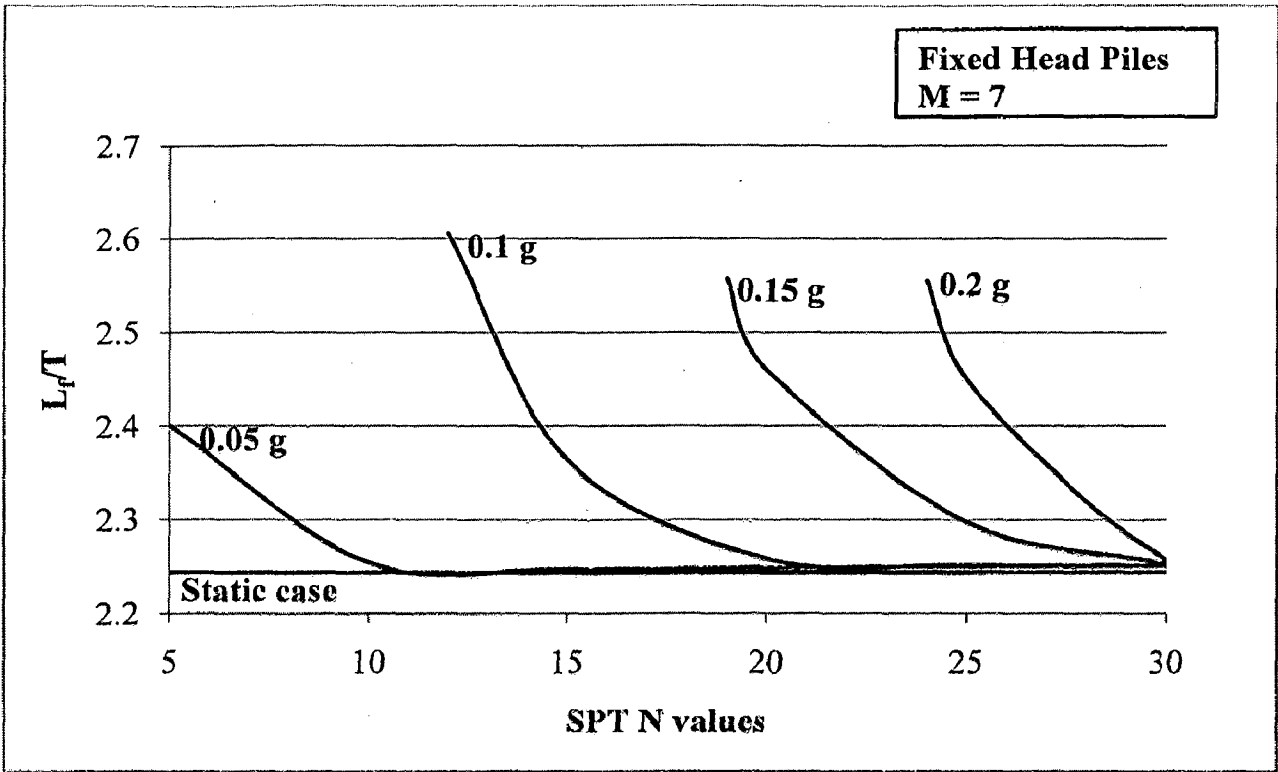

Fig. 6.11 L_f/T Vs N for M=6.5
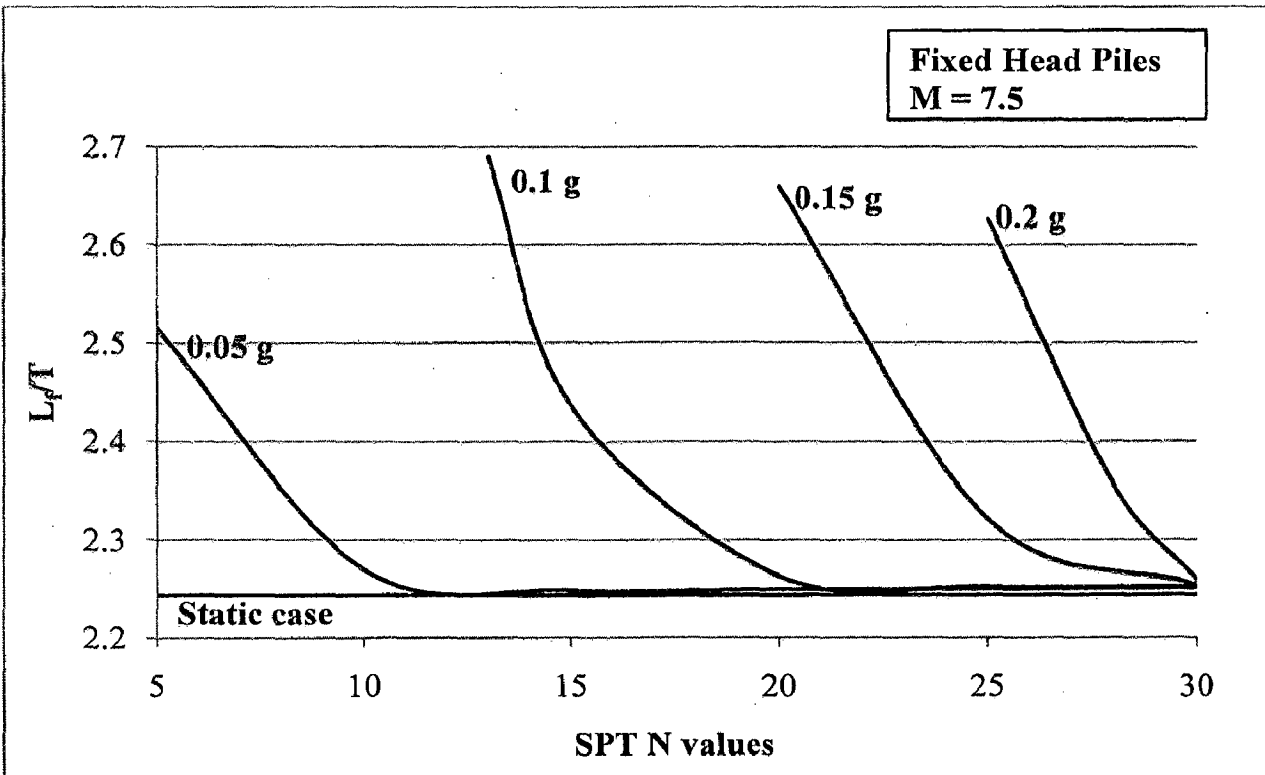
Fig. 6.12 L_f/T Vs N for M=7

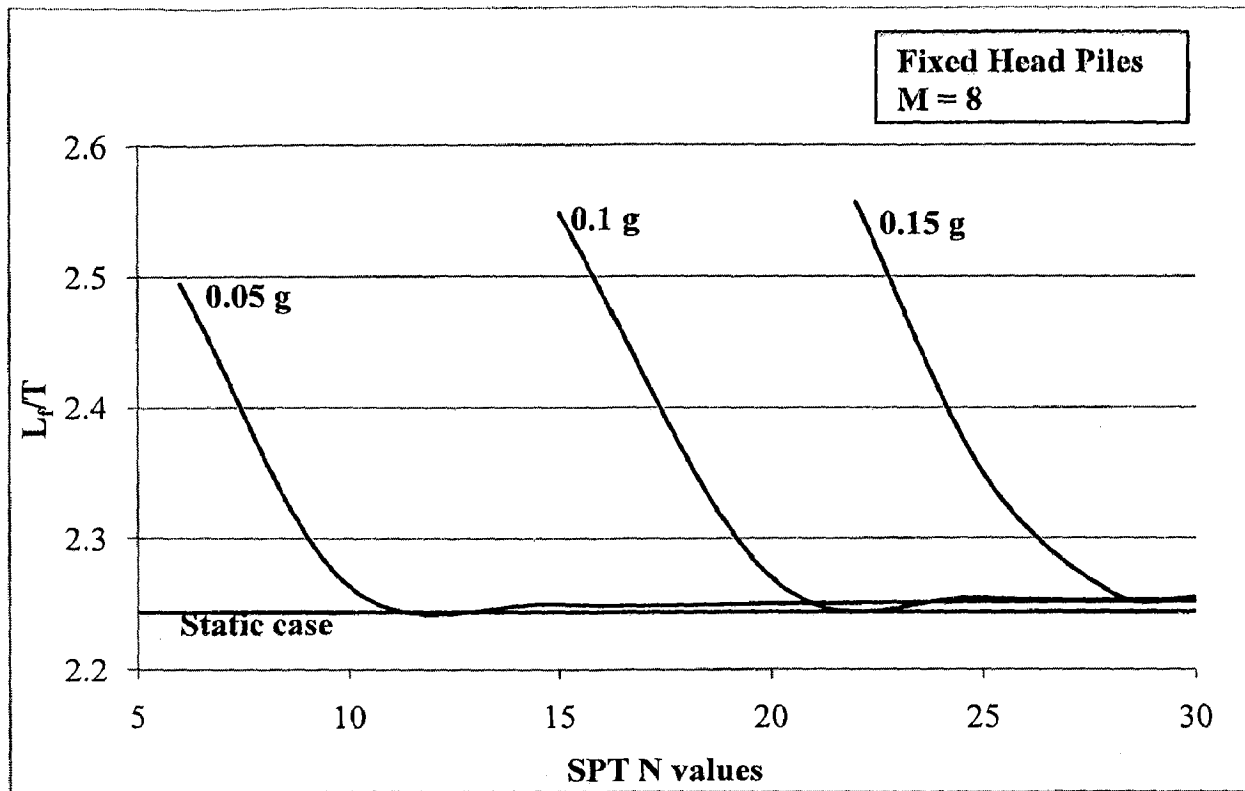
Fig. 6.13 L_f/T Vs N for M=7.5

80

Fig. 6.14 L_f/T Vs N for M=8

6.4 Problem to Illustrate the Use of Design Charts

Determine the pile head deflection for a 20 m long pile in homogenous liquefiable soil deposit having an SPT N value of 15. Pile head is fixed. The data required are given below.

Lateral load at the top = 25 kN.

Pile diameter = 0.5 m

Modulus of Elasticity of Pile, $E = 2.5*10^7$ kN/m²

Water table = at ground level

Earthquake magnitude = 6.5

Maximum ground surface acceleration is 0.1g.

Saturated unit weight = 19 kN/m³

Solution

1. Use the chart, i.e. corresponding to M = 6.5 and a_{max} = 0.1g for fixed head piles, i.e. Fig. 6.11. From this the value of L_f/T corresponding to N = 15 is obtained as 2.33.

2. For N = 15, find the value of n_h using Eq. 4.3 and for that the value of A is obtained from Table 4.1 by interpolation. A is obtained as = 464.6.

   $n_h = (A*\gamma_{sub})/1.35$

   $= 464.6 *(19-9.81)/1.35$

   $= 3158.637 \text{ kN/m}^3$

3. Calculate the value of T from Eq. 4.18.

   $T = (EI/n_h)^{0.2}$

   $= 1.893 \text{ m}$

4. Then calculate the value of 'L_f' by multiplying L_f/T obtained in step 1 by 'T' obtained in step 3. L_f is obtained as 4.41.

5. Using Eq. 4.19b, find the value of pile head deflection, y. In the equation, the unsupported length, L_1 = 0, since only fully embedded piles are considered.

   So $y = (Q*L_f^3) / (12*E*I)$

   $= 0.00233m = 2.33 \text{ mm}$

Thus using these design charts, the value of pile head deflection can be easily calculated manually.

SUMMARY AND CONCLUSIONS

7.1 SUMMARY

This dissertation deals with the analysis of lateral response of piles in liquefiable cohesionless soils due to lateral loads. For this, analytical studies are carried out and a computer code in C++ is developed. The basic idea is to develop a simple procedure to determine the lateral capacity of a single pile in liquefiable soil using commonly available field test data. The "Modulus of Subgrade Reaction" approach is adopted for studying the lateral response of the pile.

The procedure adopted is summarized as follows. The basic inputs required are the soil profile i.e. SPT N values with depth, magnitude of earthquake and maximum earthquake surface acceleration. Using the "simplified procedure", recommended by Youd et al. (2001), the liquefaction susceptibility of the soil is evaluated. For the layers which are completely liquefied, the value of modulus of horizontal subgrade reaction (K_h) is taken as zero. The soil layers which are not fully liquefied but there is a reduction in shear strength due to generation of excess pore pressure, will experience a reduction in the value of K_h. In order to calculate the extent of degradation occurred in the value of K_h, the amount of pore pressure generated is evaluated adopting the method proposed by Seed et al. (1976) and the net reduced value of effective stress is determined. Corresponding to this reduced value of effective stress, modified value of K_h is obtained and is used in the analysis to determine the lateral capacity of pile. In the "Modulus of Subgrade Reaction approach", linear elastic spring models (Winkler's hypothesis) are used. Finite Difference scheme is adopted for solving the above approach to determine lateral capacity.

Using the above developed method, the lateral capacity of piles in layered soil deposits prone to liquefaction can be analyzed. A real problem from case history is worked out using the developed procedure. The effect of position of liquefiable layer on pile response is illustrated. Design charts are developed to determine the pile head deflection for free and fixed head, fully embedded piles in homogenous soil deposits prone to liquefaction

using Equivalent Cantilever Approach. A numerical problem is worked out to illustrate the use of design charts.

The proposed method and the program developed can be used to assess the safe lateral capacity of piles embedded in any non-homogenous deposit of cohesionless soil.

7.2 CONCLUSIONS

The following major conclusions may be drawn from the study.

1. A simple method to determine the lateral capacity of single pile in liquefiable soils is developed. The method is based on the commonly available field tests data (SPT).

2. This method can be used for both long and short piles.

3. The lateral capacity of a single pile in liquefiable soil deposit reduces drastically as compared to the static case.

4. The results from the analysis of a few case histories show that the maximum bending moment increases by about 3 to 4 times in liquefied soils than in the static case. This explains the structural failure of piles reported in these cases.

5. Parametric studies conducted shows that the presence of liquefiable layers at the top is more critical than intermediate liquefiable layers as far as lateral capacity is considered.

6. Design charts developed for fully embedded piles in homogenous, cohesionless liquefiable soil deposits provide a quick means of estimating pile head deflection for a given magnitude of Earthquake and Peak ground acceleration (a_{max}).

7.3 FUTURE DIRECTIONS

1. The dissipation of pore water pressure is not considered in the present study. In the case of medium and coarse grained soils, there will be high dissipation due to high value of permeability. If dissipation is considered here, the net pore pressure generated will be sufficiently reduced and will give a more economical design.

2. Here only a single pile is considered, however the procedure can be extended to pile groups in liquefiable soils.

3. In this study one dimensional analysis is considered. Using Finite element method, three dimensional analysis can be carried out which can give more accurate results.

4. At strong excitation the behaviour of soil is non linear, therefore the linear elastic spring models used here can be replaced by non linear spring models which can represent the non linearity of soil.

REFERENCES

1 Andrus, R. D., and Stokoe, K. H., II (1997). "Liquefaction resistance based on shear wave velocity." *Proceedings: NCEER Workshop on Evaluation of Liquefaction Resistance of Soils*, Nat. Ctr. for Earthquake Engineering. Res., State Univ. of New York at Buffalo, 89–128.

2 Banerjee, P.K., and Davies, T.G. (1978). "The behaviour of axially and laterally loaded single piles embedded in non – homogenous soils." *Geotechnique*, 28(3), 309-326.

3 Barber, E. S. (1953). "Discussion to paper by S. M. Gleser." *ASTM, STP*, 154, 94-101.

4 Bhattacharya, S. (2003). "Pile instability during Earthquake liquefaction." Ph. D. Thesis, University of Cambridge, Cambridge, U.K.

5 Boulanger, R.W., and Idriss, I.M. (2004). "Evaluating the potential for liquefaction or cyclic failure of silts and clays" *Report no UCD/CGM-04/01*, Center for Geotechnical Modeling, Department of Civil & Environmental Engineering, University of California, Davis, California.

6 Boulanger, R.W., Kutter, B.L., Bradenberg, S.J., Singh, P., and Chang, D. (2003). "Pile foundations in liquefied and laterally spreading ground during earthquakes: centrifuge experiments & analyses." *Research report chapter 1*, supported by the California Department of Transportation under contract 59A0162, Department of Civil & Environmental Engineering, College of Engineering, University of California at Davis, report no UCD/CGM-03/01.

7 Bransby, M.F. (1999). "Selection of p-y curves for the design of single laterally loaded piles." *International Journal for Numerical and Analytical Methods in Geomechanics*, 23(15), 1909-1926.

8 Brennan, A.J., Govindaraju, L., and Bhattacharya, S. (2007). "Liquefaction – susceptibility, assessment and remediation." *Design of foundations in seismic areas: principles and applications, NICEE Publication, IIT Kanpur, India*. 86-122.

9 Brown, D.A., Shie, C.F., and Kumar, M. (1989). "*p-y* curves for laterally loaded piles derived from three dimensional finite element model." *Proc., 2nd Int. Symp., Numerical Models in Geomechanics*, Niagra Falls, Canada, Elsevier Applied Sciences, New York. 683-690.

10 Budhu, M., and Davies, T.G. (1988). "Analysis of laterally loaded piles in soft clays." *Journal of Geotechnical Engineering*, 114 (1), 21-39.

11 Byrne, P. (1991) "A Cyclic Shear-Volume Coupling and Pore-Pressure Model for Sand," *Proceedings of the Second International Conference on Recent Advances in*

Geotechnical Earthquake Engineering and Soil Dynamics, St. Louis, Missouri, Vol. 1, 47-55.

12 Byrne, P.M., and McIntyre, J. (1994). "Deformation in granular soils due to cyclic loading." *Vertical and horizontal deformations of foundation and embankments*, ASCE GSP 40, 1864-1896.

13 Dash, S.R., Govindaraju, L., and Bhattacharya, S. (2009). "A case study of damages of the Kandla Port and Customs Office tower supported on a mat– pile foundation in liquefied soils under the 2001 Bhuj earthquake." *Soil Dynamics and Earthquake Engineering*, 29, 333-346.

14 Davies, T.G., and Budhu, M. (1986). "Non-linear analysis of laterally loaded piles in heavily over consolidated clays." *Geotechnique*, 36(4), 527-538.

15 Davisson, M. T., and Gill, H. L. (1963). "Laterally loaded piles in a layered soil." *Journal of Soil Mechanics and Foundation Division*, ASCE, 89(3), 63-94.

16 Davisson, M.T., and Robinson, K.E. (1965). "Bending and buckling of partially embedded piles." Sixth international conference on Soil Mechanics and Foundation Engineering, Montreal, Vol. 2, 243-246.

17 Desai, C.S., and Appel, G.C. (1976). "3-D analysis of laterally loaded structures." *Proc., 2nd Int. Conf. on Numerical Methods in Geomechanics*, Blacksburg, ASCE, Vol. 1, 405-418.

18 EERI Special Earthquake Report (2001). "Preliminary observations on the origin and effects of the January 26, 2001 Bhuj (Gujarat, India) Earthquake", Earthquake Engineering Research Institute, Oakland, California.

19 Finn, W.D.L., and Fujita, N. (2002). "Piles in liquefiable soils: Seismic analysis and design issues." *Soil Dynamics and Earthquake Engineering*, 22, 731-742.

20 Finn, W.D.L., Lee, K.W., and Martin, G.R. (1977). "An effective stress model for liquefaction." *Journal of Geotechnical Engineering division*, ASCE, 103(6), 517-533.

21 Finn, W.D.L., Thavaraj, T. (2001). "Deep foundations in liquefiable soils: case histories, centrifuge tests and methods of analysis." *In: Proceedings of the fourth international conference on recent advances in geotechnical earthquake engineering and soil dynamics*, San Diego, 26–31.

22 Fuji, S., Cubrinovski, M., Tokimatsu, K., and Hayashi, T. (1998). "Analyses of damaged and undamaged pile foundations in liquefied soils during the 1995 Kobe Earthquake." *Proc., 1998 Conf. on Geotechnical Earthquake Engineering and Soil Dynamics III*, Seattle, Wash., 2, 1187–1198.

23 Gupta, M.K., and Prakash, S. (1977). "Sand liquefaction during shake table vibration." *Proceedings of 6th World conference on Earthquake Engineering*, New Delhi, Vol. 6, 19-24.

24 Gupta, M.K., and Prakash, S. (1986). "A new realistic approach for liquefaction analysis." *ISET Bulletin*, 23(3), 118-137.

25 Gupta, M.K., and Sharma H.M. (1977). "Possibility of liquefaction during an earthquake." *ISET Bulletin*, 14(3), 101-109.

26 Hamada, M. (1992). "Large ground deformations and their effects on lifelines: 1964 Niigata earthquake." *Case Studies of liquefaction and lifelines performance during past earthquake. Technical Report NCEER-92-0001*, Volume-1, Japanese case studies, National Centre for Earthquake Engineering Research Buffalo, NY.

27 Hamada, M., Sato, H., and Nakamura, T. (1994). "An Experimental and Numerical Study on Liquefaction induced Ground Displacement." *Proceedings of the 5th US National Conference on Earthquake Engineering*, California, 4, 169-178.

28 Idriss, I.M. (1991). "Earthquake ground motions at soft soil sites." *Proceedings: Second international conference on recent advances in Geotechnical Earthquake engineering and Soil Dynamics*, St. Louis, Missouri. Vol. 3, 2265-2272.

29 Idriss, I.M., and Boulanger, R.W. (2006). "Semi-empirical procedures for evaluating liquefaction potential during earthquakes." *Soil Dynamics and Earthquake Engineering*, 26, 115-130.

30 IS 1893 (Part 1) (2002). Indian Standard criteria for earthquake resistant design of structures, part 1 – General provisions and buildings. Bureau of Indian Standards, New Delhi.

31 IS 2911 (Part 1/Sec 4) (2002). Indian Standard code of practice for design and construction of pile foundation, part 1 - concrete piles (Section 4 - Bored Precast Concrete Piles). Bureau of Indian Standards, New Delhi.

32 Ishihara, K. (1993). "Thirty third Rankine Lecture: Liquefaction and flow failure during earthquakes." *Géotechnique*, 43(3), 349–415.

33 Ismael, N. F. (1990) "Behavior of laterally loaded bored piles in cemented sands." *Journal of Geotechnical Engineering Division*, ASCE, 116(11), 1678-1699.

34 Jefferies, M., and Been, K. (2006). "Soil liquefaction: A critical state approach." *Taylor and Francis*, New York.

35 Juirnarongrit. T., and Ashford, S.A. (2005). "Effect of pile diameter on the modulus of subgrade reaction." *Report Submitted to Caltrans under Contract No. 59A0051*, Department of Structural Engineering, University of California, San Diego, California. Report No. SSRP–2001/22.

36 Kagawa, T. (1992). "Effect of liquefaction on lateral pile response." *Geotechnical Special Publication, ASCE*, 34, 207-223.

37 Kagawa, T., and Kraft, L.M. (1981). "Modeling the liquefaction process." *Journal of Geotechnical Engineering*, 107(12), 1593-1607.

38 Kayen, R.E., Mitchell, J.K., Seed, R.B., Lodge, A., Nishio, S., and Coutinho, R. (1992). "Evaluation of SPT-, CPT-, and shear wave-based methods for liquefaction potential assessment using Loma Prieta data." *Proc., 4th Japan-U.S. Workshop on Earthquake-Resistant Des. of Lifeline Fac. and Countermeasures for Soil Liquefaction,* Vol. 1, 177–204.

39 Klar, A., Baker, R., and Frydman, S. (2004). "Seismic soil-pile interaction in liquefiable soil." *Soil Dynamics and Earthquake Engineering,* 24, 551-564.

40 Kooijman, A. P. (1989). "Comparison of an elastoplastic quasi three-dimensional model for laterally loaded piled with field tests." *Proc. of the III International Symposium, Numerical Models in Geomechanics, (NUMOG III),* Niagara Falls, Canada, Elsevier Applied Science: New York. 675-682.

41 Kramer, S.L. (1996). "Geotechnical Earthquake Engineering." *Pearson Education, Inc,* New Delhi.

42 Liao, S.S.C., and Whitman, R.V. (1986). "Catalogue of liquefaction and non-liquefaction occurrences during earthquakes." *Res. Rep.,* Department of Civil Engineering., Massachusetts Institute of Technology.

43 Liyanapathirana, D.S., and Poulos, H.G. (2002a). "Numerical simulation of soil liquefaction due to earthquake loading." *Soil Dynamics and Earthquake Engineering,* 22, 511-523.

44 Liyanapathirana, D.S., and Poulos, H.G. (2002b). "A numerical model for dynamic soil liquefaction analysis." *Soil Dynamics and Earthquake Engineering,* 22, 1007-1015.

45 Liyanapathirana, D.S., and Poulos, H.G. (2005a). "Seismic lateral response of piles in liquefying soil." *Journal of Geotechnical and Geoenvironmental Engineering,* ASCE, 131(12), 1466-1479.

46 Liyanapathirana, D.S., and Poulos, H.G. (2005b). "Pseudostatic approach for seismic analysis of piles in liquefying soil." *Journal of Geotechnical and Geoenvironmental Engineering,* ASCE, 131(12), 1480-1487.

47 Maheshwari, B.K., Nath, U.K., and Ramasamy, G. (2008). "Influence of liquefaction on pile-soil interaction in vertical vibration." *ISET Journal of Earthquake Technology,* 45(1-2), 1-12.

48 Martin, G.R., Finn, W.D.L., and Seed, H.B. (1975). "Fundamentals of liquefaction under cyclic loading." *Journal of Geotechnical Engineering division,* ASCE, 101(GT5), 423-438.

49 Martin, P.P., and Seed, H.B. (1979). "Simplified procedure for effective stress analysis of ground response." *Journal of Geotechnical Engineering division,* ASCE, 105 (GT6), 739-758.

50 Matlock, H. (1970). "Correlations for design of laterally loaded piles in soft clay." *Proc., 2nd Annual Offshore Technology Conf., Paper No. OTC 1204*, Houston, Texas, 577-594.

51 Matlock, H. and Reese, L.C. (1960). "Generalized solutions for laterally loaded piles." *Journal of Soil Mechanics and Foundation Division*, ASCE, 86(5), 63-91.

52 Matlock, H., and Reese, L.C. (1961). "Foundation analysis of Offshore Pile supported structures, Proceedings: Fifth international conference of Soil Mechanics and Foundation Engineering., Paris, Vol. 2, 91-97.

53 Matlock, H., and Reese, L.C. (1962). "General solutions for laterally loaded piles." *Trans. ASCE*, 127(1), 1220-1247.

54 Miura, F., Stewart, H.E., and O'Rourke, T.D. (1991). "The effect of liquefaction-induced lateral spreading on pile foundations." *Soil Dynamics and Earthquake Engineering*, 10(5), 271-279.

55 Nath, U.K. (2006). "Pile-Soil Interaction in Liquefiable Soils." M. Tech. Dissertation, Dept. of Civil Engineering, Indian Institute of Technology Roorkee, Roorkee.

56 Novak, M. (1974). "Dynamic stiffness and damping of piles." *Canadian Geotechnical Journal*, 11, 574-598.

57 Peck, R.B. (1979). "Liquefaction potential: Science versus practice." *Journal of Geotechnical Engineering Division*, ASCE, 105 (GT3), 393-398.

58 Peck, R.B., Hanson, W.E., and Thornburn, T.H. (1974) "Foundation Engineering," *John Wiley & Sons*, New York.

59 Poulos, H. G. (1973). "Analysis of piles in soil undergoing lateral movement." *Journal of Soil Mechanics and Foundation Division*, ASCE, 99(5), 391-406.

60 Poulos, H.G. (1971). "Behaviour of laterally loaded piles I – single piles." *Journal of Soil Mechanics and Foundation Division*, ASCE, 97(5), 711–731.

61 Poulos, H.G., and Davis, E.H. (1980). "Pile foundation analysis and design", John Wiley and Sons, New York.

62 Prakash, S. (1981). "Soil dynamics." *McGraw-Hill Book Company*, New York.

63 Ramasamy, G. (1974). "Flexural behavior of axially and laterally loaded individual piles and group of piles." Ph. D. Thesis, Indian Institute of Science, Bangalore.

64 Ramasamy, G., Ranjan, G., and Jain, N.K. (1987). "Modification of Indian standard procedure on lateral capacity of piles." *Indian Geotechnical Journal*, 17(3), 249-258.

65 Reese, L.C., and Welch, R.C. (1975). "Lateral loading of deep foundation in stiff clay." *Journal of Geotechnical Engineering Division*, ASCE, 101(7), 633-649.

66 Reese, L.C., Cox, W.R. and Koop, F.D. (1975). "Field testing and analysis of laterally loaded piles in stiff clay." *Proc., 7th Offshore Technology Conf., Paper No. OTC 2321*, Houston, Texas, 671-690.

67 Reese, L.C., Cox, W.R., and Koop, F.D. (1974). "Analysis of laterally loaded piles in sand," *Proc. 6th Offshore Technology Conference, Paper 2080*, Houston, Texas, 473-483.

68 Sakajo, S., Chai, J.C., Nakajima, K., and Maeda, M. (1995). "Effect of group pile on liquefaction resistance of sandy ground." *Proc., First Conf. on Earthquake Geotechnical Engineering*, Tokyo, 755–760.

69 Seed, H.B. (1979). "Soil liquefaction and cyclic mobility evaluation for level ground during earthquakes." *Journal of Geotechnical Engineering Division*, ASCE, 105(2), 201–255.

70 Seed, H.B., and Idriss, I.M. (1967). "Analysis of soil liquefaction, Niigata Earthquake." *Journal of Soil Mechanics and Foundation Division*, ASCE, 93(3), 83–108.

71 Seed, H.B., and Idriss, I.M. (1971). "Simplified procedure for evaluation soil liquefaction potential." *Journal of Soil Mechanics and Foundation Division*, ASCE, 97(9), 1249–1273.

72 Seed, H.B., and Idriss, I.M. (1982). "Ground motions and soil liquefaction during earthquakes." Earthquake Engineering Research Institute Monograph, Oakland, Calif.

73 Seed, H.B., Martin, P.P., and Lysmer, J. (1976). "Pore-water pressure changes during soil liquefaction." *Journal of Geotechnical Engineering Division*, ASCE, 102 (GT4), 323-346.

74 Seed, H.B., Tokimatsu, K., Harder, L.F., and Chung, R.M. (1985). "The influence of SPT procedures in soil liquefaction resistance evaluations." *Journal of Geotechnical Engineering*, ASCE, 111(12), 1425–1445.

75 Seed, R.B., Cetin, K.O., Moss, R.E.S., Kammerer, A. M., Wu, J., Pestana, J.M. and Riemer, M.F. (2001). "Recent advances in soil liquefaction engineering and seismic site response evaluation", *Proc. 4th Int. Conf. on Recent Adv. in Geotechnical Earthquake Engineering and Soil Dynamics*, San Diego.

76 Shahrour, I., and Ousta, R. (1998). "Numerical analysis of the behavior of piles in saturated soils under seismic loading." *Proc., 11th European Conf. on Earthquake Engineering*.

77 Spillers, W.R., and Stoll, R.D. (1964). "Lateral response of piles" *Journal of Soil Mechanics and Foundation Division*, ASCE, 90(6), 1–9.

78 Tokimatsu, K., Mizuno, H., and Kakurai, M. (1996). "Building damage associated with geotechnical problems." *Soils and Foundations*, Special Issue on Geotechnical

Aspects of the January 17 1995 Hyogoken-Nambu Earthquake, Japanese Geotechnical Society.

79 Uzoka, N., Sento, N., Kazama, M., Zhang, F., Yashima, A., and Oka, F. (2007). "Three-dimensional numerical simulation of earthquake damage to group-piles in a liquefied ground." *Soil dynamics and earthquake engineering*, 27, 395-413.

80 Website: www. ce. Washington. edu/ ~liquefaction /html /main.html.

81 Website: www.smate.wwu.edu/teched/geology/eq-Alaska64.html.

82 Wilson, D. W., Boulanger, R. W., and Kutter, B. L. (2000). "Seismic lateral resistance of liquefying sand." *Journal of Geotechnical & Geoenvironmental Engineering, ASCE*, 126(10), 898-906.

83 Yao, S., and Nogami, T. (1994). "Lateral cyclic response of piles in viscoelastic Winkler subgrade." *Journal of Engineering Mechanics*, 120(4), 758-775.

84 Yegian, M.K., Ghahraman, V.G., and Harutiunyan, R.N. (1994). "Liquefaction and embankment failure case histories, 1988 Armenia earthquake." *Journal of Geotechnical Engineering Division*, ASCE, 120(3), 581-596.

85 Youd, T.L., Idriss, I.M., Andrus, R.D., Arango, I., Castro, G., Christian, J.T., Dobry, R., Finn, W.D.L., Harder Jr., L.F., Hynes, M.E., Ishihara, K., Koester, J. P., Liao, S.S.C., Marcuson III, W.F., Martin, G.R., Mitchell, J.K., Moriwaki, Y., Power, M.S., Robertson, P.K., Seed, R.B., and Stokoe II, K.H. (2001). "Liquefaction resistance of soils: Summary report from the 1996 NCEER and 1998 NCEER/NSF workshops on evaluation of liquefaction resistance of soils." *Journal of Geotechnical and Geoenvironmental Engineering*, ASCE, 127(10), 817-833.

86 Zheng, J., Susuki, K., and Ohbo, N. (1996). "Evaluation of Sheet Pile-ring Countermeasure against Liquefaction for Oil Tank Site." *Soil Dynamics and Earthquake Engineering*, 15(6), 369-379.

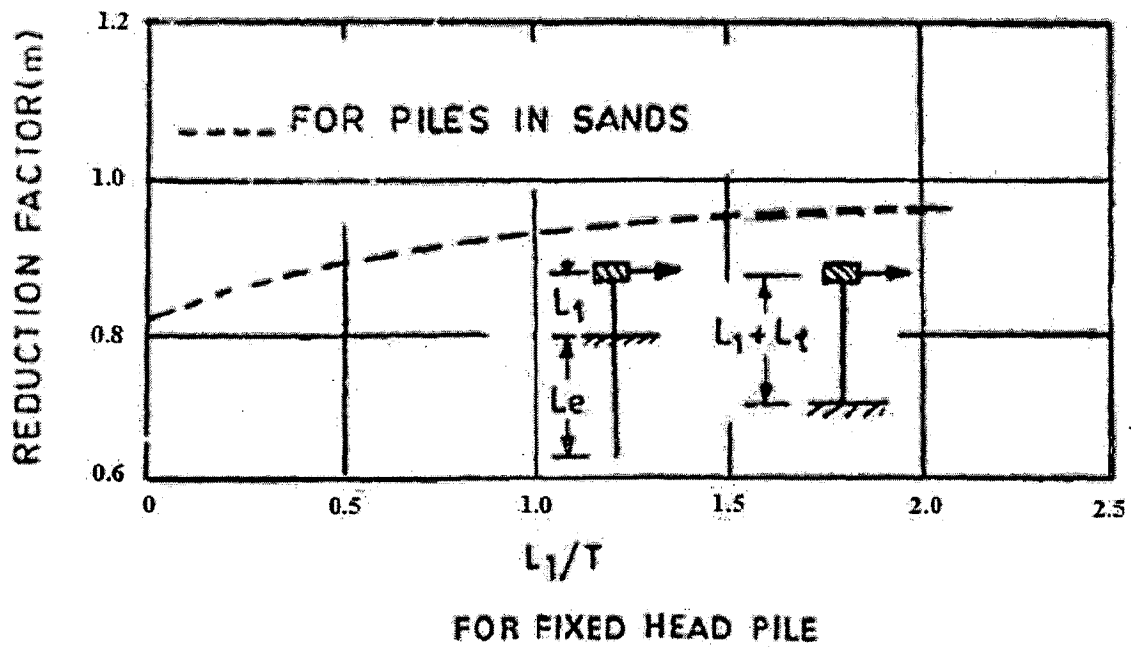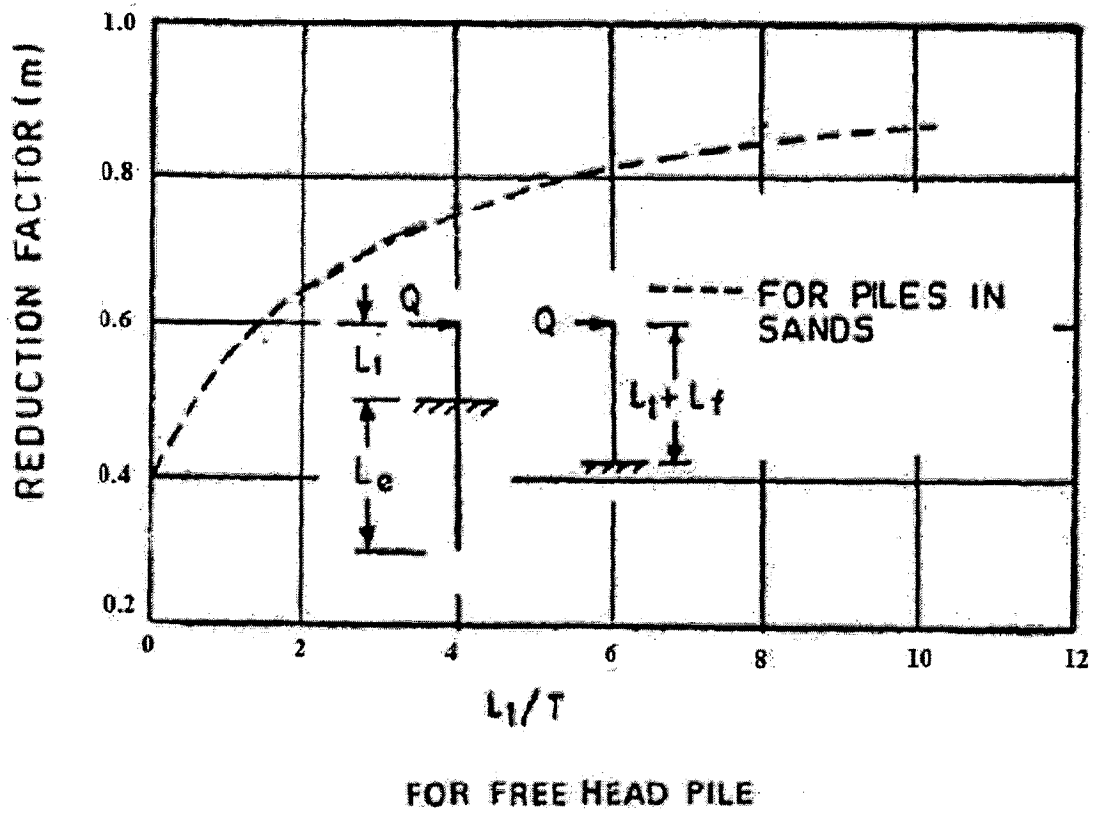FOR FREE HEAD PILE

FOR FIXED HEAD PILE

Fig. 4.4 Determination of Reduction Factors for Computation of Maximum Moment in Pile (IS: 2911 (Part 1/Sec 4) – 2002).